THE ^{1}H AND ^{13}C DYNAMIC NUCLEAR POLARIZATION (DNP) ENHANCEMENT FOR NOVEL SILICA PHASE IMMOBILIZED NITROXIDE (SPIN) SAMPLES

by

Rossitza K. Gitti

Dissertation submitted to the Faculty of the

Virginia Polytechnic Institute and State University

in partial fulfillment of the requirements for the degree of

DOCTOR OF PHILOSOPHY

in

Chemistry

APPROVED:

H. C. Dorn, Chairman

L. T. Taylor

J. M. Tanko

J. S. Merola

M. R. Anderson

August, 1991

Blacksburg, Virginia

c.2

LD
5655
V856
1991
f577
c.2

THE ^{1}H AND ^{13}C DYNAMIC NUCLEAR POLARIZATION (DNP) ENHANCEMENTS FOR NOVEL SILICA PHASE IMMOBILIZED NITROXIDE (SPIN) SAMPLES

by

Rossitza K. Gitti

Committee Chairman: Harry C. Dorn
Chemistry

(ABSTRACT)

The solid/liquid intermolecular transfer (SLIT) flow dynamic nuclear polarization (DNP) experiment potentially provides new methodology for studying interfacial phenomena (e.g., weak hydrogen bonding). In addition, the high efficiency of the transfer also ensures dramatically enhanced NMR signals. These large DNP enhancements could alleviate sensitivity limitations in various flow NMR experiments. Previous studies have established that silica phase immobilized nitroxide (SPIN) radical system are advantageous in the SLIT experiment. In favorable cases (e.g. $DCCl_3$/SPIN system) a ^{13}C DNP enhancement 60 times in excess of the high magnetic field (4.7 T) magnetization has been achieved.[12] However a number of factors still limit the SPIN system presently available. For example, low magnetogyric ratio nuclides, ^{13}C, ^{15}N, which are not dominated by scalar relaxation mechanism require high surface radical concentrations.

The focal point of the present study is the preparation and characterization of several new SPIN radical systems and can be divided into two parts:

1). Preparation, EPR, and DNP Characterization of Achiral SPIN Radicals: a number of SPIN samples were prepared in order to examine the dependence of the observed SLIT DNP

enhancements as a function of the surface spin concentration and also isotope-substitution of the immobilized radicals. The SPIN samples were characterized by EPR and DNP. The results show that the increase in the spin concentration does not offer any advantage for ^{1}H DNP studies. In contrast, ^{13}C SLIT DNP results in improved SPIN sample demonstrate the possibility of monitoring dipolar dominated ^{13}C DNP enhancements as a result of better leakage factors and suppressed three-spin effects at higher radical concentration. The effect of substitution of deuterons for protons in the immobilized radical also suggest an appreciable contribution of a solid-state three-spin effect.

2). Preparation, EPR, and DNP Characterization of Chiral SPIN Samples: This part of the study provides a chiral SPIN radical suitable for monitoring enantioselective ^{13}C DNP enhancements. The DNP results suggest that selective enantiomer/chiral SPIN interactions are feasible. Specifically, differences in the ^{13}C DNP enhancements for a model system: (R)- and (S)- enantiomers of bromocamphor, and a (R) chiral SPIN sample were observed.

To Apo

ACKNOWLEDGEMENTS

First and most of all, I would like to express my gratitude to my research director Dr. Harry Dorn for providing me with the opportunity to work in such an exciting area, which kept me going even when the results were not quite encouraging; for his guidance and support during the course of this investigation and the preparation of this manuscript; and for his understanding and patience regarding my two children who were born during the course of this study.

I would like to thank Tom (Mr. Thomas Glass) who has always gladly shared his knowledge and experience. I would like to thank Mrs. Juan Gu for helping me set up the instrumentation conditions for ^{13}C DNP measurements and for her help with the computer. Also the thanks are extended to Dr. Carl Wild and Mr. Rob Keyes for their help and suggestions throughout the synthetic portion of this work; and to Mr. Steven Stevenson and Mrs. Barbara Bunn for reading the manuscript. I would like to acknowledge Mr. Jim Coulter and Mr. Larry Jackson for maintaining the instrumentation as well as Dr. Merola's group for being so kind to let me use some of the facilities in their laboratory. Thanks are also extended to the members of my committee and Dr. H. Bell for their time and helpful comments. I would like to acknowledge my parents who helped me take care of my little sons during the last two busy years of this study.

Finally, I would like to thank my husband for his love and for his encouragement while I was going through the difficult moments during my studies here in Va. Tech.

TABLE OF CONTENTS

ABSTRACT. II

DEDICATION IV

ACKNOWLEDGEMENTS V

LIST OF FIGURES VIII

LIST OF TABLES XI

LIST OF SCHEMES XII

CHAPTER 1: INTRODUCTION 1

1.1 General 1
1.2 Static and Flow DNP 3
1.3 Research Goal 9
1.4 EPR Line - Broadening 13

CHAPTER 2: THEORY OF DNP 18

2.1 General 18
2.2 DNP in Liquids 19
2.3 Mechanism of the Radical Induced Nuclear Relaxation 22
2.4 Electron-Nuclear Interactions 25
2.4.1 Dipolar Electron-Nuclear Interaction 26
2.4.2 Scalar Electron-Nuclear Interaction 28
2.5 Static DNP - Equations 34
2.6 Three-Spin Effect in Solutons 44
2.7 Three-Spin Effect in Solids 48

CHAPTER 3: FLOW DNP 50

3.1 Low Field Flow DNP 50
3.2 Low to High Field Transfer DNP 55

CHAPTER 4: REVIEW OF SYNTHESES AND APPLICATIONS OF SPIN SAMPLES 64

4.1 SPIN Radicals for Premagnetization of Samples for Flow NMR Experiments 66
4.2 SPIN Radicals for EPR Studies of Chromatographic Surfaces 67
4.3 SPIN Radicals for SLIT DNP Experiment 69

CHAPTER 5: EXPERIMENTAL 72

5.1 Preparation of SPIN Samples 72
5.1.1 Rationale for Preparation of SPIN Samples 72

5.1.2 Preparation of Short Chain Achiral SPIN Samples 77
5.1.3 Preparation of Chiral SPIN Samples 90
5.1.4 Preparation of Long Chain Achiral SPIN Samples 96
5.2 EPR Measurements 101
5.3 DNP Measurements 102
5.3.1 Experimental Design 102
5.3.2 Sample Preparation 103
5.3.4 Estimation of the Ultimate Enhancement 104

CHAPTER 6: RESULT AND DISCUSSIONS 107

6.1 EPR Characterization of SPIN Samples 107
6.1.1 EPR Characterization of Achiral SPIN Samples 107
6.1.2 EPR Characterization of Chiral SPIN Samples 120
6.2 ^{1}H and ^{13}C SLIT DNP for Achiral SPIN Samples 127
6.2.1 ^{1}H SLIT DNP Studies of Achiral SPIN Samples 127
6.2.2 ^{13}C SLIT DNP Studies of Achiral SPIN Samples 134
6.3 ^{13}C SLIT DNP of Chiral SPIN Samples 141

CONCLUSIONS 159

FUTURE STUDIES 162

APPENDIX 164

REFERENCES 175

VITA 179

LIST OF FIGURES

Fig. 1.1 Concentration effects on EPR spectra of an immobilized nitroxide radical.....17

Fig. 2.1 The energy level diagram for the electron-nuclear spin system (I=1/2, S=1/2) and transition probabilities.....20

Fig. 2.2 Types of pulses to describe scalar interaction..... 33

Fig. 2.3 Transfer of magnetization from an unpaired electron, (e) to a carbon atom, (C)..... 45

Fig. 3.1 Low to high magnetic field transfer DNP apparatus..... 56

Fig. 3.2 Immobilized nitroxide radicals used for low to high field SLIT DNP studies..... 57

Fig. 3.3 Improved experimental set-up for low to high transfer DNP studies.....60

Fig.5.12 Plots for calculations of: (a) the enhancement without either build up or transfer losses, A/K, and (b) the saturation factor.....106

Fig. 6.1 Effect of the length of the alkyl chain on the EPR line width.....108

Fig. 6.2 Effect of the reaction conditions on the spin concentration.....110

Fig. 6.3 Effect of the silica gel pretreatment on the spin concentration.....112

Fig. 6.4 EPR spectra of directly immobilized radical, (a), and of the oxidized amino-precursor, (b)..114

Fig. 6.5 Effect of the solvent on the EPR line width (a) **SPIN 5**/benzene; (b) **SPIN 5**/methanol.....115

Fig. 6.6 EPR spectra of the SPIN momoradicals: (a) $1.7*10^{19}$ and (b) $3.6*10^{19}$ spins/g, and of the SPIN biradical,(c) $4.9*10^{19}$ spins/g 118

Fig. 6.7 EPR spectra in benzene of: (a) **SPIN 8**, and (b) it deuterated analog, **SPIN 9**.....119

Fig. 6.8 EPR spectra in benzene of (a) **SPIN 8** and (b) **SPIN 10**.....121

Fig. 6.9 EPR spectra of the chiral **SPIN 12**: (a) in benzene, and (b) in methanol.....122

Fig.6.10 EPR spectra of the chiral **SPIN 13**: (A) in benzene, and (b) in benzene in the presence of R-(+)-methyl 2-chloropropionate....124

Fig.6.11 EPR spectrum of the chiral **SPIN 13** in 1,4-dioxane.....126

Fig.6.12 Proposed mechanism for the three-spin effect analog of the solid-state three-spin effect....132

Fig.6.13 ^{13}C SLIT DNP spectrum for **SPIN 7**/$CHCl_3$: (A) static NMR spectrum, M_o^H, (B) Flow DNP spectrum, M_z^* 136

Fig.6.14 LLIT DNP spectra for 1-chlorobutane 50% (v/v) in CCl_4[11]..... 139

Fig.6.15 SLIT DNP spectra of 1-chlorobutane 50% (v/v) in CCl_4 for SPIN radicals: (b) **SPIN 7**; (c) **SPIN 8**; d) **SPIN 11**,and the static NMR spectrum, M_o^H,(a) 140

Fig.6.16 Scheme of the (R(+)-SPIN)/(R(+)-bromocamphor) model system for SLIT DNP studies.....146

Fig.6.17 ^{13}C SLIT DNP spectra of 45% bromocamphor in 1,4-dioxane: (a) chiral **SPIN 13**/R-isomer; (b) chiral **SPIN 13**/S-isomer; 147

Fig.6.18 Plots of the observed ^{13}C SLIT DNP enhancements, M_z^*, relative to the static Boltzman magnetization, M_o^H vs. 1/Flow Rate for carbons C-2; C-1; and C-7.....148

Fig.6.19 Plots of the observed ^{13}C SLIT DNP enhancements, M_z^*, relative to: (a) M_o^H and (b) $M_{C\text{-}6}$, vs. 1/Flow Rate for carbons C-1 and C-8.....150

Fig.6.20 (a) Static ^{13}C NMR spectrum of R-(+)-bromocamphor in 1,4-dioxane, M_o^H; (b)-(g) ^{13}C SLIT DNP spectra of (R-(+)-bromocamphor)/**SPIN 13**.....152

Fig.6.21 Plots of the observed ^{13}C SLIT DNP enhancements,

M_z^*, relative to M_o^H vs. 1/Flow Rate for carbons C-10 (a), and C-3 (b).....154

Fig.6.22 Plots of the observed ^{13}C SLIT DNP enhancements, M_z^*, relative to M_o^H vs. 1/Flow Rate for carbons C-8 and C-9.....157

LIST OF TABLES

Table 2.1 Requirements and experimental conditions for maximum values of ξ, f, and s parameters.....42

Table 3.1 Flow DNP enhancements, (A_∞), for TTBP/benzene solutions.....52

Table 5.1 Reaction conditions for preparation of SPIN samples.....89

Table 6.1 EPR data and reactant's mole ratios for **SPIN 7, 8,** and **11**.....117

Table 6.2 ^{1}H SLIT DNP data for **SPIN 7, 8** and **11**..... 128

Table 6.3 ^{1}H SLIT DNP of chloroform for **SPIN 8**, **SPIN 9** and **SPIN 10**.....130

Table 6.4 ^{13}C SLIT DNP enhancements for R-(+)- and S-(-)-bromocamphor at flow rate 2 ml/min.....145

Table 6.5 Relaxation tines for 1M bromocamphor in CCl_4.. 151

LIST OF SCHEMES

Scheme 4.1 General reaction sequences for the syntheses of SPIN samples with the linking reagents: (a) Me_2SiCl_2 and $MeSiCl_3$, and (b) cyanuric chloride.....65

Scheme 5.1 Synthetic route for the preparation of SPIN monoradicals; linking reagent - Me_2SiCl_2. 79

Scheme 5.2 Synthetic route for the preparation of **SPIN 6**; linking reagent - Me_2SiCl_2..... ...83

Scheme 5.3 Syntetic route for the preparation of **SPIN 11**; linking reagent - $MeSiCl_3$.....88

Scheme 5.4 (I) Preparation of R-(+)-3-carboxy-PROXYL radical, (a). (II) Preparation of R-(+)-3-hydroxymethyl-PROXYL radical, (b).....91

Scheme 5.5 Synthetic route for the preparation of the chiral **SPIN 12**.....94

Scheme 5.6 Synthetic route for the preparation of the chiral **SPIN 13**.....95

Scheme 5.7 Synthetic route for the preparation of a long-chain SPIN biradical; linking reagent-cyanuric chloride.....97

Scheme 5.8 Synthetic route for the preparation of a long-chain SPIN radical; linking reagent-1,8 bis (chlorodimethyl-sylil) octane.....100

CHAPTER 1

INTRODUCTION

1.1 General

Since its discovery 45 years ago, nuclear magnetic resonance (NMR) spectroscopy has evolved as a powerful technique for studying molecular structures and interactions. The introduction of pulse Fourier transform methods started a new era of NMR spectroscopy that resulted in an intensive development of new experimental techniques. Enhancement of sensitivity has been the most important aspect with attention focused on less sensitive nuclei (with low magnetic moments), such as ^{13}C and ^{15}N, where the situation is aggravated by a low natural abundance and long relaxation times. The use of high magnetic fields, B_o and fast data accumulation has helped alleviate the sensitivity problem for protons and other nuclei with relatively large magnetic moments, such as ^{19}F, ^{203}Tl, ^{205}Tl, and ^{31}P. Although the use of double resonance techniques (e.g. Nuclear Overhauser Effect, NOE, INEPT and DEPT) result in improvement in ^{13}C NMR sensitivity, amplification factors of an order of magnitude at most have been achieved. For the polarization transfer methods (DEPT and INEPT), the gain in the signal intensity is a result of polarization transfer (under appropriate conditions) from one nucleus to another (e.g. from an abundant, usually ^{1}H to a rare nuclear spin, ^{13}C

or ^{15}N). The magnitude of the obtained enhancement is proportional to the ratio of the magnetogyric ratios (γ_i) of the nuclei of interest. For example, for the ^1H - ^{13}C case the enhancement factor is given by the ratio $(\gamma_{1H}/\gamma_{13C})$[1]. The interaction which gives rise to the NOE is the dipolar coupling between the two nuclei, where the enhancement is proportional to the sum $(1+\gamma_S/2\gamma_I)$, (S = ^1H and I = ^{13}C or ^{15}N).[2]

A particularly attractive double resonance technique in terms of potential NMR enhancements is the Dynamic Nuclear Polarization (DNP) or nuclear-electron Overhauser effect. The DNP enhancement is induced by two simultaneous processes: saturation of the electron spin transitions and nuclear-electron relaxation[3]. In the double resonance techniques mentioned above, the DNP enhancements (A) are ultimately proportional to the electron to nuclear gyromagnetic ratio ($A \sim \gamma_e/\gamma_n$) which is very large. For example a factor of 660 and 2640 for the ^1H and ^{13}C nuclei, respectively, can be predicted. Equally important, the magnitude and the sign of the enhancement is crucially dependent on the spatial and time dependence of the electron-nuclear interaction (also denoted by electron-nuclear coupling).

Thus the DNP technique has evolved as a powerful technique not only for a dramatic improvement of NMR

sensitivity but also for the study of intermolecular interactions in solutions and at solid-liquid interfaces. For example, DNP studies in liquids have been used to study molecular motion, mean distances for species in solutions, and weak radical/solvent (or solute) complex formation. For an extensive review of the subject, there exists a number of excellent review papers of static DNP studies in liquids[4-6] and solids[7].

1.2 Static and Flow DNP

As stated earlier, DNP is a double magnetic resonance technique which can be described as an increase of a nuclear magnetic resonance (NMR) signal when the electron spin resonance (EPR) transitions are saturated. The drastic change in the intensities of the observed NMR signal is induced by cross-relaxation processes due to time-dependent interactions of the coupled electron-nuclear spin system. The magnitude of the enhancement depends on how effective these interactions are and on the degree of saturation of the EPR transitions.

The DNP experiment can be performed in two ways: under static conditions or by a flow approach.

In most previous DNP studies both static liquid[4-6] or solid[7] samples in the presence of free radicals have been used. In the static DNP approach, the samples were usually placed in a relatively low external magnetic field (0.005 - 1.4 T) where a microwave oscillating magnetic field, B_{1e}, was applied to irradiate (saturate) the EPR transitions at or near the electron Larmor frequency, ω_e. The strength of the microwave magnetic field (B_{1e}) at the sample determines the efficiency of saturation at a given output microwave power, (P). The magnitude of B_{1e} varies as square of the applied power ($B_{1e} \propto P^2$), and the saturation can always be achieved at the expence of higher applied power. Since the NMR coil (placed within the microwave cavity) shields the microwave field, an increased power is needed for saturation which in turn results in sample heatings. More importantly, in the static configuration, the NMR detection is not optimized and the NMR resolution is limited by the low external magnetic field used. Although large enhancements have been reported utilizing the low field static DNP method[4-7], the lack of resolution and the poor NMR sensitivity have limited this approach to nuclei with high NMR sensitivity (^1H, ^{19}F, ^{31}P) in small molecules with one resonance line[4-7].

Several years ago, different research groups[5,7,] suggested the possibility of overcoming the difficulties of

the low field static DNP by spatial separation of the EPR region (where the dynamic polarization is generated) and the NMR detection region, but the idea had not been implemented.

Recently, a flow DNP method has been developed, in our laboratory, which utilizes a flowing liquid to detect the DNP enhancement in a region spatially separated from the region of polarization build up. In general, there are two ways for the polarization transfer utilizing the flow DNP experiment. In one case, liquid/liquid intermolecular transfer (LLIT) DNP, the radical (usually a stable nitroxide free radical) is dissolved in the flowing liquid (benzene, chloroform etc.) and is thus present in both the polarization (EPR) and detection (NMR) regions of the experiment. An alternative method is the solid/liquid intermolecular transfer (SLIT) DNP when the radical is immobilized on a silica gel surface and placed in the microwave cavity.

Initially, the polarization part (the microwave cavity) and the detection part (the NMR coil) of the flow experiment were placed in one and the same magnetic field (0.33 T) [8,9]. Recent studies have reported the succesful transfer of a polarized bolus from a low to high magnetic field[10].

The low field flow DNP approach provides several

advantages over the static one[8]. First, with the removal of the NMR coil from the microwave cavity (e.g. no shielding effects) better saturation factors, s (s=0.8), were obtained compared to the static value (s=0.2) for significantly lower applied microwave power. Furthermore, the flow DNP experiment alleviates deleterious sample heating effects by efficient flow removal of a given bolus from the microwave electric field thus allowing an independent optimization of both EPR and NMR regions. As a result better NMR detector sensitivity can be achieved. However, the low magnetic field (0.34 T) flow DNP experiment still suffered the disadvantage of having very limited chemical shift resolution.

With the recent development of the low (0.34 T) to high (4.7 T) magnetic field transfer DNP experiment[10,11] the severe limitation of the low field experiments to simple molecules with a single resonance line has been largely overcome. The transfer DNP experiment provides an order of magnitude improvement in the NMR detector sensitivity and improved chemical shift resolution.

Thus, the development of the transfer approach has extended the application of the DNP method for the study of selective enhancements of different nuclei in one and the same molecule. In addition, the improved sensitivity and resolution

allows DNP studies of magnetic nuclei with low sensitivity and low natural abundance such as ^{13}C, ^{15}N, and ^{29}Si as well as studies of weak intermolecular interactions such as hydrogen bond formation.

The ^{1}H and ^{13}C low to high field SLIT DNP studies comprise the majority of this thesis. The SLIT DNP experiment is particularly attractive because in addition to the high sensitivity and improved spectral resolution it provides high efficiency in the low to high magnetic field transfer experiment. Also, the absence of the radical in the flowing bolus stream (after polarization transfer) avoids a potential problem of paramagnetic line broadening of the NMR signals.

The theory of the flow DNP experiment and a review of previous studies utilizing different developments of this approach will be discussed in detail in Chapter 3. However, some important low to high magnetic field transfer DNP results which are relevant to the subject of this thesis are discussed in this chapter. In particular preliminary results demonstrated:

i). Large flow ^{1}H SLIT DNP enhancements[12]. The reported ^{1}H SLIT DNP enhancements exceed the Boltzmann thermal magnetization at 4.7 T by factors of 2-4 for flowing liquids

(benzene and chloroform).

ii). Selective ^{1}H and ^{13}C LLIT DNP enhancements for 1-chlorobutane with the nitroxide spin label TEMPO[11]. This result demonstrated that at low radical concentrations only a scalar dominated ^{13}C DNP was observed for the C-1 carbon. Much higher radical concentrations were necessary to observe the dipolar enhancements for the remaining carbons (C-2, C-3, and C4). This result is consistent with three-spin effects which tend to cancel the observed polarization at low radical concentrations for dipolar dominated enhancements. The latter observation is of particular importance for the case of SLIT DNP studies due to the relatively low achievable unpaired spin density presumably achievable on silica gel surfaces.

iii). Selective SLIT ^{1}H DNP enhancements for taxol (an anticancer drug) in contact with the nitroxide radical immobilized on silica gel[13]. These results indicate selective proton enhancements for protons on two different acetate groups, even though these acetate groups have similar spin-lattice relaxation times (e.g. 0.5 and 0.58 sec. respectively).

iv). Large flow DNP enhancements for low γ nuclei. For example, the LLIT ^{15}N DNP and ^{29}Si DNP are the first liquid ^{15}N and ^{29}Si DNP results reported to date[14]. A large SLIT ^{13}C DNP enhancement 61 times the thermal Boltzmann magnetization at 4.7 T is the largest ^{13}C DNP value reported to date; however,

it was obtained for a favorable case of a scalar dominated DNP ($CDCL_3$/immobilized nitroxide spin system). The difficulties of observing dipolar dominated ^{13}C DNP were consistent with dominant three-spin effects and low leakage factors for these immobilized spin system.[10]

In summary, the preliminary DNP results obtained for 1-chlorobutane and taxol suggest selective DNP enhancements which depend on weak intermolecular interactions. On the other hand, the three-spin effects and poor leakage factors limit the application of the SLIT ^{13}C DNP experiment to studies of scalar dominated DNP enhancements.

1.3 Research Goal

With the recent flow DNP developments a lot of progress has been achieved in terms of instrumentation as well as chemical systems used for DNP studies. The focal point of this thesis was to extend further the application of the flow SLIT DNP experiment by developing new silica phase immobilized nitroxide (SPIN) radicals which will hopefully solve the problems encountered with the immobilized spin labels used in previous studies. In particular, the goal of this study was to provide SPIN radicals with high surface spin concentration

wich will suppress the three-spin effect and thus extent the application of the ^{13}C SLIT DNP for dipolar dominated mechanisms.

Equally important was the goal to synthesize chiral SPIN systems (by analogy of the chiral stationary phases used for gas chromatography, GC, and liquid chromatography, LC) which will provide chiral environment appropriate for monitoring of enantioselective ^{13}C SLIT DNP enhancements of enantiomeric pairs (R- and S-stereoisomers).

During the last several years, there has been a rapid development of chromatographic methods for separation of enantiomers. Studies of a number of new chiral stationary phases for GC and LC have shown that a necessary condition for chiral recognition leading to enantioseparation is either the presence of a bonding interaction between the enantiomers and the stationary phase, or differences in the distance the conponents under separation have to travel through the column, i.e. steric exclusion chromatography.[15] The bonding interaction may arise from hydrogen bonding, ionic or dipolar interactions. In early studies of chiral GC stationary phases, a minimum of three simultaneously operating interactions (the three-points interaction model) between enantiomer and stationary phase were found necessary for a chiral

discrimination[16]. This minimum number of contact points, however, does not necessary mean points of attachment. Situations where only steric interactions cause a molecular steric discrimination were possible.[15] It should be noted that although the three-point interaction model has been widely used to construct chiral recognition models there has not been sufficient experimental support for its validity. There are examples of resolution of very simple hydroxy or carbonyl compounds having only one hydrogen bonding site[17,18].

Research today on chiral stationary phases for GC is concentrated primarily around polysiloxane-bonded chiral phases. If all hydrogen-bonding GC phases, polysiloxane-linked L-valine tert-butyl-amide ("Chirasil-val") is by far the most fully investigated. In this case multiple hydrogen bonding interactions are assumed to operate[19]. Another type of chiral stationary phases for capillary GC is based on chiral metal complexes. A chiral β-dicarbonyl ligand of the same type as used in NMR shift reagents[20] complexed to a transition metal by two oxygen functions, constitutes the enantioselective component. In addition, chiral phases based on inclusion effects (the ability of certain compounds to use their particular structure to include suitable guest molecule) have been utilized for GC enantioseparations.[15]

The stationary phases used in chiral LC can be based on metal complexes - the method is based on the ability of transition metals to participate in complex formation. For example, in a study by Davankov[21], L-proline was immobilized on a chloromethylated styrene-divinylbenzene copolymer. Because diastereomeric complexes are formed from amino-acid ligands of opposite configuration, any difference in the stability of these complexes will result in different chromatographic mobilities of the amino-acid enantiomers. Another type of chiral stationary phases for LC is based on charge transfer complexation. This particular interaction requires π-electron system (aromatic systems, nitroaromatics, etc.) and the π-π interaction is the source of retention. Also, phases based on hydrogen-bonding (specifically, two-point diastereomeric hydrogen-bonding[22]) solute-sorbent association have been extensively used in liquid chiral separation.

In this thesis, the hypothesis to be explored is enantioselective DNP enhancements based on a possible transient hydrogen-bond complex formation between chiral nitroxide group of the SPIN radicals and R-/S- enantiomeric pairs.

1.4 EPR Line-broadening

One of the major requirements in the present study is a relatively high unpaired electron spin density on the silica gel surface. Since an increase of the surface radical concentration results in an increase in the EPR linewidth which in turn affects the magnitude of the DNP enhancements it is important to discuss here the different mechanisms responsible for the EPR line-broadening.

The nitroxide free radicals are characterized by a sharp three-line EPR spectrum due to the ^{14}N hyperfine interaction only at very low radical concentrations in solutions. As the radical concentration increases the lines of the triplet move together and broaden. When the spin concentration becomes large enough, the triplet collapses to a single broad line. In general there are three mechanisms responsible for the EPR line broadening: anisotropic electron-nuclear hyperfine interaction, electron-electron exchange and electron-electron dipole-dipole interaction.

1. Anisotropic Hyperfine Interaction:

The dependence of the linewidth, $(1/T_2)$ upon the nuclear quantum number, m_I, specifying the transitions can be described by the equation[33]:

$$(T_2)^{-1} = X + Ym_I + Zm_I^2 \qquad 1.1$$

where the terms Y and Z defined the anisotropies in the (g) factor and in the hyperfine coupling (A), respectively, and can be defined by the equations below[33]:

$$Y = \frac{4}{15} b(\Delta\gamma) B_o \tau_c \qquad 1.2$$

$$Z = \frac{1}{8} b^2 \tau_c \qquad 1.3$$

where $b = (4\pi/3)[A_{zz} - (1/2)(A_{xx}+A_{yy})]$ with corresponding components of the hyperfine coupling along the x,y and z axis denoted by A_{xx}, A_{yy} and A_{zz}; $\Delta\gamma = \beta_e \hbar^{-1}[g_{zz} - (1/2)(g_{xx}+g_{yy})]$, where g_{zz}, g_{xx} and g_{zz} are the anisotropic components of the g factor; and τ_c is the molecular correlation time which is a measure of the length of time over which the molecules persist in a given orientation. If τ_c is sufficiently fast, the anisotropies in the g factor and the coupling factor, A, are efficiently averaged out and no linewidth effects are observable. However, in the case of slow motion the line shape reflects directly the random frequency distribution which results in asymmetric, broad EPR lines.

The term X in eq. 1.1 includes contributions to the line broadening resulting from mechanisms that are not dependent on anisotropy. These broadening effects arise, for example, from the presence of oxygen in the solution or from instrumental

factors. The Y and Z terms can be determined experimentally from the peak to peak line widths for the three lines in the EPR spectrum of a given nitroxide radical if an isotropic motion is assumed.

2. Electron-Electron Exchange Interaction

The exchange interaction is due to an overlap of unpaired electron orbitals which occur at the moment of collision. At low rates of collision (that is, large overlap) the EPR spectrum will reflect electron-nuclear interactions and a well resolved triplet for the nitroxide radical will be observed. The greater the frequency of collision the greater will be the contribution of the electron exchange to the EPR line width. At high rates of collision (at high radical concentration) a single resonance line will appear - this is the so called exchange narrowing limit.

3. Electron -Electron Dipolar Interaction

The electron-electron dipole-dipole interaction depends on the relative orientation and mutual separation of the two electron spins. At short molecular correlation times τ_c (fast motion) both spins reorient rapidly in the applied magnetic field and this interaction is averaged to zero regardless of the concentration. If they reorient at an intermediate rate relative to the frequency corresponding to the energy

difference between the electron-electron energy states, line broadening will be observed. The electron-electron dipole-dipole interaction is observed usually in solids while predominant exchange interaction occurs in solutions.

Concentration effects on the EPR line shape of a SPIN radical are demonstrated in Fig. 1.1 the observed asymmetry and the increase in the EPR line width can be attributed to the presence of an anisotropic motion (due to restricted mobility) as well as perhaps electron-exchange interaction for this immobilized nitroxide radical.

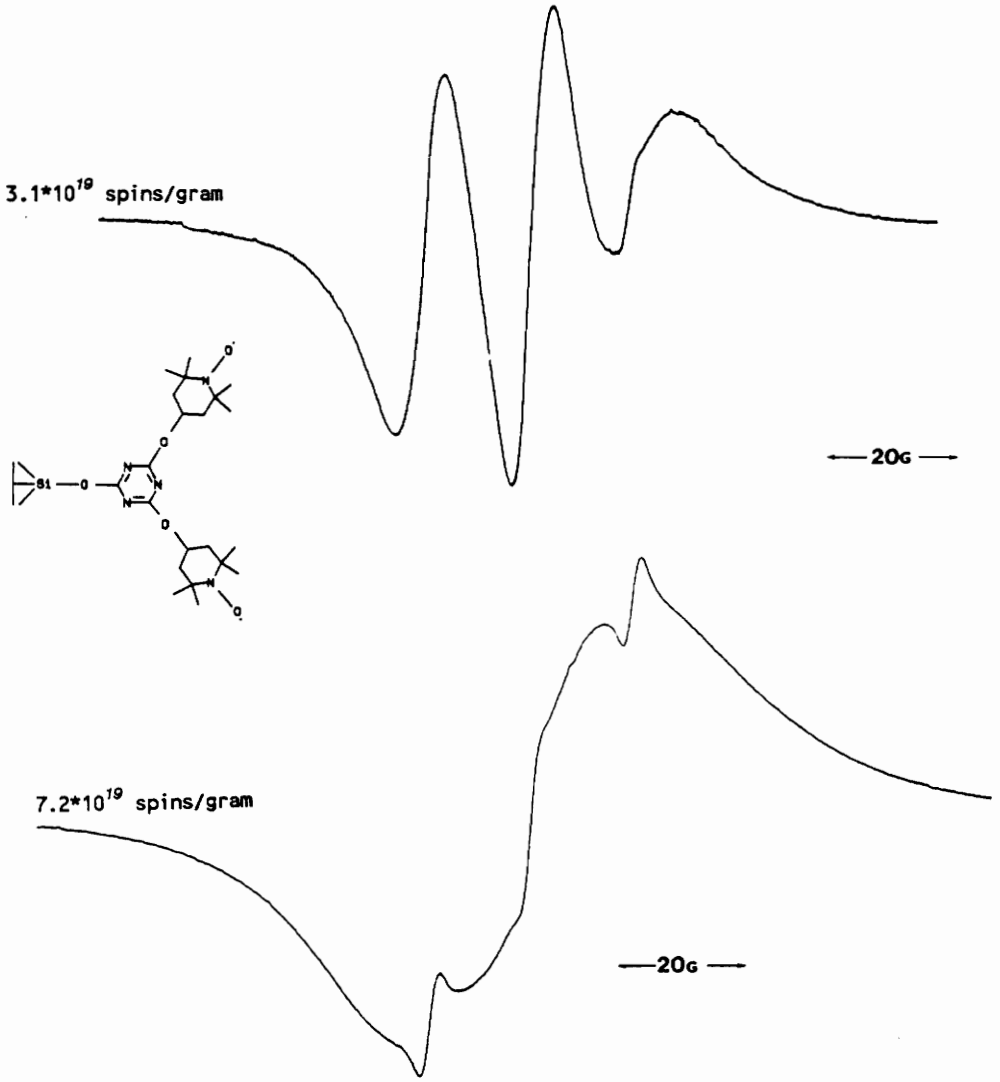

Fig. 1.1 Concentration effects on EPR spectra of an immobilized nitroxide radical[9].

CHAPTER 2

THEORY OF DNP

2.1 General

In general the Hamiltonian of two interacting spins in an external magnetic field B_o is given by[6]:

$$\hat{H} = \gamma_S \hbar (\hat{S} . B_o) + \gamma_I \hbar (\hat{I} . B_o) + \hat{H}_{SS} + \hat{H}_{SI} + \hat{H}_{II} \qquad 2.1$$

where, S and I are the electron and nuclear spin angular momentum operators and γ_S and γ_I denote the gyromagnetic ratios of the electrons and nuclei, respectively. H_{SS}, H_{SI}, and H_{II} represent the spin-spin interactions between the electrons, between the electrons and the nuclei and between the nuclei, respectively. For the DNP the most important term in eq. (2.1) is the interaction term H_{SI}. Depending on the nature and the time dependence of the nuclear-electron coupling, H_{SI} several different DNP mechanisms can be encountered[7]:

i). Overhauser Effect: This mechanism occurs in liquids and solids containing mobile electrons. The nuclear-electron interaction is time-dependent, ($H_{SI} = H_{SI}(t)$) on a scale comparable to the electron larmor frequency, ω_e. In this case, the maximum enhancement of the nuclear polarization is obtained when the EPR transition is irradiated at a frequency

$\omega = \omega_e$.

ii). In addition to the Overhauser effect, two other mechanisms are important in solid samples which contain fixed paramagnetic centers. One is a solid state effect, a time-independent nuclear-electron interaction which achieves a maximum enhancement for $\omega = (\omega_e \pm \omega_n)$, where ω_n is the nuclear larmor frequency. Also, a direct and indirect thermal mixing effect can occur when there is a large number of fixed paramagnetic centers, so that the nuclear larmor frequency, ω_n, becomes comparable to the EPR linewidth, $\omega_{1/2}$. In this case a maximum enhancement occurs at $\omega=(\omega_e \pm \omega_{1/2})$

2.2 DNP in Liquids

The physical reason for the DNP enhancement can be explained in terms of simultaneous action of the applied oscillating magnetic field B_{1e} and nuclear spin relaxation processes induced by relaxation of electron spins. Let us consider weakly coupled electron, S, and nuclear, I, spins in an external magnetic field, B_o (Fig. 2.1). The transition probabilities between the energy levels of the two spin system are represented by W_1^S (which arises from the interaction $H_S(t)$), W_1^I (from the interaction $H_I(t)$), and W_o, W_2, (from the interaction $H_{SI}(t)$, eq. 2.1). The unperturbed eigenstates $|M,m\rangle$

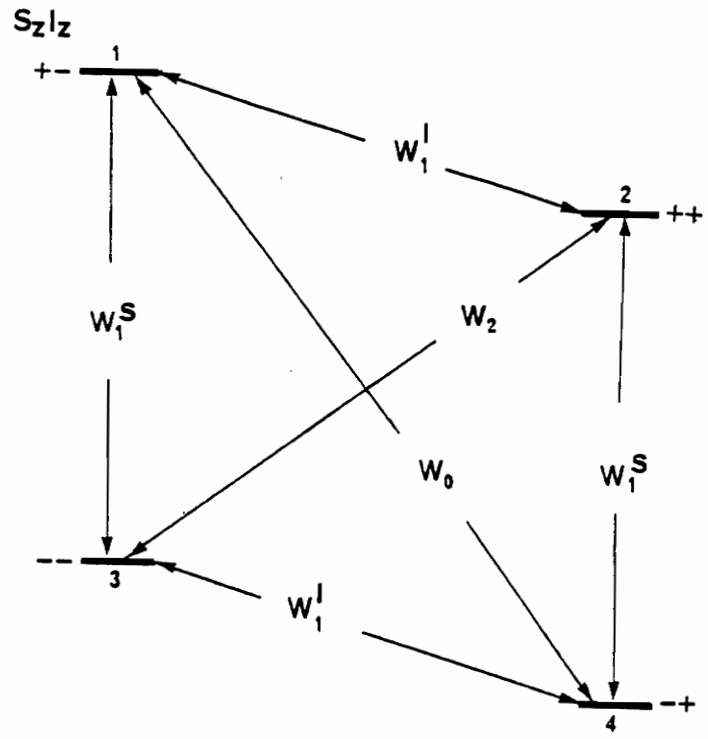

Fig. 2.1: The energy level diagram for the electron-nuclear spin system (I=1/2, S=1/2) and transition probabilities.

of H_o are denoted by a sign (+) or (-). The first sign represents the orientation in the magnetic field of the electron spin,S, and the second that of the nuclear spin,I.

If an oscillating field, B_{1e} is turned on, the net effect will be spin flips up ($\Delta M = \pm 1$, $\Delta m = 0$) so that the number of electron spins in each energy level tend to equalize. If the electron resonance is completely saturated the net rate of electron spin flips in one direction due to B_{1e} will be balanced by a similar rate in the opposite direction due to relaxation interaction. Although all paths, W_1, W_2, and W_o (Fig.2.1) are allowed for relaxation only W_o and W_2 will change the nuclear polarization because these relaxation transitions result in simultaneous flips of both nuclear and electron spins (e.g. ++ → --; or +- → -+, and -+ → +-). In other words, the flip of a nuclear spin, I, is induced by a flipping electron spin, S. Following saturation, the spin system tries to reestablish the thermal equilibrium, and the electron spins will flip predominantly to the lower energy level. Under the assumption that a flipping spin S always flips one spin I in the opposite direction, the nuclear flips will be mostly to the higher energy level. The transitions that flip nuclear spins in the reverse direction are forbidden, because the final states are already occupied.

Therefore the polarization action (the deviation from the equilibrium population of the nuclear spin system) takes place because nuclear spins are diverted in excess in one direction by relaxation processes.

Thus the intensity of the NMR signal $\langle I_z \rangle$ becomes proportional to[4]:

$$p \equiv \frac{\langle I_z \rangle}{I} = \tanh \frac{h\nu_e}{2kT} \qquad 2.2$$

which is enhanced by $\nu_e/\nu_n \approx 10^3$ over the thermal equilibrium polarization $p_o = h\nu_n/2kT$. In the above equation, p denotes the nuclear dynamic polarization; I is the intensity of the NMR signal at thermal equilibrium; ν_e and ν_n are the electron and nuclear Larmor frequencies respectively; and k is the Boltzmann factor.

2.3 Mechanism of the Radical Induced Nuclear Relaxation

In general, a relaxation process occurs when there exists a magnetic interaction fluctuating at the resonance frequency (e.g. $\omega = \omega_e \pm \omega_n$), for the cross-relaxation transitions W_o and W_2. In the case of DNP, the magnetic interaction is the interaction between local magnetic fields generated by the electron and nuclear magnetic moments. In

solutions, the fluctuations in the above magnetic interaction are usually induced by random molecular motion. Also, the molecular motion ensures that any nucleus is in continuous interaction with the unpaired electron and all nuclei are equally affected. The above model was suggested by Müller-Warmuth[6] and is known as the "two-spin" or electron-nuclear spin pairwise interaction. The random molecular motion is characterized by a molecular correlation time, τ_c, which sets the time scale for the random motion. As the mutual relaxation transitions W_o and W_2 demand an exchange of energy quanta ($\hbar(\omega_e \pm \omega_n) \approx \hbar\omega_e$) with the lattice, these transitions are effective only when the molecular motion has a frequency component comparable to ω_e. The frequencies of the magnetic interactions (and therefore) DNP are related to the frequencies of the molecular motion and have been utilized for a number of DNP studies[4-6] - which give information about molecular correlation times, distances between species in solution, weak complexations, etc.

The transition relaxation probabilities W_o and W_2 (Fig.2.1) can be expressed by the equation:[23]

$$W = (\overline{b_{loc}})^2 J(\omega_e) \qquad 2.3$$

where b_{loc} is the root mean square average amplitude of the fluctuating field, and $J(\omega_e)$ is the spectral density function.

$J(\omega_e)$ gives the intensities or probabilities of the molecular motion at frequencies $(\omega_e \pm \omega_n) \approx (\omega_e)$ that is, the intensities of the fluctuations of the local magnetic fields at these frequencies. Since the magnetic moment of the electron spin, μ_e, is on the order of 10^3 times greater than those of the nuclei, the intensities of the local magnetic fields generated by the paramagnetic electrons are correspondingly greater, which makes the electron-nuclear interaction a predominant mechanism for nuclear relaxation.

However, the electron spin system has in addition to the electron-nuclear interaction other powerful relaxation mechanisms such as dipolar magnetic interaction between themselves, exchange interaction, and spin-orbit interaction.[4] These electron interactions do not effect the DNP enhancement directly and will be discussed only in so far as their time constants are relevant for nuclear relaxations.

2.4 Electron-Nuclear Interactions

The term, $\hat{H}_{SI} = \hat{H}_{SI}(t)$, (eq. 2.1) represents the time-dependent electron-nuclear interaction that gives rise to the electron spin induced nuclear relaxation and the DNP enhancement. In principle, the time dependence can be caused by fluctuations in the amplitude of $\hat{H}_{SI}$, arising from motional effects or from the time dependence of the orientation of the electron spin, S, because of relaxation effects (also called Overhauser effects of the first and second kind, respectively[6]). The second kind of relaxation mechanism arises from a rapid flipping of the electron spin, S, and is effective for radicals with much shorter spin-lattice relaxation times relative to ω_e. For example such a relaxation mechanism was observed when Mn^{++} was used for ^1H DNP studies of water molecules[24]. Short relaxation times (on the order of 10^{-9} sec.) are usually characteristic of transition metal ions. However, the relaxation times of the nitroxide free radicals used in present DNP experiments (about 10^{-6} sec.) are much longer than ω_e^{-1} ($\approx 5.8*10^{-10}$ sec. in our case) so that only Overhauser effects of the first kind will be expected.

The time-dependent electron-nuclear interaction, $\hat{H}_{SI}$, is composed of dipolar and scalar terms[5]:

$$\hat{H}_{SI} = \hat{H}^{D}_{SI} + \hat{H}^{Sc}_{SI} \qquad 2.4$$

The nature and the time dependence of both dipolar and scalar interaction are considered in detail in the next two sections.

2.4.1 Dipolar Electron-Nuclear Interaction

The $\hat{H}_{SI}{}^{D}$ term (Eq. 2.4) represents the dipolar interaction of the nuclei with electrons located in non-spherically symmetric orbitals and can be described by the classical Hamiltonian for two interacting dipoles[5]:

$$\hat{H}_{SI} = \gamma_S \gamma_I \hbar^2 \left[\frac{3(\hat{S}.r)(\hat{I}.r)}{r^5} - \frac{(\hat{S}.\hat{I})}{r^3} \right] \qquad 2.5$$

The dipolar term can be expressed in polar coordinates and written in components.[23] One finds that it is proportional to $(3\cos^2\theta - 1)/r^3$, where $r = |\mathbf{r}|$ is the distance between the two spins and θ is the angle between $\mathbf{r}$ and the static field B_o. Since the angle θ varies rapidly due to the random molecular motion in low viscosity liquids, the dipolar part of the interaction is averaged to zero and does not contribute to the time-independent interactions of the system: that is, it does not affect the energy levels. However, it does provide a time-

dependent interaction (that is, relaxation and DNP). The time dependence can be described in terms of different models for molecular motion, each of which is characterized by a corresponding molecular correlation time, τ_c

The modulation mechanisms for dipolar interactions are summarized below:

i). Relative translational diffusion. In this case the electron and nuclear spins are in the center of different molecules and the time dependence arises from fluctuations in the interspin distance **r**. The molecular motion is characterized by a translational correlation time, τ_t.

ii). Rotational diffusion. The S and I spins are in the same molecule. The model is effective for nuclei within a free radical molecule, or also for tight bond complexes. (The S spin is assumed to be localized). The time dependence is due to fluctuations in the angle θ (reorientational or rotational correlation time, τ_r is the characteristic correlation time).

iii). Mixed translational and rotational diffusion . This modulation mechanism can be explained by assuming a weak complex formation (for instance hydrogen bonding) between the

solvent molecules and the free radical. When the molecules which bear the S and I spins are stuck together, the dipolar coupling is only modulated by fluctuations in the polar angles. When the molecules are apart the dipolar coupling is again modulated by translational diffusion.

2.4.2 Scalar Electron - Nuclear Interaction

The Hamiltonian for the scalar interaction (usually referred to as the Fermi contact term) is given by[6]:

$$\hat{H}_{SI}^{Sc}(t) = \gamma_S \gamma_I \hbar^2 \left(\frac{8\pi}{3}\right) |\psi(0)|^2 (\hat{S}.\hat{I}) \qquad 2.6$$

where $\Psi(0)$ represents the wave function of the unpaired electron, S, at the nucleus, I. Thus $\hat{H}_{SI}^{Sc}$ is due to a finite electron spin density at the site of the nucleus and occurs when the unpaired electrons are transferred to s-type orbitals. There are two possible mechanisms which can describe this interaction[5]. In one case, the radical approaches a molecule and a transient bond is formed whereby some electron spin density is transferred from the radical to the molecule. If the unpaired electron density is transferred to an s-orbital, the s-orbital has a nonvanishing value at the nucleus and there will be finite electron density at the nucleus. Thus, scalar coupling can occur. Another possible mechanism is

provided by the overlap of the charge clouds for the filled orbitals of the molecule. Because of the Pauli exclusion principle, there will be a contraction of atomic orbitals containing electrons parallel to the unpaired spin of the radical (no overlap)) and corresponding expansion of the atomic orbital containing the antiparallel spin. The latter case will lead to a slight unpairing of the electrons in the vicinity of the nucleus and in the case of s-orbitals a finite spin density will occur at the nucleus in question. It should be emphasized that when electrons are located in p-orbitals, this does not necessarily mean that $\hat{H}_{SI}^{Sc} = 0$. Exchange forces between these electrons and the bonding s-type electrons can polarize the bonding electrons leading to non-zero electron-spin density at the nuclear site.

Thus the unpaired electron spin density is transmitted from the free radical to the nucleus by a similar mechanism to that giving rise to the nuclear hyperfine structure in a regular EPR spectrum. However, for the case of EPR experiment the scalar coupling is effectively time-independent and produces the isotropic component of the hyperfine sructure (splitting of the electron energy levels). This is due to the relatively long nuclear relaxation times, (T_{1n} and $T_{2n} > 1/A$; A is the hyperfine electron-nuclear coupling constant) and nuclear exchange time, τ_n ($\tau_n > 1/A$, τ_n is the time for the

electron-nuclear interaction).

In the DNP experiment, the unpaired electron and the nucleus are usually in different molecules. The rapid molecular motion ensures that the scalar interaction (which occurs only when the unpaired electron and the nucleus are close to one another) will vary rapidly. Formally, this means a time-dependence of the coupling constant. On the time scale of the NMR experiment (that is, very short electron spin relaxation and exchange times, T_{1e}, T_{2e}, $\tau_e \ll 1/A$, τ_e is the time for the electron-nuclear interaction and equals 10^{-10} to 10^{-11} sec), the energy part of the scalar coupling is averaged to zero. However, the unpaired electron density produced at the nucleus can induce a shift in the NMR frequency (NMR contact shift) given by:[25]

$$\Delta\delta = -A\frac{|\gamma_S|}{\gamma_I}\frac{1}{4kT} \qquad 2.7$$

where A_{SI} is the electron-nuclear hyperfine coupling constant, k is the Boltzmann factor, and T is the absolute temperature. Since larger paramagnetic electron spin density at a given nucleus produces larger chemical shifts, the NMR contact shift provides a direct measure of the scalar interaction.

The hyperfine electron-nuclear interaction term, $\hat{H}_{SI}^{Sc}$ is

frequently written briefly as[4]:

$$\hat{H}_{SI}^{Sc}(t) = hA\hat{S}.\hat{I} \qquad 2.8$$

where A is the hyperfine coupling constant.

The time-dependence of the above interaction may arise either from the time-dependence of A, or from the time-dependence of the orientation of the electron spin, S. Since relaxation mechanisms of the first kind are relevant to this study (see Ch.2.4), the possible models for the time dependence of the scalar interaction due to modulations of the coupling constant, A are summarized below:[26]

i). The Sticking Model : in this case there is a finite scalar interaction only during the time when the spin S and the spin I are "stuck" together, for example, as a result of weak complex formation between a solvent molecule and a free radical. During that time the scalar interaction is characterized by a coupling constant, (A), and is zero at all other conditions. The time-dependence of A arises because the time of sticking is a random variable.

ii). The Diffusion Model[26]: the scalar interaction is assumed here to be a function of the distance between I and S spins. As in the dipolar case, the variation of the **r** with time is responsible for the time dependence of the

interaction. Thus, unlike the sticking model, the unpaired electron density produced at the nucleus is not at one instant finite and then zero (e.g. switched on and then off) but it approaches maximum value as the radical and solvent molecules collide and then decays to zero again as the molecules move away from each other. Since the scalar interaction can only arise from an electron-orbital overlap with the nucleus, the interaction is assumed to be of a very short range interaction and highly dependent on the internuclear distance. It is therefore postulated that the overlap varies exponentially with the internuclear distance.

iii). The Pulse Model[27]: in the pulse model (as in the diffusion model) it is assumed that the time between the radical-solvent collisions during which the scalar interaction can occur is a random variable. The rate of change of this scalar interaction will depend on the geometry of the interaction between I and S spins. For example, different radicals (S) may approach different I spins with preferred orientations, with the result that the electron orbital overlap with the nucleus may be described by a different function in each case (Fig. 2.2).

The difference between this model and the diffusion model is that the latter explicitly assumes a definite function for

the scalar coupling which is invariant in all systems. More specifically, the diffusion model is just one special case of the pulse mode. When both dipolar and scalar interactions are present, it is necessary to combine a model for the dipolar interaction with one model for the scalar interaction.

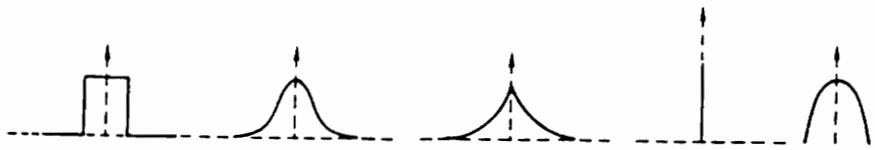

Fig. 2.2 Types of pulses to describe scalar interaction. (From Noack et al.[18]).

Because of the strong time dependence of the DNP enhancement on a particular electron-nuclear interaction, a number of low field DNP studies have been used as a sensitive method for distinguishing between scalar and dipolar parts of the electron-nuclear relaxation[6]. The low field measurements are appropriate because in this case the nuclear relaxation (e.g. DNP) is independent of ω_e and ω_n, and hence the external magnetic field, B_o. Thus the observed enhancements will provide information about the geometry of the colliding molecules and on the characteristics of the molecular motion when dipolar interactions are predominant. For the case of scalar interactions, the DNP will mirror the chemical environment of both the receptor nucleus and the unpaired

electron.

A general procedure for extracting the scalar and dipolar components involves experimentally measured enhancements at several different frequencies. The experimental data are then fitted to models such as those discussed above, thereby allowing the ratio of dipolar and scalar coupling to be estimated.

In principle, by combining measurement of the relaxation times and DNP enhancements, it is possible to determine values for molecular correlation times τ_c, radical-solvent distances of closest approach, energy of activation ΔE, and average diffusion constants, D.

2.5 Static DNP - Equations

In liquid DNP experiments, the polarization, A, for the time-dependent electron-nuclear interaction is usually expressed as a deviation from the static polarization:[4-6]

$$A \equiv \frac{\langle I_z \rangle - I_o}{I_o} \qquad 2.9$$

where $\langle I_z \rangle$ is the expectation value of the nuclear magnetization and I_o is the same value in thermal equilibrium. $\langle I_z \rangle$ and $\langle S_z \rangle$ (the expectation value for the electron polarization) are not independent of each other, but are coupled because of the time-dependence of the electron-nuclear interaction, $\hat{H}_{SI} = \hat{H}_{SI}(t)$. Thus the rate of change of $\langle I_z \rangle$ and $\langle S_z \rangle$ (which are experimentally observable quantities) is expressed by the coupled differential equations[28]:

$$\frac{d\langle I_z \rangle}{dt} = -(W_o+2W_1+W_2)(\langle I_z \rangle - I_o) - (W_2-W_o)(\langle S_z \rangle - S_o) \qquad 2.10$$

$$\frac{d\langle S_z \rangle}{dt} = -(W_2-W_o)(\langle I_z \rangle - I_o) - (W_o+2W_1^S+W_2)(\langle S_z \rangle - S_o) \qquad 2.11$$

Equations 2.10 and 2.11 describe properly the relaxation of the nuclear spins I, but they are negligible for the relaxation of the electron spins S since these possess, as previously mentioned in Ch.1, other stronger relaxation mechanisms.

For the nuclear spins, I, the total relaxation rate, ($W_t = 1/T_1$) can be expressed as:

$$W_t = W_o+2W_1+W_2+W^o \qquad 2.12$$

where the term W° represents those relaxation processes not involving the electron spins, S and therefore not included in Fig. 2.1.

In the double resonance experiment, the NMR signal, which is proportional to I_z, is observed under steady-state conditions, e.g.:

$$\frac{d\langle I_z\rangle}{dt} = 0 = -(W_o+2W_1+W_2+W^{\circ})(\langle I_z\rangle - I_o) - (W_2-W_o)(\langle S_z\rangle - S_o) \qquad 2.13$$

or from equations 2.12 and 2.13 we obtain:

$$\langle I_z\rangle = I_o + \frac{W_2-W_o}{W_t}(S_o - \langle S_z\rangle) \qquad 2.14$$

multiplying numerator and denominator by $S_o(W_o + 2W_1 + W_2)$ gives:

$$\langle I_z\rangle = I_o\left(1+\frac{W_2-W_o}{W_o+2W_1+W_2}\right)\left(\frac{W_o+2W_1+W_2}{W_t}\right)\left(\frac{S_o-\langle S_z\rangle}{S_o}\right)\left(\frac{S_o}{I_o}\right) \qquad 2.15$$

If the following parameters are introduced:

coupling factor, ξ: $\xi = (W_2 + W_o)/(W_o + 2W_1 + W_2)$

leakage factor, f: $f = (W_o + 2W_1 + W_2)/(W_o + 2W_1 + W_2)+W^{\circ}$

saturation factor, s: $s = (S_o - \langle S_z\rangle)/S_o$

and the ratio of the equilibrium magnetization $M_S^{\circ}/M_I^{\circ} = S_o/I_o$ is replaced by the identical quotient of the magnetogyric ratios γ_s/γ_I, the basic equation for the DNP enhancement, A is

given by:

$$A = \frac{\langle I_z \rangle - I_o}{I_o} = \xi f s \frac{|\gamma_s|}{\gamma_I} \qquad 2.16$$

It should be noted that both the dipolar and the scalar interactions contribute to the relaxation rate W_o ($W_o = W_o^D + W_o^{Sc}$), while the only contribution to the relaxation rate W_2 is the scalar interaction ($W_2 = W_2^{Sc}$).

Coupling Factor, ξ:

The coupling factor, ξ, dictates the type of electron-nuclear interaction and is defined by

$$\xi = \frac{(W_2^D - W_o^D - W_o^{Sc})}{(W_2^D + W_o^D + W_o^{Sc} + 2W_1^D)} \qquad 2.17$$

Eqn. 2.17 gives the contribution of the different transition probabilities to the nuclear relaxation rate. The superscripts D and Sc denote dipolar and scalar coupling, respectively. If we consider only dipolar interactions, ($W_o^{Sc} = 0$), it can be calculated[15] that: $W_o^D = 1/20 (d_{ij})^2 J(\omega_s, \tau_c)$, $W_2^D = 6/20 (d_{ij})^2 J(\omega_e, \tau_c)$, and $W_1^D \equiv W_n^e = 3/20 (d_{ij})^2 J(\omega_n, \tau_c)$ with $(d_{ij})^2 = \gamma_S \gamma_I \hbar^2 / r^3_{ij}$, where J is the spectral density function. In the extreme narrowing case, when ($\omega \tau_c << 1$), the ratios of the different dipolar

transition probabilities are $W_o^D:W_1^D:W_2^D = 2:3:12$ and $W_2^D - W_o^D = 1/2(W_2^D+W_o^D+2W_1^D)$. Thus, the coupling factor, ξ attains its maximum value of 0.5 in the case of pure scalar coupling, $(W_1^D = W_o^D = W_2^D = 0)$ and the coupling factor, ξ is equal to -1. The coupling factor can range from -1 to 0.5 and consequently the DNP enhancement is negative or positive. The coupling factor can be calculated using eqn. (2.16), if the leakage factor,(f) and saturation factor, (s) are known or can be determined separately.

Leakage Factor, f:

The leakage factor, f, measures the fraction of the total nuclear relaxation rate due to electron-nuclear interactions and in terms of transition probabilities is given by:

$$f = \frac{(W_o+2W_1+W_2)}{(W_o+2W_1+W_2)+W^o} \qquad 2.18$$

where, $(W_o + 2W_1 + W_2) \equiv \rho$ represents the part of the nuclear relaxation rate that arises from interactions with the electrons, while W^o represents contributions from other interactions and can be expressed also as $W^o = 1/T_{1no}$; T_{1no} is the nuclear relaxation time in the absence of electron spins.

Thus, equation (2.18) becomes:

$$f = \frac{\rho}{W_t} = \frac{\rho}{\rho + W^o} = 1 - \frac{W^o}{W_t} = 1 - \frac{T_{1n}}{T_{1no}} \qquad 2.19$$

where T_{1n} is the nuclear relaxation time in the presence of the radical. When f=0 the electron-nuclear interactions are negligible (e.g. $T_{1n} \approx T_{1no}$). In contrast, they are dominant when ($T_{1n} << T_{1no}$) f=1. It follows from eq. (2.19) that the leakage factor, (f), can be measured experimentally by measuring the nuclear spin relaxation times in the presence (T_{1n}) and in the absence (T_{1no}) of the radical. An alternative way is to measure the DNP enhancements (A) at different radical concentrations, C[4,29]. The relaxation rate of the nuclear spins in the presence of free radicals, ($1/T_{1n}$) can be express as: $1/T_{1n} = 1/T_{1no} + \Gamma C$, where Γ is a measure of the strength of the electron-nuclear interaction, and C is the free radical concentration. Then the leakage factor, f, can be expressed as:

$$f = \frac{\Gamma C T_{1no}}{1 + \Gamma C T_{1no}} \qquad 2.20$$

From equations 2.16 and 2.20 we get:

$$A^{-1} = (\xi s \frac{\gamma_s}{\gamma_I})^{-1} (1 + \frac{1}{\Gamma C T_{1no}}) \qquad 2.21$$

A plot of reciprocal polarization, A^{-1} as a function of reciprocal concentration, C^{-1} of the unpaired electron will extrapolate to $\{\xi s(\gamma_s/\gamma_I)\}^{-1}$, the inverse of which is the enhancement at infinite concentration, i.e. the enhancement for f=1. The second approach can be applied only for the case when the nuclei of interest are on different molecules from the paramagnetic radicals and is based on the fact that W^o is independent of the concentration, C, while W_o, W_1 and W_2 are proportional to the concentration.

Saturation Factor, s:

The saturation factor, s is a measure of the degree of saturation of the electron spin resonance transition (for complete saturation, s=1) and is defined by the equation:

$$s = \frac{S_o - \langle S_z \rangle}{S_o} \qquad 2.22$$

enhanced at high radical concentrations may even become positively enhanced at low radical concentrations if the three-spin effect outweighs the direct polarization mechanism[5].

The presence of the three-spin effect can be revealed by triple irradiation experiments, where both the electron and the proton spin transitions are strongly irradiated. This has the effect of removing the indirect pathway for the transfer of spin polarization from the electron to the carbon via the proton, leaving only the direct electron-carbon mechanism[4].

Under the conditions of triple resonance, the enhancement is given by[4]:

$$A-\xi_C^S f_C^S s \frac{\gamma_S}{\gamma_C}+\xi_C^H f_C^H s^H \frac{\gamma_H}{\gamma_c} \qquad 2.27$$

Since the proton spin system can be saturated more easily because of the longer relaxation times and the lower resonance frequency, ν_{1H}, the value of s^H can usually be equal to 1.

The second term in eq. (2.27) can be neglected because $\gamma_H << \gamma_S$. Thus, simultaneous saturation of the proton spin system is effectively equivalent to a reduction of the three-spin system to the simpler two-spin system.

2.7 The Three-Spin Effect in Solids

A solid-state analog of the three-spin effect in solutions was reported for a solid sample containing three kinds of spins (unpaired electrons, ^{13}C, and ^{1}H)[31]. The unpaired electrons were confined to islands of polyacetylene embedded in a matrix of polyethylene. Although the effect is very closely related to the three-spin effect in solutions, the spin polarization is transferred in a different way, via spin diffusion (see Fig. 2.3 (b)). The reported negative ^{13}C DNP enhancement due to the solid-state three-spin effect was explained by the following sequence of spin dynamic processes: i). first a fluctuating scalar electron-proton coupling generates a positive enhancement for the protons in the region of polyacetylene; ii). rapid spin diffusion between these protons on polyacetylene and those on nearby polyethylene chains spreads this positive ^{1}H polarization into regions of polyethylene far removed from the unpaired electrons; iii). dipolar coupling between the positively polarized protons and the ^{13}C spins in bulk polyethylene results in a negative enhancement of the bulk ^{13}C spins. The ^{13}C DNP enhancement in this case is given by:

$$A_C = -\left(\frac{\gamma_H}{\gamma_C}\right) f_{CH} \xi_{CH} A_H \qquad 2.28$$

where A_H = 1.8 and ξ_{CH} = 1/2 (e.g. pure ^{13}C - ^{1}H dipolar coupling). In this study the role of the electron as a third spin is implicitly contained in the expectation value of the proton spin operator, $\langle I_z^H \rangle$ through A_H, the ^{1}H DNP enhancement factor.

In general, there is alway an interplay between the direct and indirect effect in both solids and liquids. However, for the above solid-study the direct dipolar coupling between the unpaired electrons and the ^{13}C nuclei does not contribute to the total ^{13}C DNP enhancement. This conclusion was based on the fact that a negative ^{13}C DNP enhancement was not observed when the protons in the polyacetylene region were irradiated (e.g. the saturation of the EPR signal during the polarization period has no effect on the protons or ^{13}C nuclei in bulk polyethylene under simultaneous saturation of the protons in the region of polyacetylene).

CHAPTER 3

FLOW DNP*

3.1 Low Field Flow DNP

In the low field flow DNP experiment, a flowing sample bolus can be defined as having residence time in three different spatial regions in one and the same magnetic field (.34 T). First the bolus enters the microwave region, region A and develops the nuclear Boltzmann magnetization in a relatively short time ~3--4T_{1n}, where T_{1n} is the nuclear relaxation time in this region.

Also during this time period, the microwave field, B_{1s} irradiates the EPR transitions, and the polarization for the flowing bolus builds up with the time constant T_{1n}. Subsequently, the polarized bolus flows through the transfer region, region B, where some relaxation process will occur and enters the NMR region, region C, where the enhancement is detected.

* This chapter gives a review of the different flow DNP experiments. The reported DNP enhancement as well as the instrumentational aspects will be discussed in detail.[8,9]

Some results from LLIT ^1H DNP enhancements utilizing the above experimental set-up are reproduced in Table 3.1[8]. Although much better saturation factors are reported (s=0.8) relative to the static values of (s = 0.2 - 0.3,), the data in the table show that the enhancement decreases with an increase of the radical concentration. This was explained by polarization losses in the transfer region, region B, due to relaxation processes. At large radical concentrations the nuclear spin-lattice relaxation time, T_{1n}, becomes smaller than the residence time of the sample bolus in region B ($T_{1n} < \tau_B$). The above result demonstrated that the flow DNP enhancement depends crucially on the relative magnitude of τ_B and the spin-lattice relaxation time, T_{1n}, of the nuclei in region B.

In a different study[9], the SLIT version of the flow DNP experiment was utilized. Phenoxy and nitroxide free radicals immobilized on a silica gel surface (placed in region A) were used to monitor ^1H DNP enhancements of flowing benzene. In this case, the dependence of the nuclear polarization on the relative magnitude of τ_B and T_{1n} can be described by the equation below, assuming that the Boltzmann equilibrium magnetization as well as the dynamic polarization have been completely built up in region A. In other words at the time the bolus enters region B (τ_B=0) the magnitude of the polarization is given by $A_z = A_o(1 + \xi fs(\gamma_S/\gamma_I))$.[32]:

Table 3.1 Flow DNP enhancements, (A_∞), for TTBP/benzene solutions.[8]

Sample	A_∞ (enhancement)
0.01 M TTBP/benzene	-80.6
0.05 M TTBP/benzene	-79.9
0.10 M TTBP/benzene	-76.3
0.50 M TTBP/CCl_4	~+3

$$\frac{A_Z - A_o}{A_o} = \xi f s \frac{\gamma_S}{\gamma_I} e^{-\frac{\tau_B}{T_{1no}}} \qquad 3.1$$

The above equation contains an additional term, $\exp(-\tau_B/T_{1no})$ (in comparison to the classic DNP equation, eq.(2.16)) which describes the exponential decay of the polarized magnetization in region B with time constant T_{1no}. If the condition $\tau_B < T_{1no}$ holds, eq.(3.1) becomes identical to eq. (2.16).

Although the above result demonstrated one of the major advantages of the SLIT DNP experiment over the LLIT experiment (e.g., better transfer efficiency), the reported SLIT enhancements (-10 to -16) were smaller than the corresponding LLIT enhancement(-88) for flowing benzene. The low enhancements were attributed to the reduced molecular motion (long τ_c) for these immobilized spin label/benzene interactions which was also supported by EPR linewidth measurements.

An important result in the above study was the different DNP mechanisms encountered with the nitroxide and phenoxy radical system, respectively. While the Overhauser effect (usually observed in solutions at irradiation frequency $\omega=\omega_e$) was the predominant mechanism for the nitroxide spin system,

the immobilized phenoxy spin label had a dominant solid-state effect (enhancements at $\omega_e \pm \omega_n$) with a minor Overhauser contribution. This result suggested that the immobilized phenoxy spin label has significant contributions from the time-independent nuclear-electron interaction. In conclusion, the authors suggested the potential application of the method as a new technique for the study of liquid/surface intermolecular interactions because the reporter group (the flowing bolus) reflects the properties of the surface[9].

In summary, in spite of the significant advantage of the low field flow DNP in providing independent optimization of the B_{1s} microwave field and the FT NMR detector (see Ch.1), the technique still suffered from two major problems. One is related to the instrumentation, e.g. the disadvantage of low NMR chemical shift resolution imposed by the low field magnet. Equally important, the immobilized systems were not optimized in terms of good surface coverage of the unpaired spin system as well as chemical stability. For example,the significant "bleeding" of the nitroxide spin label from the silica gel surface in the presence of chloroform and acetone suggests unstability of the SPIN system in polar solvents.[12]

3.2 Low to High Field Transfer DNP

Dorn et al. first utilized the flow transfer SLIT experiment to monitor at high field the proton magnetization which was generated at a low magnetic field[10]. The low to high magnetic field transfer flow DNP experiments were performed with instrumentation schematically illustrated in Fig. 3.1. With this instrumentation set-up the total volume of the microwave region was ≈ 160 μl (without the immobilized radical sample); the transfer volume in region B was ≈ 50 μl; the volume in the high magnetic field region, region C, before detection was ≈ 10 μl; and the active NMR volume in the detection region was ≈ 20 μl[10]. The major improvement with this apparatus is the increased chemical shift dispersion achievable by monitoring the DNP signals at high magnetic field (4.7 T). This was illustrated for the case of flowing ethylbenzene where all three enhanced proton resonances were resolved[10]. The major remaining contribution to the NMR linewidths was the flow lifetime broadening. An inherent advantage of the SLIT experiment is the fact that no radical is present in the detection region to cause an additional decrease in the NMR resolution.

The immobilized silica gel sample used in the above study is illustrated in Fig. 3.2 (a). Although this system exhibited

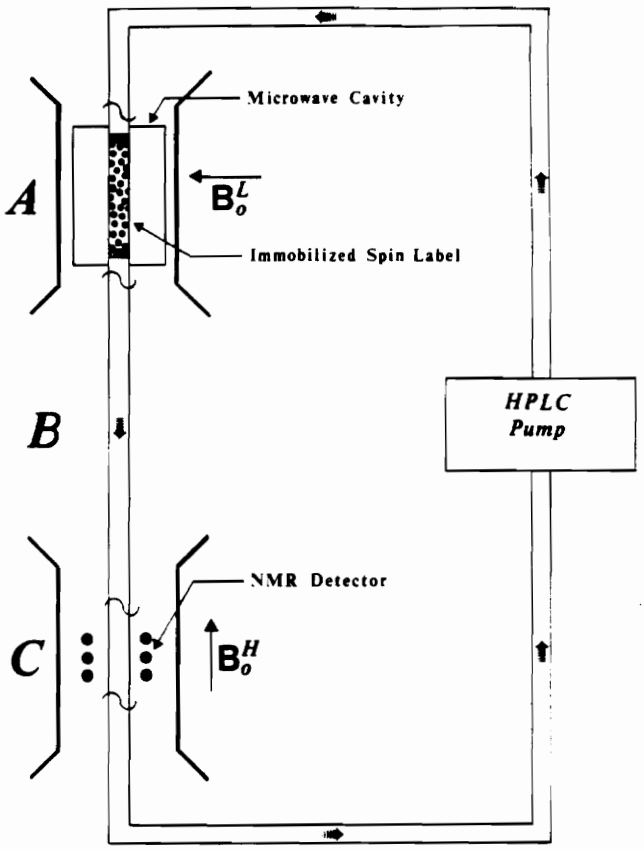

Fig. 3.1: Low to high magnetic field transfer DNP apparatus.[10]

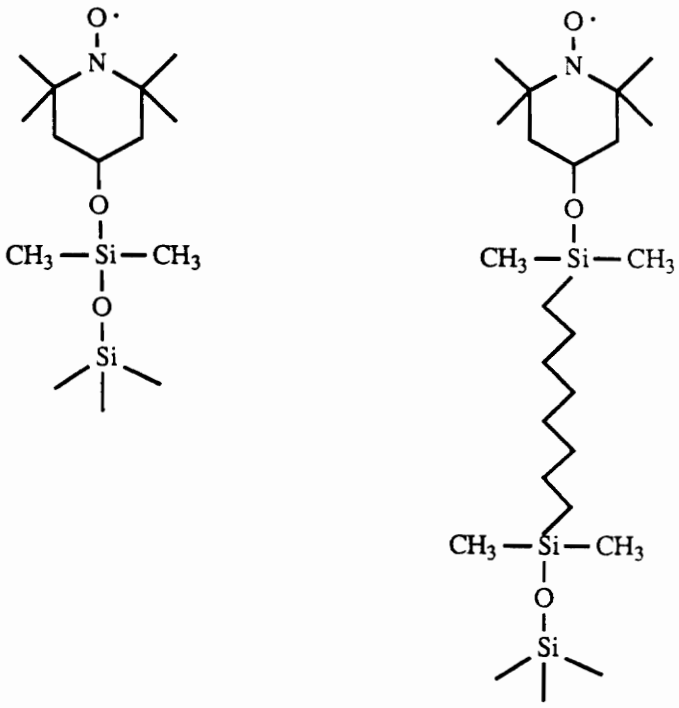

Fig. 3.2 Immobilized nitroxide radicals used for low to high field SLIT DNP studies[10]

improved chemical stability[14] in the presence of a wide variety of different solvents, the surface spin concentration as well as the DNP linewidths were not significantly different when compared to the systems used in the low field flow DNP studies. For all flowing liquids (hexane, benzene, ethylbenzene and propylbenzene),the enhancement of the low field polarized signal which exceeds the normal thermal Boltzmann magnetization at high field (4.7) were reported. However, there still remained the desire for better transfer efficiency and optimized immobilized spin-label system for higher DNP enhancements, especially when the enhancements for low γ nuclei are monitored.

It should be noted that Sagdeev et al.[33] also reported a similar transfer DNP experiment which was used to study reactions of short-lived radicals. The short-lived radicals were generated by UV irradiation in a magnetic field (0.5-50 mT). An oscillating magnetic field, B_{1s} induced a dynamic magnetization during the life time of the radicals. The polarization was then "transferred" to the reaction products. The enhanced MNR spectrum of the products was monitored at a high magnetic field (4.7 T).

Further improvement in the transfer efficiency of the low to high transfer DNP experiment was achieved in our laboratory

with a new instrumentation set-up represented in Fig.3.3[29]. With this instrumentation set-up the transfer volume in region b was reduced to 15 μl (relative to the set-up in Fig. 3.1 where the volume in region be was 50 μl).

A mathematical model for the low to high magnetic field transfer DNP experiment was developed by Tsai et al.[11] The model makes possible the calculation of the low field enhancements, A ($A = \xi fs(\gamma_S/\gamma_I)$ for the transfer DNP experiment and their direct comparison with results from the classic DNP. According to this model, the enhanced magnetization, M_z^* relative to the high field equilibrium Boltzmann magnetization, M_o^H is given by the equation:

$$A_{obs} = \frac{\langle M_z^* \rangle - \langle M_z^{HL} \rangle}{M_o^H} = \frac{A}{K}(1-e^{\frac{-t_a}{T_{1a}}})e^{\frac{-t_b}{T_{1b}}}e^{\frac{-t_c}{T_{1c}}} \qquad 3.2$$

where M_z^{HL} denotes the contribution of both low and high field magnetizations of the flowing bolus in the absence of microwave power. The constant K is the ratio of the two magnetic fields (B_o^H/B_o^L). For the above experimental set-up, the value of K was 14.4. In comparison with eq.(3.1) there are two additional exponential terms. The first one, $(1-\exp(-t_a/T_{1a}))$ accounts for the decrease in A_{obs} due to incomplete dynamic polarization build-up under the assumption that the thermal equilibrium magnetization has been

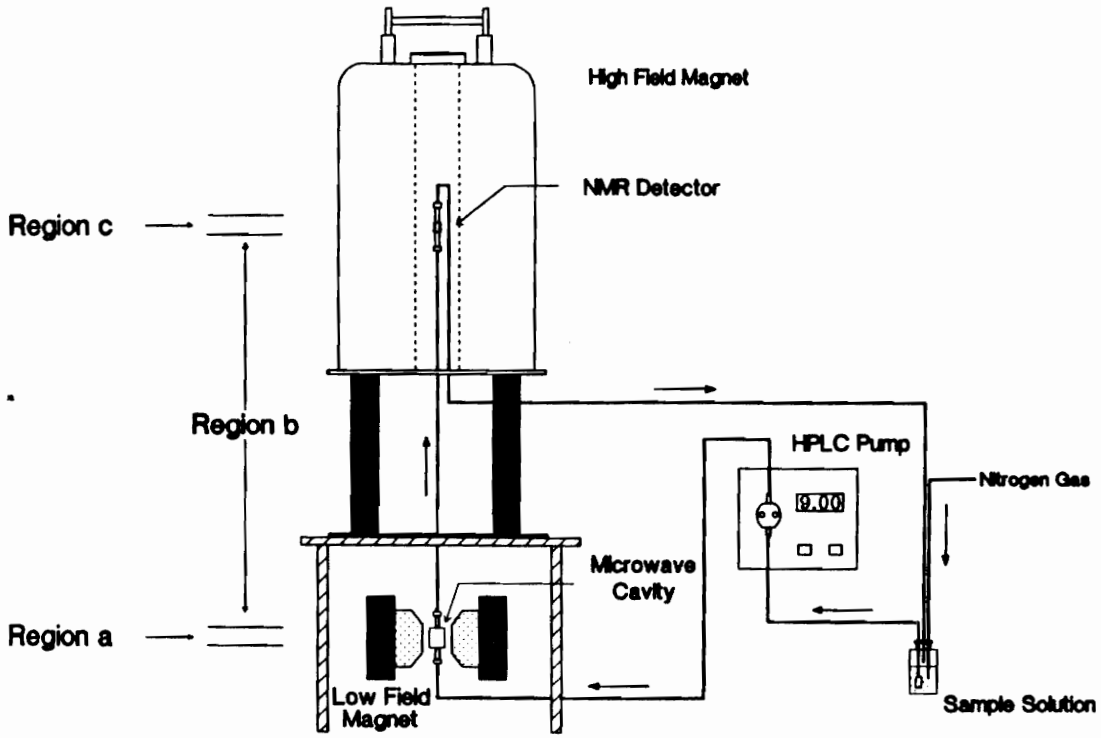

Fig. 3.3 Improved experimental set-up for low to high transfer DNP studies"

established during the residence time of the bolus in region a. The second additional term, $\exp(-t_c/T_{1c})$, represents an exponential decrease of the enhanced polarization due to relaxation processes in region c. Both A and the term $\exp(-t_b/T_{1b})$ have the same meaning to that of the corresponding terms in eq.(3.1). It is important to note that the observed enhancement, A_{obs} monitored at the high magnetic field in the low to high magnetic field transfer experiment is attenuated by the ratio K relative to the equivalent corresponding high field DNP enhancement at B_o^H.

A very convenient form for expressing eq. (3.2) is[11]:

$$A_{obs} = \left(\frac{A}{K}\right)\left(1-e^{-\frac{V_a}{T_{1a}}\frac{1}{F}}\right)e^{-\left(\frac{V_b}{T_{1b}}+\frac{V_c}{T_{1c}}\right)\frac{1}{F}} \qquad 3.3$$

where $t_a=V_a/F$, $t_b=V_b/F$, and $t_c=V_c/F$ (where F is the flow rate and V_a, V_b, and V_c are the volumes of regions a, b, and c respectively), assuming a plug flow pattern. Eq. (3.3) contains three unknown parameters: A, V_a/T_{1a} and $(V_b/T_{1b} + V_c/T_{1c})$. On the other hand, the quantities $\langle M_z^* \rangle$, $\langle M_z \rangle$, and M_o^H (eq.3.2) can be measured experimentally. Thus if a set of A_{obs} data are measured at different flow rates the above unknown parameters can be obtained by fitting the data according to eq. (3.3) using a nonlinear regression method.[11]

When the condition $t_a > 5T_{1a}$ holds, the eq. (3.3) reduces to:

$$A_{obs} = \left(\frac{A}{K}\right) e^{-\left(\frac{V_b}{T_{1b}} + \frac{V_c}{T_{1c}}\right)\frac{1}{F}} \qquad 3.4$$

Eq. (3.4) can also be written as follows:

$$\ln(A_{obs}) = \ln\left(\frac{A}{K}\right) - \left(\frac{V_b}{T_{1b}} + \frac{V_c}{T_{1c}}\right)\frac{1}{F} \qquad 3.5$$

A plot of $\ln(A_{obs})$ versus $1/F$ yields a straight line with intercept $\ln(A/K)$. Thus, eq. (3.5) provides an alternative way for the calculation of enhancement A[11]. The condition $t_a = V_a/F > 5T_{1a}$ is normally met at low flow rates and when T_{1a} is small.

The above model neglects possible three-spin contributions to the various relaxation rates. The three-spin effects as well as electron-electron exchange influences can alter the ultimate derived enhancement, A_∞. However, at high radical concentrations the above effects are suppressed. So the model provides a convenient method for estimating the ultimate enhancement, A_∞, in the low to high magnetic field transfer experiment at high radical concentration.

The improved experimental setup (see above) utilized for low to high transfer DNP studies resulted in significant improvements in the magnitude of the observed enhancements for both the LLIT and SLIT experiments. A study by Tsai et al.[14]

reported for the first time ^{29}Si DNP in liquids. Also, large LLIT and SLIT enhancements were obtained for other low abundance nuclei such as ^{15}N and ^{13}C[29]. In addition, there were a number of studies[12,13,29] which demonstrated the detection of selective DNP enhancements for different nuclei in one and the same molecule (which has been briefly discussed in chapter 1). However, in spite of the above important experimental improvements, the problems encountered in the case of ^{13}C SLIT DNP studies still remained unsolved.

CHAPTER 4

REVIEW OF SYNTHESES AND APPLICATIONS OF SPIN SAMPLES

Within the past 15 years several studies utilizing immobilized spin labels on different silica supports have been reported. In terms of applications, the silica phase immobilized nitroxide (SPIN) radicals can be divided into three groups: i) SPIN radicals for premagnetization of samples for flow NMR experiments; ii) SPIN radicals for EPR studies of chromatographic surfaces; iii) SPIN radicals for SLIT DNP studies.

In general, spin labeling of silanols by means of covalently bonded radicals requires functional groups that bond to both the silanol hydroxyl groups and to the organic spin labels. Two types of linking agents have been utilized to date: silanes (dimethyldichloro-silane and methyltrichloro-silane) and cyanuric chloride. The two general modes of surface attachment used are represented in scheme 4.1. (For most synthesis, the TEMPOL free radical has been used, as illustrated in scheme 4.1) The different procedures for the synthesis of the immobilized samples utilized to date will be reviewed briefly below.

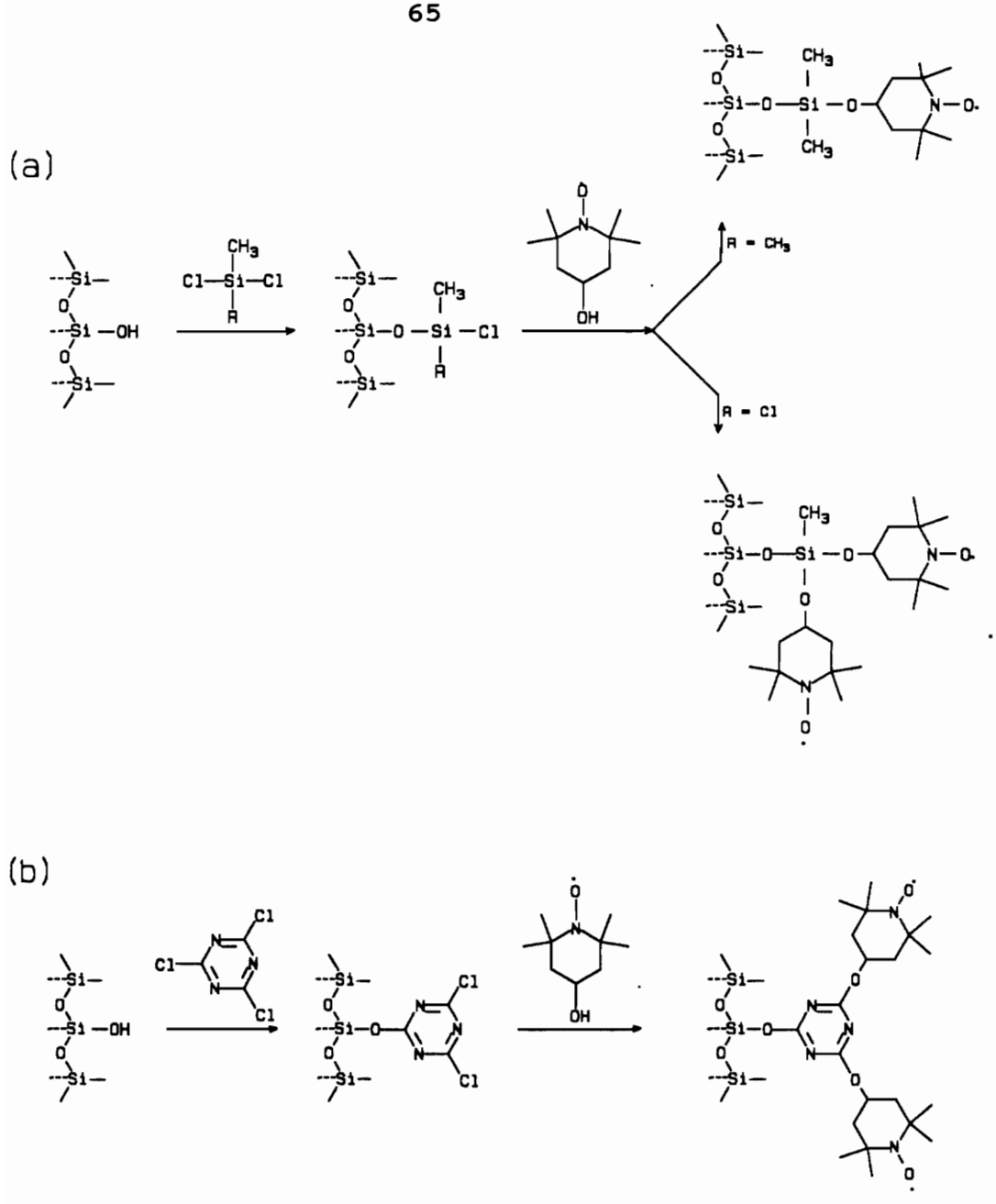

Scheme 4.1 General reaction sequences for the syntheses of SPIN samples with the linking reagents: (a) Me_2SiCl_2 and $MeSiCl_3$, and (b) cyanuric chloride.

4.1 SPIN Radicals for Premagnetization of Samples for Flow NMR Experiment

Bruck et al.[34] employed immobilized free radicals for efficient premagnetization of samples in the main magnetic field for flow NMR experiments. The general approach used in this work was to make use of the efficient electron-nuclear relaxation processes in the presence of free radicals to quickly bring the nuclear spins in a flowing liquid to equilibrium in the magnetic field. This approach avoids line broadening by immobilizing the free radicals on a solid substrate and placing them prior to detection in the NMR region. The approach is not only very important for obtaining optimal NMR signal intensity, but also for obtaining reliable relative peak intensities.

Controlled-pore glass beads of several different surface areas (29 to 350 m^2/g) were used as a solid support. The immobilized spin labels were prepared by linking TEMPOL (4-hydroxy-2,2,6,6,tetramethylpiperidinoxyl) free radical to the high-surface-area glass beads composed of microporous silica. It should be noted that cross-linked polystyrene beads were also used as a support. The linking reactions were carried out in anhydrous benzene using dimethyldichlorosilane

and cyanuric chloride according to scheme 4.1(a and b respectively). The degree of loading for beads of a given surface area was controlled by variation of the relative proportion of the linking agent - the higher the proportion, the higher the degree of derivatization. The surface spin concentrations have not been reported.

4.2 SPIN Radicals for EPR Studies of Chromatographic Surfaces.

Gilpin and co-workers[35] have investigated the effect of various polar and nonpolar solvents on the EPR spectra of chromatographic grade silica modified with immobilized TEMPOL molecules and reported changes in the hyperfine coupling constant with solvent polarity. Large differences in the hyperfine line shapes between the bound TEMPOL and that free in solution was observed for the nonpolar solvents. In the case of polar solvents, the line shapes were significantly more narrower, indicative of increased group mobility on the surface. The results were rationalized in terms of a major conformational change in the immobilized nitroxide probe as a result of the solvents ability to strongly interact with unreacted silanol groups on the surface.

The first step in the preparation of the SPIN sample in

the above study was the synthesis of a spin-labelled precursor by a reaction of dichlorodimethylsilane and TEMPOL free radical. Subsequently, the spin-labeled silane was covalently attached to the silica gel surface. The reaction was carried out in anhydrous toluene. The porous chromatographic support was LiChrosorb Si-60 silica (particle diameter = 10 μm, surface area = 550m^2/g) from Merck (EM Labs.,Elmsford, NY). The authors reported 0.002 μmol of TEMPOL per square meter area of silica surface which corresponds to ~0.07*10^{19} spins/gram silica gel.[35]

In a study by Wagner et al.[36], several SPIN samples were used for structural identification and quantitative determination of surface silanol groups by EPR spectroscopy. The number of bonded radicals was correlated with the relative concentration of vicinal and isolated silanols. The spin labeling susceptibility of the silica surface was found to be drastically modified by pre-treatment with inorganic and organometallic reagents. High temperature pre-treatment (dehydration) was found to remove the vicinal silanol groups, thus increasing the fractional population of the more reactive isolated silanol groups on the surface. If the dehydration temperature was increased from 200 to 800°C, then an increase in the concentration of derivatized spin labels from 3.7*10^{19} to 2.2*10^{20} per gram of silica was reported. The labeling was

found to be quantitative and complete when the vicinal silanols were totally removed by treatment above 600°C. Thus, the limited labeling at low temperature was attributed to the resistance of the vicinal silanol groups to labeling reagents rather than steric effects.

Both, dimethyldichlorosilane and methyltrichlorosilane were use to attach the TEMPOL free radical on the silica gel surface (Scheme 4.1(a)) in the above study. Commercial Xerogel (W.R. Grace & Co), surface area 230-260 m^2/g, pore diameter 200 Å, ave. particle size 70 μm was used for all experiments. An increase of surface spin concentration for $MeSiCL_3$/TEMPOL by a factor of 2 relative to that for Me_2SiCl_2/TEMPOL under identical conditions has been reported.[36]

4.3 SPIN Radicals for SLIT DNP Studies

In the low field ^1H SLIT DNP study by Gitti and co-workers[9], the immobilized nitroxide radicals were analogous (except for the type of silica gel support) to those employed by Bruck et al., described above. Two different solid supports have been used: silica gel bonded to 30-38 μm glass beads(Whatman), and silica gel - 40 μm particle diameter (Baker), Scheme 4.1(b). In addition, phenoxy free radicals

immobilized on aminocapped silica gel (Baker), have been used in the low field SLIT DNP study discussed above. Overhauser SLIT ^{1}H DNP enhancements of -5 to -16 for flowing benzene have been reported for the nitroxide spin-labeled system, Scheme 4.1(b). In contrast, a phenoxy spin labelled system, exhibited a dominant solid-state effect (enhancements of +3 and -6), relative to the thermal Boltzmann magnetization at 0.34 T for a flowing benzene sample. The low enhancements were attributed to reduced molecular motion for these immobilized spin label/benzene interactions. The immobilized phenoxy radical ($R=CH_3$) exhibited low stability within the time required for a DNP experiment.

In a later low to high transfer SLIT DNP study by Dorn et al.[10], the SPIN radicals were prepared by a modification of the Gilpin's procedure described above. TEMPOL free radicals were immobilized on 40 μm silica gel (Baker) in anhydrous benzene, Scheme 4.1 (a). A surface spin concentration of $1.56*10^{19}$ spins/g silica gel has been reported (Sample #113, which is **SPIN 1** in the present study)[10]. The observed Overhauser ^{1}H SLIT DNP enhancements were in the range of -11 to -25 relative to the equilibrium Boltzmann magnetization at 0.34 T which corresponds to enhancements of -0.9 to -1.4 relative to the equilibrium Boltzmann magnetization at 4.7 T.

Although a large improvement in the ^{1}H SLIT DNP enhancement (that is A_{obs}= -4.6 relative to the equilibrium Boltzmann magnetization) was reported in a subsequent study by Dorn et al[12] for the same immobilized spin system, the surface unpaired spin density provided by this sample was considered insufficient for ^{13}C SLIT DNP enhancements which are dominated by dipolar time-dependent interactions.

Based on the above results we can conclude that the spin loading on a silica gel surface depends on: i) the type of silica support (particle size and surface area); ii) the thermal and chemical pretreatment of the silica gel; iii) the type and the relative amount of the linking agent.

Three-Spin Effect in Solutions

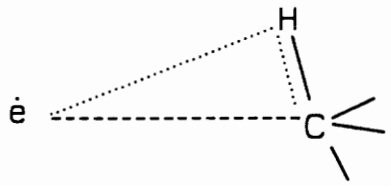

····· Three-spin effect

---- DNP

Three-Spin Effect in Solids

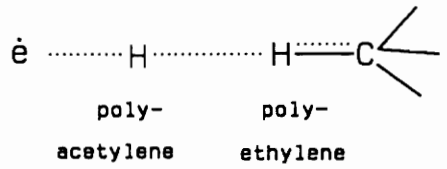

Fig. 2.3 **Transfer of magnetization from an unpaired electron, (ė) to a carbon atom, (C)**

interaction is described by coupled differential equations similar to eqs. 2.10 and 2.11. In the case of the three-spin effect, the enhancement in given by the equation below[30]:

$$A=(\xi_C^S f_C^S-\xi_C^H f_C^H \xi_H^S f_H^S)\, s\frac{\gamma_s}{\gamma_C} \qquad 2.26$$

The first term in eq.(2.26) is identical to the result for the two-spin system (e.g. eq.2.16). The quantity f_C^S represents the fraction of the ^{13}C relaxation due to the direct carbon-electron interaction which is usually dipolar in solutions and results in negative ^{13}C DNP enhancements. On the other hand, the indirect transfer of magnetization from the radical to the carbon (via the proton spin) will result in positive ^{13}C DNP enhancements (see the second term, eq. 2.26). Thus, the three -spin effect results in a decrease of the dipolar dominated DNP enhancements in solutions.

The significance of the three-spin effect for a particular system depends on the effectiveness (e.g. f_C^H) of the carbon-proton interaction. The quantity f_C^H measures the fraction of the total ^{13}C relaxation rate due to carbon-proton interactions in the presence of the unpaired electrons. At high radical concentrations ($f_C^H \simeq 0$) the ^{13}C relaxation will be governed exclusively by the carbon-electron interaction ($f_C^S \simeq 1$). It is possible that a signal which is negatively

enhanced at high radical concentrations may even become positively enhanced at low radical concentrations if the three-spin effect outweighs the direct polarization mechanism[5].

The presence of the three-spin effect can be revealed by triple irradiation experiments, where both the electron and the proton spin transitions are strongly irradiated. This has the effect of removing the indirect pathway for the transfer of spin polarization from the electron to the carbon via the proton, leaving only the direct electron-carbon mechanism[4].

Under the conditions of triple resonance, the enhancement is given by[4]:

$$A=\xi_C^S f_C^S s\frac{\gamma_S}{\gamma_C}+\xi_C^H f_C^H s^H\frac{\gamma_H}{\gamma_c} \qquad 2.27$$

Since the proton spin system can be saturated more easily because of the longer relaxation times and the lower resonance frequency, ν_{1H}, the value of s^H can usually be equal to 1.

The second term in eq. (2.27) can be neglected because $\gamma_H << \gamma_S$. Thus, simultaneous saturation of the proton spin system is effectively equivalent to a reduction of the three-spin system to the simpler two-spin system.

2.7 The Three-Spin Effect in Solids

A solid-state analog of the three-spin effect in solutions was reported for a solid sample containing three kinds of spins (unpaired electrons, ^{13}C, and ^{1}H)[31]. The unpaired electrons were confined to islands of polyacetylene embedded in a matrix of polyethylene. Although the effect is very closely related to the three-spin effect in solutions, the spin polarization is transferred in a different way, via spin diffusion (see Fig. 2.3 (b)). The reported negative ^{13}C DNP enhancement due to the solid-state three-spin effect was explained by the following sequence of spin dynamic processes: i). first a fluctuating scalar electron-proton coupling generates a positive enhancement for the protons in the region of polyacetylene; ii). rapid spin diffusion between these protons on polyacetylene and those on nearby polyethylene chains spreads this positive ^{1}H polarization into regions of polyethylene far removed from the unpaired electrons; iii). dipolar coupling between the positively polarized protons and the ^{13}C spins in bulk polyethylene results in a negative enhancement of the bulk ^{13}C spins. The ^{13}C DNP enhancement in this case is given by:

$$A_C = -\left(\frac{\gamma_H}{\gamma_C}\right) f_{CH} \xi_{CH} A_H \qquad 2.28$$

where A_H = 1.8 and ξ_{CH} = 1/2 (e.g. pure ^{13}C - ^{1}H dipolar coupling). In this study the role of the electron as a third spin is implicitly contained in the expectation value of the proton spin operator, $\langle I_z^H \rangle$ through A_H, the ^{1}H DNP enhancement factor.

In general, there is alway an interplay between the direct and indirect effect in both solids and liquids. However, for the above solid-study the direct dipolar coupling between the unpaired electrons and the ^{13}C nuclei does not contribute to the total ^{13}C DNP enhancement. This conclusion was based on the fact that a negative ^{13}C DNP enhancement was not observed when the protons in the polyacetylene region were irradiated (e.g. the saturation of the EPR signal during the polarization period has no effect on the protons or ^{13}C nuclei in bulk polyethylene under simultaneous saturation of the protons in the region of polyacetylene).

CHAPTER 3

FLOW DNP*

3.1 Low Field Flow DNP

In the low field flow DNP experiment, a flowing sample bolus can be defined as having residence time in three different spatial regions in one and the same magnetic field (.34 T). First the bolus enters the microwave region, region A and develops the nuclear Boltzmann magnetization in a relatively short time ~3--4T_{1n}, where T_{1n} is the nuclear relaxation time in this region.

Also during this time period, the microwave field, B_{1s} irradiates the EPR transitions, and the polarization for the flowing bolus builds up with the time constant T_{1n}. Subsequently, the polarized bolus flows through the transfer region, region B, where some relaxation process will occur and enters the NMR region, region C, where the enhancement is detected.

* This chapter gives a review of the different flow DNP experiments. The reported DNP enhancement as well as the instrumentational aspects will be discussed in detail.[8,9]

Some results from LLIT ^1H DNP enhancements utilizing the above experimental set-up are reproduced in Table 3.1[8]. Although much better saturation factors are reported (s=0.8) relative to the static values of (s = 0.2 - 0.3,), the data in the table show that the enhancement decreases with an increase of the radical concentration. This was explained by polarization losses in the transfer region, region B, due to relaxation processes. At large radical concentrations the nuclear spin-lattice relaxation time, T_{1n}, becomes smaller than the residence time of the sample bolus in region B ($T_{1n} < \tau_B$). The above result demonstrated that the flow DNP enhancement depends crucially on the relative magnitude of τ_B and the spin-lattice relaxation time, T_{1n}, of the nuclei in region B.

In a different study[9], the SLIT version of the flow DNP experiment was utilized. Phenoxy and nitroxide free radicals immobilized on a silica gel surface (placed in region A) were used to monitor ^1H DNP enhancements of flowing benzene. In this case, the dependence of the nuclear polarization on the relative magnitude of τ_B and T_{1n} can be described by the equation below, assuming that the Boltzmann equilibrium magnetization as well as the dynamic polarization have been completely built up in region A. In other words at the time the bolus enters region B (τ_B=0) the magnitude of the polarization is given by $A_z = A_o(1 + \xi fs(\gamma_S/\gamma_I))$.[32]:

Table 3.1 Flow DNP enhancements, (A_∞), for TTBP/benzene solutions.[8]

Sample	A_∞ (enhancement)
0.01 M TTBP/benzene	-80.6
0.05 M TTBP/benzene	-79.9
0.10 M TTBP/benzene	-76.3
0.50 M TTBP/CCl_4	~+3

$$\frac{A_Z - A_o}{A_o} = \xi f s \frac{\gamma_S}{\gamma_I} e^{-\frac{\tau_B}{T_{1no}}} \qquad 3.1$$

The above equation contains an additional term, $\exp(-\tau_B/T_{1no})$ (in comparison to the classic DNP equation, eq.(2.16)) which describes the exponential decay of the polarized magnetization in region B with time constant T_{1no}. If the condition $\tau_B < T_{1no}$ holds, eq.(3.1) becomes identical to eq. (2.16).

Although the above result demonstrated one of the major advantages of the SLIT DNP experiment over the LLIT experiment (e.g., better transfer efficiency), the reported SLIT enhancements (-10 to -16) were smaller than the corresponding LLIT enhancement(-88) for flowing benzene. The low enhancements were attributed to the reduced molecular motion (long τ_c) for these immobilized spin label/benzene interactions which was also supported by EPR linewidth measurements.

An important result in the above study was the different DNP mechanisms encountered with the nitroxide and phenoxy radical system, respectively. While the Overhauser effect (usually observed in solutions at irradiation frequency $\omega = \omega_e$) was the predominant mechanism for the nitroxide spin system,

the immobilized phenoxy spin label had a dominant solid-state effect (enhancements at $\omega_e \pm \omega_n$) with a minor Overhauser contribution. This result suggested that the immobilized phenoxy spin label has significant contributions from the time-independent nuclear-electron interaction. In conclusion, the authors suggested the potential application of the method as a new technique for the study of liquid/surface intermolecular interactions because the reporter group (the flowing bolus) reflects the properties of the surface[9].

In summary, in spite of the significant advantage of the low field flow DNP in providing independent optimization of the B_{1s} microwave field and the FT NMR detector (see Ch.1), the technique still suffered from two major problems. One is related to the instrumentation, e.g. the disadvantage of low NMR chemical shift resolution imposed by the low field magnet. Equally important, the immobilized systems were not optimized in terms of good surface coverage of the unpaired spin system as well as chemical stability. For example,the significant "bleeding" of the nitroxide spin label from the silica gel surface in the presence of chloroform and acetone suggests unstability of the SPIN system in polar solvents.[12]

3.2 Low to High Field Transfer DNP

Dorn et al. first utilized the flow transfer SLIT experiment to monitor at high field the proton magnetization which was generated at a low magnetic field[10]. The low to high magnetic field transfer flow DNP experiments were performed with instrumentation schematically illustrated in Fig. 3.1. With this instrumentation set-up the total volume of the microwave region was ≈ 160 μl (without the immobilized radical sample); the transfer volume in region B was ≈ 50 μl; the volume in the high magnetic field region, region C, before detection was ≈ 10 μl; and the active NMR volume in the detection region was ≈ 20 μl[10]. The major improvement with this apparatus is the increased chemical shift dispersion achievable by monitoring the DNP signals at high magnetic field (4.7 T). This was illustrated for the case of flowing ethylbenzene where all three enhanced proton resonances were resolved[10]. The major remaining contribution to the NMR linewidths was the flow lifetime broadening. An inherent advantage of the SLIT experiment is the fact that no radical is present in the detection region to cause an additional decrease in the NMR resolution.

The immobilized silica gel sample used in the above study is illustrated in Fig. 3.2 (a). Although this system exhibited

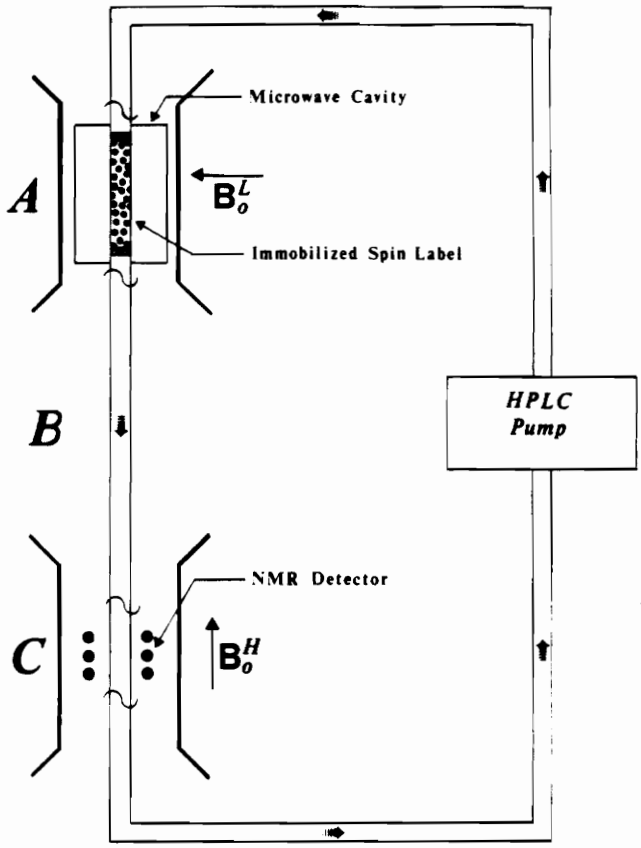

Fig. 3.1: Low to high magnetic field transfer DNP apparatus.[49]

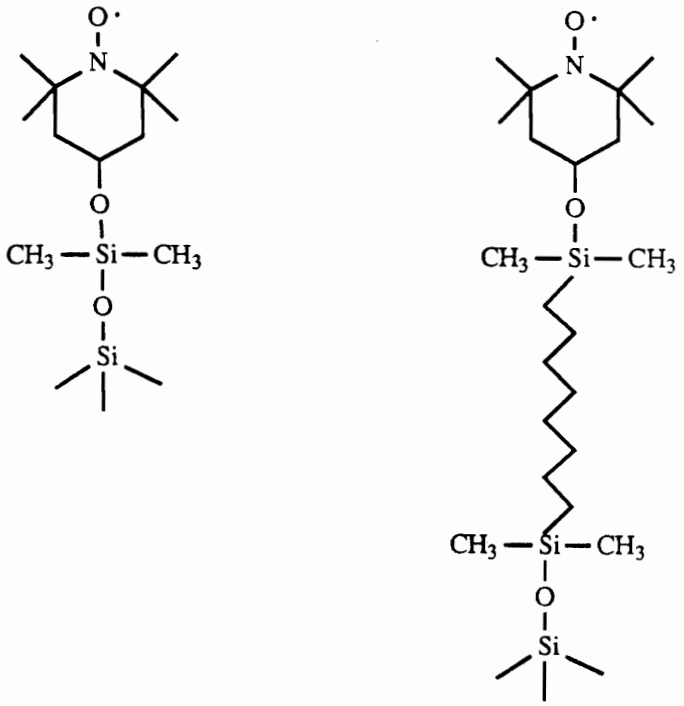

Fig. 3.2 Immobilized nitroxide radicals used for low to high field SLIT DNP studies[10]

improved chemical stability[14] in the presence of a wide variety of different solvents, the surface spin concentration as well as the DNP linewidths were not significantly different when compared to the systems used in the low field flow DNP studies. For all flowing liquids (hexane, benzene, ethylbenzene and propylbenzene),the enhancement of the low field polarized signal which exceeds the normal thermal Boltzmann magnetization at high field (4.7) were reported. However, there still remained the desire for better transfer efficiency and optimized immobilized spin-label system for higher DNP enhancements, especially when the enhancements for low γ nuclei are monitored.

It should be noted that Sagdeev et al.[33] also reported a similar transfer DNP experiment which was used to study reactions of short-lived radicals. The short-lived radicals were generated by UV irradiation in a magnetic field (0.5-50 mT). An oscillating magnetic field, B_{1S} induced a dynamic magnetization during the life time of the radicals. The polarization was then "transferred" to the reaction products. The enhanced MNR spectrum of the products was monitored at a high magnetic field (4.7 T).

Further improvement in the transfer efficiency of the low to high transfer DNP experiment was achieved in our laboratory

with a new instrumentation set-up represented in Fig.3.3[29]. With this instrumentation set-up the transfer volume in region b was reduced to 15 μl (relative to the set-up in Fig. 3.1 where the volume in region be was 50 μl).

A mathematical model for the low to high magnetic field transfer DNP experiment was developed by Tsai et al.[11] The model makes possible the calculation of the low field enhancements, A ($A = \xi fs(\gamma_S/\gamma_I)$ for the transfer DNP experiment and their direct comparison with results from the classic DNP. According to this model, the enhanced magnetization, M_z^* relative to the high field equilibrium Boltzmann magnetization, M_o^H is given by the equation:

$$A_{obs} = \frac{\langle M_z^* \rangle - \langle M_z^{HL} \rangle}{M_o^H} = \frac{A}{K}(1-e^{\frac{-t_a}{T_{1a}}})e^{\frac{-t_b}{T_{1b}}}e^{\frac{-t_c}{T_{1c}}} \qquad 3.2$$

where M_z^{HL} denotes the contribution of both low and high field magnetizations of the flowing bolus in the absence of microwave power. The constant K is the ratio of the two magnetic fields (B_o^H/B_o^L). For the above experimental set-up, the value of K was 14.4. In comparison with eq.(3.1) there are two additional exponential terms. The first one, $(1-\exp(-t_a/T_{1a}))$ accounts for the decrease in A_{obs} due to incomplete dynamic polarization build-up under the assumption that the thermal equilibrium magnetization has been

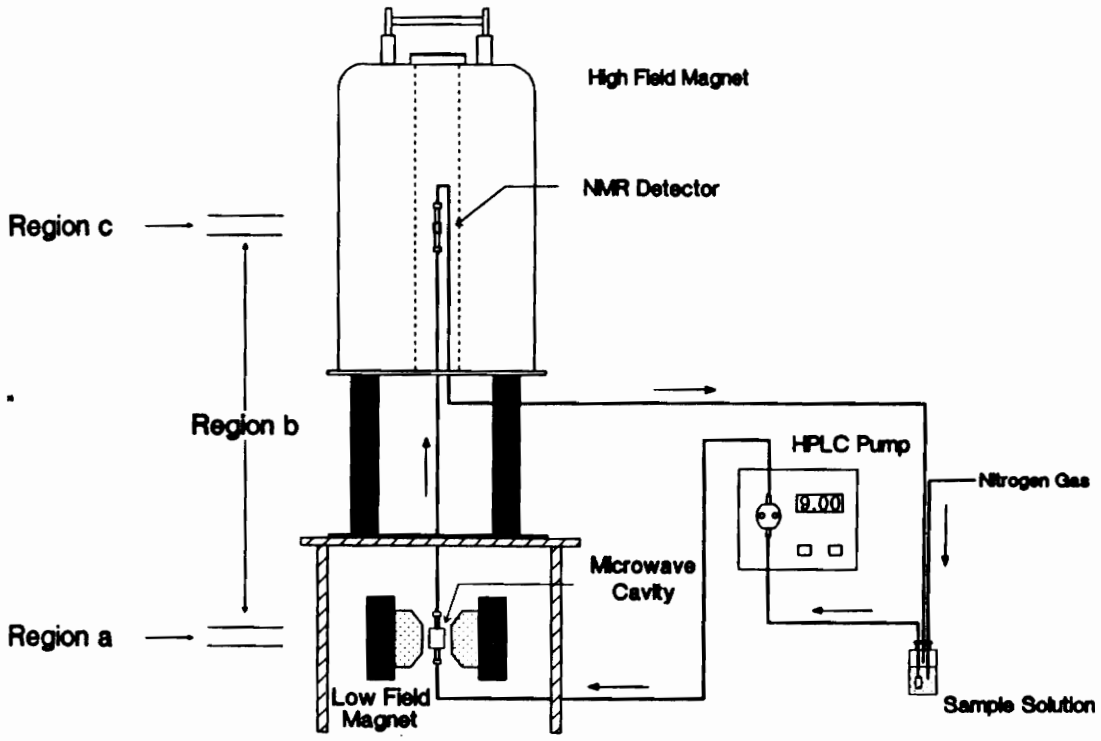

Fig. 3.3 Improved experimental set-up for low to high transfer DNP studies"

established during the residence time of the bolus in region a. The second additional term, $\exp(-t_c/T_{1c})$, represents an exponential decrease of the enhanced polarization due to relaxation processes in region c. Both A and the term $\exp(-t_b/T_{1b})$ have the same meaning to that of the corresponding terms in eq.(3.1). It is important to note that the observed enhancement, A_{obs} monitored at the high magnetic field in the low to high magnetic field transfer experiment is attenuated by the ratio K relative to the equivalent corresponding high field DNP enhancement at B_o^H.

A very convenient form for expressing eq. (3.2) is[11]:

$$A_{obs} = \left(\frac{A}{K}\right)\left(1-e^{-\frac{V_a}{T_{1a}}\frac{1}{F}}\right)e^{-\left(\frac{V_b}{T_{1b}}+\frac{V_c}{T_{1c}}\right)\frac{1}{F}} \qquad 3.3$$

where $t_a=V_a/F$, $t_b=V_b/F$, and $t_c=V_c/F$ (where F is the flow rate and V_a, V_b, and V_c are the volumes of regions a, b, and c respectively), assuming a plug flow pattern. Eq. (3.3) contains three unknown parameters: A, V_a/T_{1a} and $(V_b/T_{1b} + V_c/T_{1c})$. On the other hand, the quantities $\langle M_z^* \rangle$, $\langle M_z \rangle$, and M_o^H (eq.3.2) can be measured experimentally. Thus if a set of A_{obs} data are measured at different flow rates the above unknown parameters can be obtained by fitting the data according to eq. (3.3) using a nonlinear regression method.[11]

When the condition $t_a > 5T_{1a}$ holds, the eq. (3.3) reduces to:

$$A_{obs} = \left(\frac{A}{K}\right) e^{-\left(\frac{V_b}{T_{1b}} + \frac{V_c}{T_{1c}}\right)\frac{1}{F}} \qquad 3.4$$

Eq. (3.4) can also be written as follows:

$$\ln(A_{obs}) = \ln\left(\frac{A}{K}\right) - \left(\frac{V_b}{T_{1b}} + \frac{V_c}{T_{1c}}\right)\frac{1}{F} \qquad 3.5$$

A plot of $\ln(A_{obs})$ versus $1/F$ yields a straight line with intercept $\ln(A/K)$. Thus, eq. (3.5) provides an alternative way for the calculation of enhancement A[11]. The condition $t_a = V_a/F > 5T_{1a}$ is normally met at low flow rates and when T_{1a} is small.

The above model neglects possible three-spin contributions to the various relaxation rates. The three-spin effects as well as electron-electron exchange influences can alter the ultimate derived enhancement, A_∞. However, at high radical concentrations the above effects are suppressed. So the model provides a convenient method for estimating the ultimate enhancement, A_∞, in the low to high magnetic field transfer experiment at high radical concentration.

The improved experimental setup (see above) utilized for low to high transfer DNP studies resulted in significant improvements in the magnitude of the observed enhancements for both the LLIT and SLIT experiments. A study by Tsai et al.[14]

reported for the first time ^{29}Si DNP in liquids. Also, large LLIT and SLIT enhancements were obtained for other low abundance nuclei such as ^{15}N and ^{13}C[29]. In addition, there were a number of studies[12,13,29] which demonstrated the detection of selective DNP enhancements for different nuclei in one and the same molecule (which has been briefly discussed in chapter 1). However, in spite of the above important experimental improvements, the problems encountered in the case of ^{13}C SLIT DNP studies still remained unsolved.

CHAPTER 4

REVIEW OF SYNTHESES AND APPLICATIONS OF SPIN SAMPLES

Within the past 15 years several studies utilizing immobilized spin labels on different silica supports have been reported. In terms of applications, the silica phase immobilized nitroxide (SPIN) radicals can be divided into three groups: i) SPIN radicals for premagnetization of samples for flow NMR experiments; ii) SPIN radicals for EPR studies of chromatographic surfaces; iii) SPIN radicals for SLIT DNP studies.

In general, spin labeling of silanols by means of covalently bonded radicals requires functional groups that bond to both the silanol hydroxyl groups and to the organic spin labels. Two types of linking agents have been utilized to date: silanes (dimethyldichloro-silane and methyltrichloro-silane) and cyanuric chloride. The two general modes of surface attachment used are represented in scheme 4.1. (For most synthesis, the TEMPOL free radical has been used, as illustrated in scheme 4.1) The different procedures for the synthesis of the immobilized samples utilized to date will be reviewed briefly below.

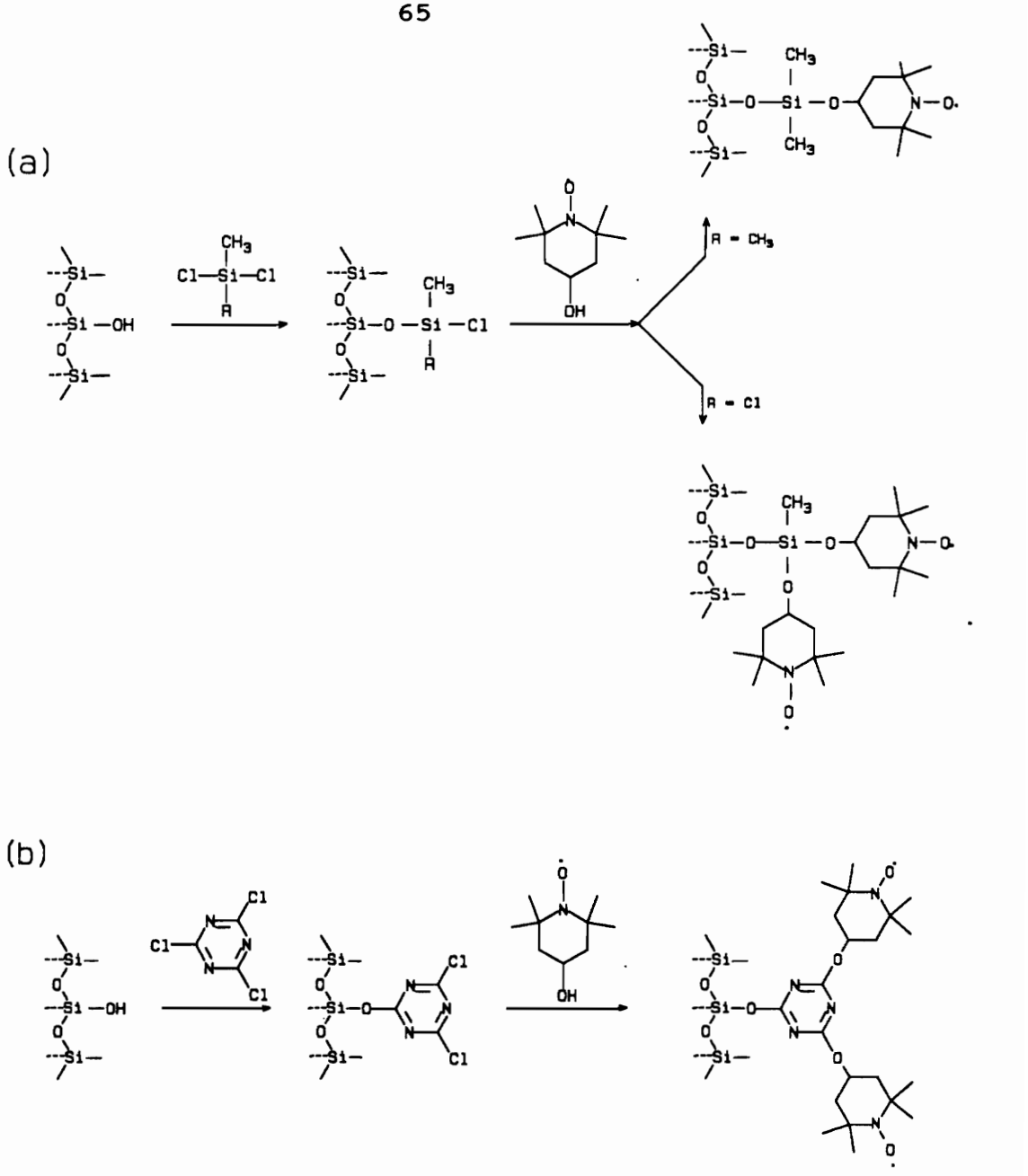

Scheme 4.1 General reaction sequences for the syntheses of SPIN samples with the linking reagents: (a) Me_2SiCl_2 and $MeSiCl_3$, and (b) cyanuric chloride.

4.1 SPIN Radicals for Premagnetization of Samples for Flow NMR Experiment

Bruck et al.[34] employed immobilized free radicals for efficient premagnetization of samples in the main magnetic field for flow NMR experiments. The general approach used in this work was to make use of the efficient electron-nuclear relaxation processes in the presence of free radicals to quickly bring the nuclear spins in a flowing liquid to equilibrium in the magnetic field. This approach avoids line broadening by immobilizing the free radicals on a solid substrate and placing them prior to detection in the NMR region. The approach is not only very important for obtaining optimal NMR signal intensity, but also for obtaining reliable relative peak intensities.

Controlled-pore glass beads of several different surface areas (29 to 350 m^2/g) were used as a solid support. The immobilized spin labels were prepared by linking TEMPOL (4-hydroxy-2,2,6,6,tetramethylpiperidinoxyl) free radical to the high-surface-area glass beads composed of microporous silica. It should be noted that cross-linked polystyrene beads were also used as a support. The linking reactions were carried out in anhydrous benzene using dimethyldichlorosilane

and cyanuric chloride according to scheme 4.1(a and b respectively). The degree of loading for beads of a given surface area was controlled by variation of the relative proportion of the linking agent - the higher the proportion, the higher the degree of derivatization. The surface spin concentrations have not been reported.

4.2 SPIN Radicals for EPR Studies of Chromatographic Surfaces.

Gilpin and co-workers[35] have investigated the effect of various polar and nonpolar solvents on the EPR spectra of chromatographic grade silica modified with immobilized TEMPOL molecules and reported changes in the hyperfine coupling constant with solvent polarity. Large differences in the hyperfine line shapes between the bound TEMPOL and that free in solution was observed for the nonpolar solvents. In the case of polar solvents, the line shapes were significantly more narrower, indicative of increased group mobility on the surface. The results were rationalized in terms of a major conformational change in the immobilized nitroxide probe as a result of the solvents ability to strongly interact with unreacted silanol groups on the surface.

The first step in the preparation of the SPIN sample in

the above study was the synthesis of a spin-labelled precursor by a reaction of dichlorodimethylsilane and TEMPOL free radical. Subsequently, the spin-labeled silane was covalently attached to the silica gel surface. The reaction was carried out in anhydrous toluene. The porous chromatographic support was LiChrosorb Si-60 silica (particle diameter = 10 μm, surface area = 550m^2/g) from Merck (EM Labs.,Elmsford, NY). The authors reported 0.002 μmol of TEMPOL per square meter area of silica surface which corresponds to ~0.07*10^{19} spins/gram silica gel.[35]

In a study by Wagner et al.[36], several SPIN samples were used for structural identification and quantitative determination of surface silanol groups by EPR spectroscopy. The number of bonded radicals was correlated with the relative concentration of vicinal and isolated silanols. The spin labeling susceptibility of the silica surface was found to be drastically modified by pre-treatment with inorganic and organometallic reagents. High temperature pre-treatment (dehydration) was found to remove the vicinal silanol groups, thus increasing the fractional population of the more reactive isolated silanol groups on the surface. If the dehydration temperature was increased from 200 to 800°C, then an increase in the concentration of derivatized spin labels from 3.7*10^{19} to 2.2*10^{20} per gram of silica was reported. The labeling was

found to be quantitative and complete when the vicinal silanols were totally removed by treatment above 600°C. Thus, the limited labeling at low temperature was attributed to the resistance of the vicinal silanol groups to labeling reagents rather than steric effects.

Both, dimethyldichlorosilane and methyltrichlorosilane were use to attach the TEMPOL free radical on the silica gel surface (Scheme 4.1(a)) in the above study. Commercial Xerogel (W.R. Grace & Co), surface area 230-260 m^2/g, pore diameter 200 Å, ave. particle size 70 μm was used for all experiments. An increase of surface spin concentration for $MeSiCL_3$/TEMPOL by a factor of 2 relative to that for Me_2SiCl_2/TEMPOL under identical conditions has been reported.[36]

4.3 SPIN Radicals for SLIT DNP Studies

In the low field ^1H SLIT DNP study by Gitti and co-workers[9], the immobilized nitroxide radicals were analogous (except for the type of silica gel support) to those employed by Bruck et al., described above. Two different solid supports have been used: silica gel bonded to 30-38 μm glass beads(Whatman), and silica gel - 40 μm particle diameter (Baker), Scheme 4.1(b). In addition, phenoxy free radicals

immobilized on aminocapped silica gel (Baker), have been used in the low field SLIT DNP study discussed above. Overhauser SLIT ^{1}H DNP enhancements of -5 to -16 for flowing benzene have been reported for the nitroxide spin-labeled system, Scheme 4.1(b). In contrast, a phenoxy spin labelled system, exhibited a dominant solid-state effect (enhancements of +3 and -6), relative to the thermal Boltzmann magnetization at 0.34 T for a flowing benzene sample. The low enhancements were attributed to reduced molecular motion for these immobilized spin label/benzene interactions. The immobilized phenoxy radical ($R=CH_3$) exhibited low stability within the time required for a DNP experiment.

In a later low to high transfer SLIT DNP study by Dorn et al.[10], the SPIN radicals were prepared by a modification of the Gilpin's procedure described above. TEMPOL free radicals were immobilized on 40 μm silica gel (Baker) in anhydrous benzene, Scheme 4.1 (a). A surface spin concentration of $1.56*10^{19}$ spins/g silica gel has been reported (Sample #113, which is **SPIN 1** in the present study)[10]. The observed Overhauser ^{1}H SLIT DNP enhancements were in the range of -11 to -25 relative to the equilibrium Boltzmann magnetization at 0.34 T which corresponds to enhancements of -0.9 to -1.4 relative to the equilibrium Boltzmann magnetization at 4.7 T.

Although a large improvement in the ^{1}H SLIT DNP enhancement (that is A_{obs}= -4.6 relative to the equilibrium Boltzmann magnetization) was reported in a subsequent study by Dorn et al[12] for the same immobilized spin system, the surface unpaired spin density provided by this sample was considered insufficient for ^{13}C SLIT DNP enhancements which are dominated by dipolar time-dependent interactions.

Based on the above results we can conclude that the spin loading on a silica gel surface depends on: i) the type of silica support (particle size and surface area); ii) the thermal and chemical pretreatment of the silica gel; iii) the type and the relative amount of the linking agent.

CHAPTER 5

EXPERIMENTAL

5.1 Preparation of SPIN Samples

5.1.1 Rationale for Preparation of SPIN Samples

In order for a SPIN system to be useful in flow SLIT DNP studies it must satisfy the following important requirements:

i). The immobilized radicals must be reasonably stable. The term "stable" is used here in the Ingold[37] sense; that is the free radical can be immobilized on the silica gel surface, stored, and handled in the laboratory with no more precaution than observed when working with conventional organic compounds. In general, this requirement is met by nitroxide free radicals. In addition, the spin samples must exhibit chemical inertness towards different polar solvents and solute molecules present in the flowing solution.

ii). High surface spin concentration is required for efficient solid/liquid interaction.

iii).In order for convenient saturation of the EPR transition, the SPIN samples must exhibit a relatively narrow EPR linewidth.

iv). The immobilized silica gel must exhibit good flow characteristics (must not cause large back pressures) so that

high flow rate DNP studies are possible.

There are some difficulties in satisfying both requirements (ii) and (iii) at the same time, specifically the large radical concentration necessary for better electron-nuclear interaction results in broad EPR line widths which are difficult to saturate.

As already mentioned, the purpose of this thesis is to provide a SPIN samples with high surface spin concentrations, decreased molecular correlation times, τ_c, and better saturation factors, s. The molecular correlation time, τ_c of an immobilized system can be decreased by high temperature studies or by immobilizing longer chain free nitroxide molecules on the surface which presumably would exhibit higher mobility. The second approach (preparation of long-chain SPIN radicals) has been applied in this thesis to help alleviate EPR linewidth and/or saturation limitations in the DNP experiment.

It should be noted that a study by Sindorf and Maciel[38] has shown that alkyl motion increases with the distance from the silica surface; however, from cross-polarization relaxation measurements they concluded that motion does not become liquid-like even for carbons far removed from the

surface. Instead, they found that the increase in alkyl motion falls off after a distance of about eight to nine carbons.

Another approach examined in this thesis was isotope substitution on the immobilized free radicals. Previous DNP studies in solutions[29] demonstrated that the three-spin effect can be suppressed if deuterium is substituted for hydrogen on the flowing samples. For example, larger ^{13}C SLIT DNP enhancement were reported for benzene-d_6 relative to that obtained for benzene. Also, deuteration eliminated the solid-state three-spin effect for a polymer system in a study by Maresch[31] discussed in Chapter 2.7. In this thesis, deuterium substituted derivatives of nitroxide free radicals were immobilized on the silica gel surface in order to examine the effect of deuteration of the covalently bonded radicals on the DNP enhancement for the SPIN system used in this study.

Another very important consideration in favor of nitrogen isotopic substitution is related to the nature of the electron-nuclear ^{14}N hyperfine splitting for nitroxide radicals. The EPR of any nitroxide radical is usually a triplet (^{14}N, I=1). With the present DNP apparatus only one line of the EPR triplet can be saturated at a time.

It has been shown in a solution study by Bates[39] that ^{14}N

labelled nitroxide radicals at very low concentration will have ultimate enhancements reduced by a factor of three, $A_o/3$ (e.g. -330/3 for ^1H DNP enhancements). In the case of the exchange narrowing limit (fast electron-electron exchange rate for the three separate transitions) observed at high radical concentration the EPR spectrum is a singlet and the extrapolated enhancements will approach the appropriate dipolar limit (-330 for protons). For all cases in between these two extremes, a correction for the electron-electron exchange is necessary for the estimation of A_o. Although corrections for electron-electron exchange can be applied in solution DNP studies using the model developed by Bates[40], corrections in the SLIT DNP experiment are more formidable. Thus, an ideal case for SLIT DNP ultimate enhancements would be a single sharp EPR line for ^{14}N nitroxide immobilized radicals.

In contrast, the EPR spectrum for a ^{15}N nitroxide radical is a doublet due to ^{15}N electron hyperfine interaction (^{15}N, I = 1/2). In this case, a reduction in the DNP ultimate enhancements by only a factor of two (-330/2) will result (for low electron-electron exchange rate) which corresponds to higher observable DNP enhancements under analogous conditions.

With the considerations above, deuterated and ^{15}N

labelled 4-Hydroxy TEMPO was immobilized on silica gel surface so that the DNP enhancement can be compared to that obtained for analogous but non-labelled SPIN system. In addition, samples were prepared with different particle size supports. The silica gel particle size was similar to that used in a previous study reported by Wagner et al.[36] (see Ch. 4) where a similar SPIN sample was prepared with significantly higher surface spin counts.

The second synthetic goal of this thesis was to prepare a chiral SPIN system appropriate for monitoring SLIT DNP enhancements for weak diastereomeric pairwise interactions.

As pointed out in Chapter 3, the SLIT experiment depends on nuclear-electron time-dependent and/or time-independent interactions between an immobilized free radical system and the flowing liquid. A number of spectroscopic techniques such as infrared and photoacoustic spectroscopy, fluorescence spectroscopy, and the ^{13}C and ^{29}Si CP MAS NMR techniques have been employed extensively in recent years to study and characterize modified silica gel surfaces. Most NMR methods have focused on chemical and motional characterization of bonded phases. Preliminary studies[9] in Dr. Dorn's laboratory suggested that a SLIT DNP experiment could evolve as a new approach for characterization of bonded phases by direct

monitoring of surface/liquid or surface/gas weak intermolecular interactions. Based on the results from the above studies and the possibility of monitoring selective enhancements of different nuclei in a given molecule, we decided to prepare a chiral SPIN system for SLIT DNP studies of enantiomeric pairs.

Potentially, selective DNP enhancements for diastereomeric pairwise complexes (that is complexes between chiral spin labels immobilized on the silica gel surface and pure enantiomers, R- or S-, dissolved in the flowing solution) could provide a new approach for determining enantiomeric purity and absolute configuration. In addition, the SLIT DNP technique could evolve as a powerful tool for monitoring the efficacy of chiral chromatographic separations without potential contamination of valuable samples with a chiral solvent and/or chiral shift reagent.

Two different chiral SPIN systems have been synthesized. The syntheses as well as the DNP results will be discussed in Chapters 5.1.3 and 6.3 respectively.

5.1.2 Preparation of Short Chain Achiral SPIN Samples

A number of SPIN samples have been prepared in order to

establish the optimum conditions in terms of radical concentration, EPR linewidth, and good flow characteristics. The procedures for the preparation of the SPIN samples are classified according to both the type of silica gel and the type of the linking reagent used.

Two types of silica gel have been employed in this study: 40 μm silica gel (Baker, flash chromatography; surface area = 480 m^2/g, pore diameter = 60 Å) and 150-75 μm silica gel (Davisil; surface area = 150 m^2/g, pore diameter = 150 Å)

In all cases 4-hydroxy-2,2,6,6-tetramethyl-piperidinyloxy (TEMPOL) free radical was used. The radical was attached to the silica gel surface using both silane and cyanuric linking agents. All procedures can be described in two steps: step one - is the attachment of the linking reagent to the silica gel surface, and step two - is the attachment of the free radical to the linking reagent. The syntheses were carried out either in benzene or in toluene (dried over Na, benzophenone) in a dry nitrogen atmosphere.

Procedure A: Preparation of **SPIN 1, 2, 3, 4, 5, and 6** Monoradicals:

The preparation of **SPIN 1**, Scheme 5.1, (which is sample

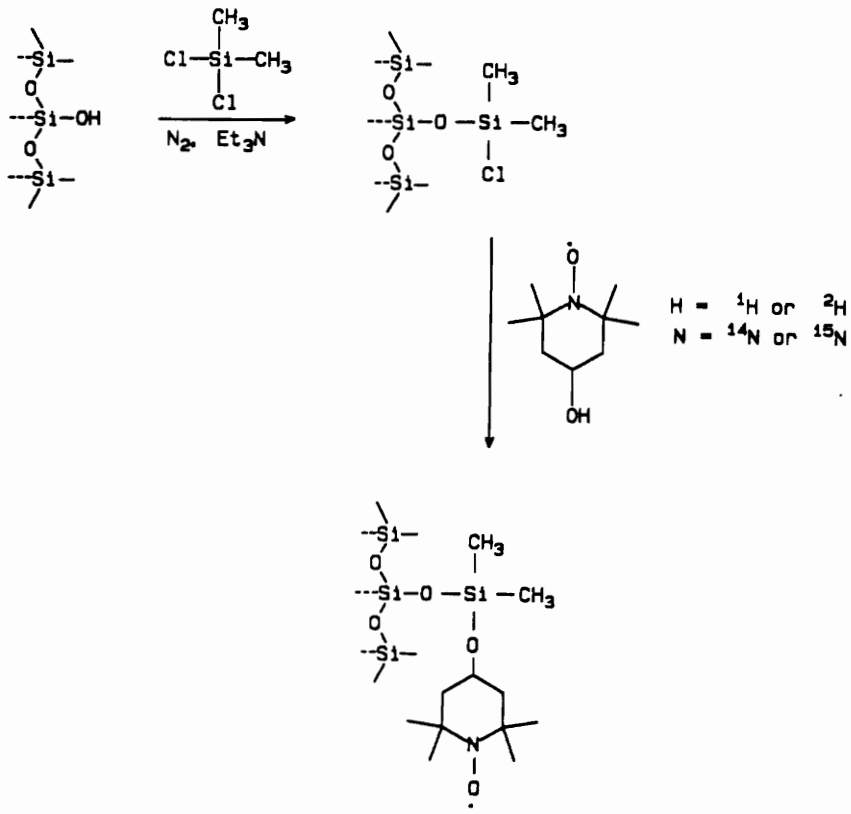

Scheme 5.1 Synthetic route for the preparation of SPIN monoradicals; linking reagent - Me_2SiCl_2.

#113[29] and "SPIN sample 2"[12] in previous studies) is described by Dorn at al.[12] A modification of the procedures described by Gilpin[35] and Wagner[36] was used to prepare two SPIN samples under different reaction conditions. In both cases the silica gel was prewashed (stirred) with concentrated HCl for 1/2 hour, subsequently distilled H_2O at room temperature, and finally dried at 80°C for about 45 min. Then the silica gel was heated to 200°C for 5 hours and cooled to room temperature in the presence of a gentle stream of dry nitrogen. The silica gel was transferred into the reaction flask in a nitrogen atmosphere in a glove box. The procedure for the preparation of the **SPIN 2** is described below:

To a stirred suspension of 2 g silica gel in 25 ml dry toluene in a three-neck flask was added 0.03 mL triethylamine (distilled over KOH and dried over 4 Å molecular sieves). The reaction flask was equipped with a soxhlet extractor containing freshly activated 3 Å molecular sieves. Step one: following the dropwise addition of a solution of 0.02 ml (0.16 mmol) dimethyldichlorosilane in ~20 ml dry toluene the reaction mixture was refluxed for 24 hours and then cooled to room temperature. Step two: A solution of 0.0234 g (~0.14 mmol) TEMPOL free radical in ~20 ml dry toluene was added dropwise to the derivatized silica gel. The suspension was refluxed for 24 hours. To ensure the absence of any remaining

unbonded material, the spin-labeled silica gel (**SPIN 2**) was washed with: 50 ml dry toluene, 100 ml water saturated toluene, 100 ml ether, 100 ml 50/50 2-propanol/water, 100 ml 2-propanol and 100 ml H_2O.

The **SPIN 3** sample was prepared under identical conditions as those described for the **SPIN 2** sample with the following difference. Following both the addition of the linking reagent in step one and the addition free radical in step two, **SPIN 3** sample was stirred for 24 hours at room temperature (according to the procedure described by Wagner[36]), while the **SPIN 2** sample was refluxed for 24 hours as described above.

In a separate experiment two SPIN radical samples (**SPIN 4** and **SPIN 5**) were prepared using the same procedure as that described for the **SPIN 2** sample above with the only difference that the silica gel was preheated at different temperatures as follows: for **SPIN 4** - the silica gel was heated at 400°C, for **SPIN 5**- the silica gel was heated at 600°C.

An additional SPIN sample (**SPIN 6**), was prepared under analogous conditions used for **SPIN 5** (that is, the silica gel was pretreated at 600°C and the procedure described above, procedure A was employed). However, procedure A was modified by treatment of the derivatized silica gel in step two with a

solution of 2,2,6,6-tetramethyl-4-piperidinol (Aldrich) instead of TEMPOL free radical. (Scheme 5.2). The immobilized amine was subsequently oxidized according to a procedure similar to that described by Bates et al.[41] as follows: to 1.3 g of the immobilized amine in 40 ml dry methylene chloride (distilled over P_2O_5) was added (for 30 min.) a solution of 0.05 g (0.3mmol) m-chloro-perbenzoic acid (mCPBA) in 6 ml dry methylene chloride. The mixture was stirred for 24 hours An additional 0.02 g (0.127 mmol) mCPBA was added for ~30 min. After another 3 hours of stirring the final product was washed the same way as described in procedure A.

In summary three groups of **SPIN** samples (**2** & **3**), (**2**, **4** & **5**), and (**5** & **6**) were prepared in order to examine the conditions for obtaining high radical concentrations on the surface of 40 μm silica gel.

Procedure B: Preparation of **SPIN 7**, **8**, **9**, and **10** Monoradicals (Scheme 5.1):

The choice of the silica gel (particle size = 150-75 μm; pore diameter = 150 Å) was based on the high surface radical concentration, reported in a study by Wagner et al.[36], where a silica gel with particle size = 70 μm and pore diameter = 200 Å was used, (See Ch. 4).

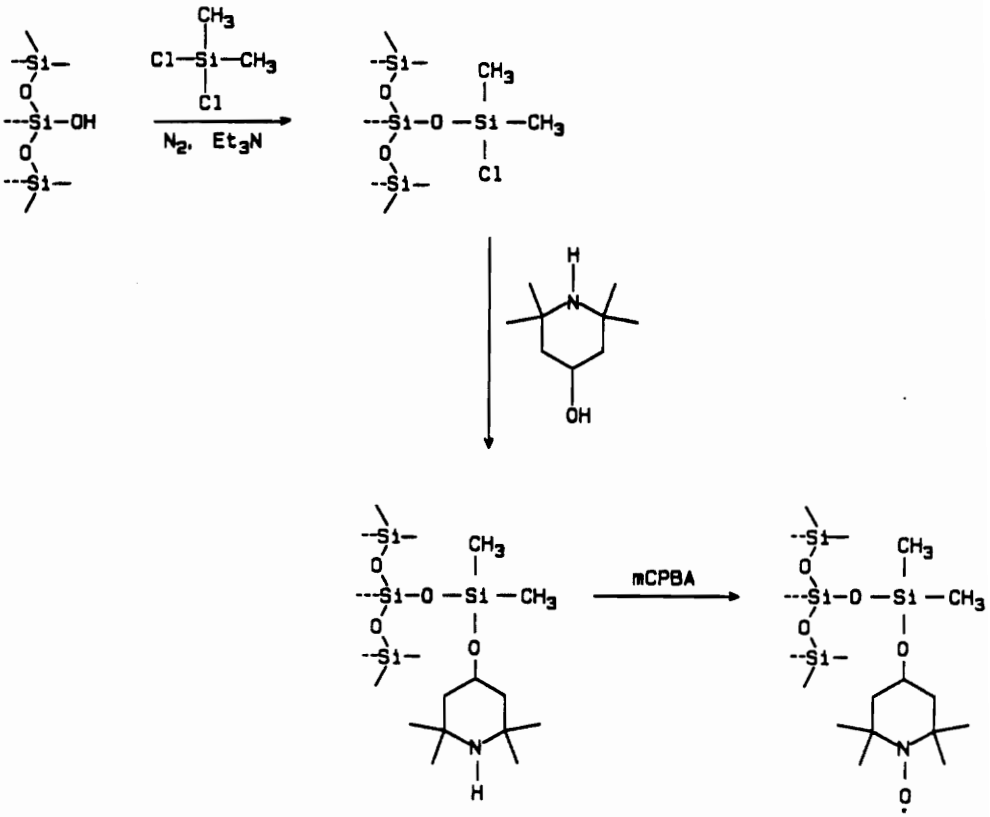

Scheme 5.2 Synthetic route for the preparation of **SPIN 6**; linking reagent - Me_2SiCl_2.

Procedure B.1: The SPIN sample (**SPIN 7**) was prepared by a modification of Wagner's[36] procedure (see Chapter 4). The silica gel used for this synthesis was prewashed with concentrated HCL and deionized H_2O, heated at 600°C in a nitrogen atmosphere for 5 hours, cooled, and transferred into a three-necked flask also in the presence of nitrogen. Step 1: to 2 g of the silica gel was added 9 ml dry triethylamine (distilled over KOH and dried over 4 Å molecular sieves) in 100 ml anhydrous toluene. To the above mixture was added dropwise a solution of 0.042 ml (0.35 mmol) dichlorodimethylsilane and 1 ml dry triethylamine in 9 ml dry toluene. The suspension was refluxed for 24 hrs, then cooled to room temperature. Step 2: A solution of 0.21 g (1.2 mmol) TEMPOL in 10 ml dry toluene was added dropwise to the above mixture which then was refluxed for 24 hours and the solvent was removed (while still hot) by filtration through a small, coarse-fritted filter stick. The final product was washed with ~ 150 ml chloroform.*

*It should be noted that a separate experiment showed no change in the number of spins for two identical samples, one which was washed with chloroform and the other washed as described in procedure A above).

It turned out that immediate filtration of the spin-labeled silica gel (while the mixture is still very hot) is very important in terms of obtaining samples with good flow characteristics. In cases where the reaction mixture was cooled or left stirring at room temperature, the removal of the by-products was incomplete, which resulted in an increase of the back pressure with the increase of the flow rate used for the DNP experiment. In some cases it was impossible to use a flow rate higher than 1.5 to 2 ml/min.

Procedure B.2: Three SPIN radicals (**SPIN 8, 9 & 10**) were prepared using a modification of the Wagner's[36] procedure according to Scheme 5.1. The three samples were prepared under identical conditions except that: TEMPOL (^{1}H, ^{14}N) was used for **SPIN 8**, TEMPOL (^{2}H, ^{14}N) was used for **SPIN 9**, and TEMPOL (^{2}H, ^{15}N) was used for **SPIN 10**.

Both isotope labelled free radicals were synthesized in our laboratory by Andrea Stossel.

In contrast to all cases described above, the silica gel was not prewashed with concentrated HCL, because a separate experiment did not confirm any improvement due to the acid wash. A thermal pretreatment employed for all three samples was analogous to that described in procedure B.1. However, the samples were heated at 800°C (instead of 600°C).

A substantial difference in the preparation of SPIN radicals: **SPIN 8, 9** and **10** relative to that for **SPIN 7** (described in Procedure B.1 above) is the relative mole ratio of the linking reagent, for a fixed amount of silica gel. In all cases, the ratio TEMPOL/linking reagent was kept equal to 3/1 (that is, a large excess of TEMPOL radical was used). As already mentioned above, **SPIN 9** and **SPIN 10** were prepared in an identical manner to that used for **SPIN 8**, however, because of the limited amount of isotope substituted TEMPOL radicals available the procedure for the preparation of **SPIN 9** and **SPIN 10** was scaled accordingly.

With the above in mind, the procedure for the preparation of **SPIN 8** is as follows: Step 1: Silica gel (1 g) in 100 ml dry toluene and 0.9 ml triethylamine was added dropwise a solution of 0.035 ml (~0.29 mmol) dimethyldichlorosilane and 0.1 ml triethylamine in 10 ml dry toluene. The suspension was refluxed for 24 hours, then cooled to room temperature. Step 2: A solution of 0.150 g (0.87mmol) TEMPOL free radical in 30 ml toluene was added dropwise to the above mixture which then was refluxed for 24 hours, filtered while it was hot, and washed over the filter with 200 ml chloroform.

Procedure C: Preparation of Sample **SPIN 11** : linking reagent methyltrichlorosilane; 150-75 μm silica gel.

Sample **SPIN 11** was prepared in a similar manner as described above for sample **SPIN 8**. However, methyltrichlorosilane was use for the linking reactions (see Scheme 5.3) and the mole ratio linking reagent/Silica gel for SPIN radical 11 was 5 times greater than that for SPIN radical 8. The ratio TEMPOL/linking reagent was kept equal to 3/1. Step 1: Silica gel (2 g) and 4 ml triethylamine in 100 ml dry toluene was added dropwise a solution 0.374 g (2.5 mmol) methyltrichloro - silane in 9 ml toluene and 1 ml triethylamine. The suspension was refluxed for 24 hours. Step 2: After cooling to room temperature, a solution of 1.27 g (7.4 mmol) TEMPOL in 40-50 ml dry toluene was added dropwise to the above mixture which was then refluxed for 24 hours, filtered while it was hot and washed with about 150 ml chloroform.

Table 5.1 summarizes the different conditions for the preparation of the achiral SPIN samples using dimethyldichlorosilane (Me_2SiCl_2) and methyltrichlorosilane ($MeSiCl_3$) as linking reagents. Representative examples are given for samples for which the conditions given in Table 5.1 were identical. In particular, the following samples are not included in the table: **SPIN 3** (see **SPIN 2**); **SPIN 6** (see **SPIN 5**);**SPIN 9** and **SPIN 10** (see **SPIN 8**).

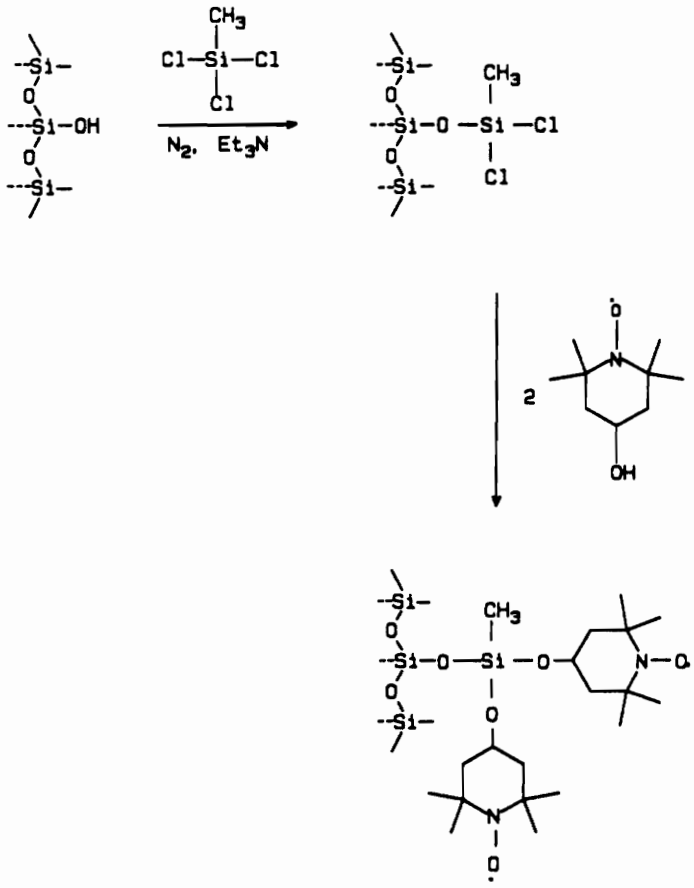

Scheme 5.3 Syntetic route for the preparation of **SPIN 11**; linking reagent - $MeSiCl_3$.

Table 5.1: **Reaction conditions for preparation of SPIN samples.**

SPIN radical	Silica gel (μm)	Silica gel grams used	Silica gel Chemical Pretreat.	Silica gel Thermal Pretreat.	Linking reagent (mmol)	TEMPOL (mmol)
1	40	2	c. HCL	110°C, vac.	Me_2SiCl_2/0.16	0.14
2	40	2	c. HCl	200°C, N_2	Me_2SiCl_2/0.16	0.14
4	40	2	c. HCl	400°C, N_2	Me_2SiCl_2/0.16	0.14
5	40	2	c. HCl	600°C, N_2	Me_2SiCl_2/0.16	0.14
7	150-75	2	c. HCL	600°C, N_2	Me_2SiCl_2/0.35	1.18
8	150-75	2	none	800°C, N_2	Me_2SiCl_2/0.58	1.74
11	150-75	2	none	800°C, N_2	$MeSiCl_3$/2.5	7.4

Sample 1 was used in previous SLIT DNP studies and it is included in the table for comparison.

5.1.3 Preparation of Chiral SPIN Samples.

The purpose of the syntheses of chiral spin samples was to provide a chiral a nitroxide radical system immobilized on a silica gel surface which can be used to measure the DNP enhancement for enantiomeric pairs (R or S) of solutes dissolved in the flowing liquid.

Two chiral SPIN samples have been prepared: **SPIN 12** and **SPIN 13** by immobilizing R-(+)-3-carboxy-2,2,5,5-tetramethyl-1-pyrrolidinyloxy (3-carboxy-PROXYL) free radical, and R-(+)-3-hydroxymethyl-2,2,5,5-tetramethyl-1-pyrrolidinyl-oxy, (3-hydroxymethyl-PROXYL) free radical, respectively.

Procedure A: Resolution of (±)-3-Carboxy-PROXYL Free Radical. The procedure for the preparation of the R-(+) 3-carboxy-PROXYL free radical Scheme 5.4 (a) was similar to that described by Flohr et al[42]. The racemic acid was resolved by making a salt from equimolar amounts of (±)-3-carboxy-PROXYL radical and the resolving agent - S-(-)-α-methylbenzylamine (S-(-)-αMeBA); the solvent used for the recrystallizations was acetone. The (±)-3-carboxy-PROXYL radical, 3.73 g (0.02 mol), (Aldrich) and 2.58 ml (0.02 mol) S-(-)-αMeBA (Aldrich) were dissolved in 150 ml acetone. The crystals, after standing at

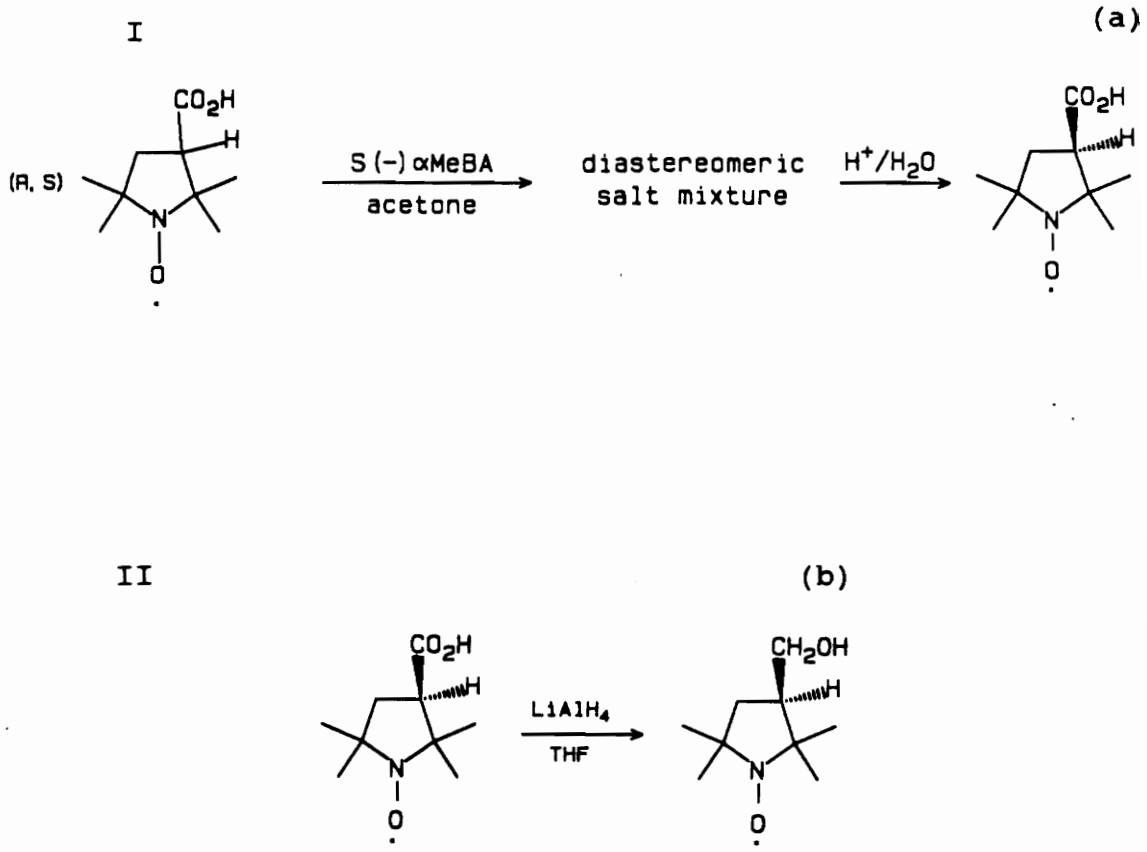

Scheme 5.4: (I)-preparation of R-(+)-3-carboxy-PROXYL radical,(a). (II)-preparation of R-(+)-3-hydroxymethyl-PROXYL radical, (b).

room temperature for 12 hours, were filtered (the weight of the crystals was 2.5 g), redissolved in about 80 ml acetone, left at room temperature for 12 hours, and filtered. The weight of the crystals after the second recrystalization was 1.3 g. The salt was dissolved in ~40 ml H_2O and acidified with ~100-120 ml 0.02N HCl (pH ~4). The resolved R-(+)-carboxy-PROXYL radical was extracted with ~200 ml ether (4×50), dried over anhydrous $MgSO_4$ and the solvent was evaporated. The final yield was 0.53 g.(28%), mp 202-205°C.

Procedure B). Preparation of R-(+)-3-Hydroxymethy-PROXYL Radical (Scheme 5.4 (b)).

The R-(+)-alcohol was prepared according to the procedure described by Gaffney[36] as follows: 0.5 g (2.68 mmol) of R-(+)-3-carboxy-PROXYL radical was dissolved in 20 mL. dry THF in nitrogen atmosphere. A 2.9 ml 1M solution of $LiAlH_4$ in THF was introduced dropwise over 1/2 hour in the above solution cooled in an ice-water bath. The reaction mixture was stirred for 4 hours at room temperature. The excess $LiAlH_4$ was decomposed by careful addition of a saturated aqueous solution of Na_2SO_4 until the white salt coagulated. The THF layer was decanted and dried over anhydrous $MgSO_4$. The dried solution was filtered and evaporated to give 0.4 g (87% yield) R-(+)-3-hydroxymethyl-PROXYL free radical. (m.p. 114-115°C, lit. m.p. 112°C).

Procedure C: Preparation of the Chiral **SPIN 12** Sample, (Scheme 5.5). The chiral **SPIN 12** sample was prepared using a modification of the procedure for a preparation of N-n-valeryl-L-valyl-aminopropylsilanized silica described by Hara et al.[43]

Aminopropyl silica gel (Baker, 10 μm) was used for this synthesis. The silica gel was dried in vacuum for 8 hours at 80°C. To a suspension of 0.2 g aminocapped silica gel in 8 ml dimethylformamide (DMF) (degassed in vacuo for 5 min) was added 1-hydroxybenzotriazole, 0.052 g (0.38 mmol), in 3 ml DMF and R-(+)-3-carboxy-PROXYL radical, 0.05 g (0.27 mmol). The resulting mixture was treated with a solution of 0.057 g (0.27 mmol) dicyclohexylcarbodiimide (DCC) in 3 ml DMF at 0°C for 30 min with stirring, and then stirred at room temperature for 48 hrs in nitrogen atmosphere. The spin-labeled silica gel was separated by centrifugation and washed with 50 ml chloroform (in small portions, centrifuged after the addition of each one). Then the sample was transferred in a small coarse-fritted filter and washed successively with 50 ml chloroform, 50 ml acetone, 50 ml methanol, and 50 ml ether.

Procedure D: Preparation of the Chiral **SPIN 13** Sample, (Scheme 5.6). The procedure employed is similar to the one used for SPIN radical 11, described above. The silica gel (150-75 μm) was preheated at 800°C for 5 hours. In Step 1, to

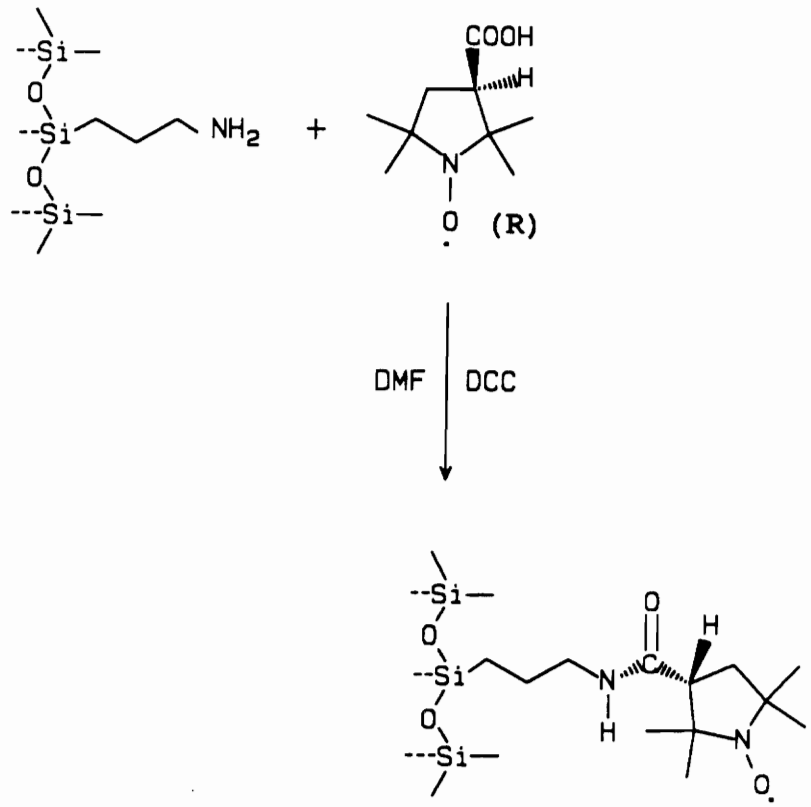

Scheme 5.5 Synthetic route for the preparation of the chiral **SPIN 12**.

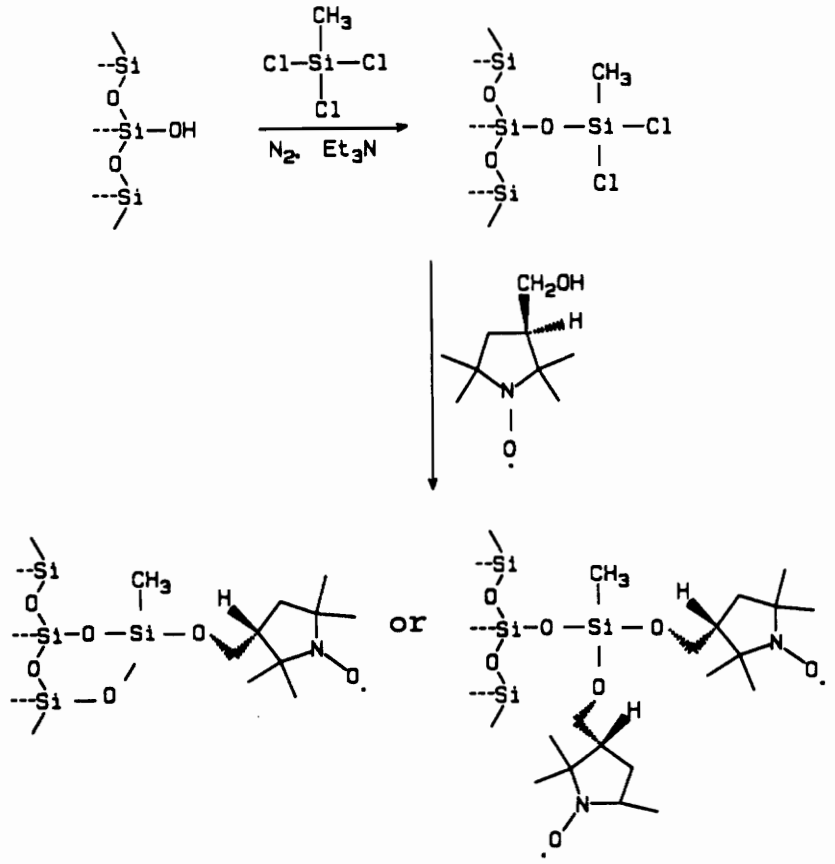

Scheme 5.6 Synthetic route for the preparation of the chiral **SPIN 13.**

silica gel (1 g) and 0.9 ml triethylamine (Et_3N) in 40 ml toluene was added a solution of 0.06 ml methyltrichlorosilane and 0.1 ml Et_3N in 10 ml toluene. The mixture was refluxed for 22 hours and then cooled to room temperature. Step 2: A solution of 0.25 g R-(+)-3-hydroxymethyl-PROXYL radical in 30 ml toluene was added for about 40 min and subsequently the suspension was refluxed for 22 hours, filtered while hot, washed with toluene and finally washed with chloroform. It should be noted that **SPIN 14** and **SPIN 15**, e.g. the racemic (±)-analog of the **SPIN 12** and **SPIN 13** respectively, were prepared by immobilizing the (±)-acid and the (±)-alcohol, respectively under identical conditions. The procedure and the amount of the reagents were identical.

5.1.4 Preparation of Long Chain Achiral SPIN Samples

Procedure A: Preparation of the Long Chain **SPIN 16** Sample: linking reagent - cyanuric chloride; 40 μm silica gel. A modification of the procedures described previously[9,34] was used to immobilize TEMPOL free radical on a silica gel surface pretreated with a long chain diol according to Scheme 5.7. The silica gel was prewashed with concentrated HCl (20 min. at room temperature) and distilled water and subsequently dried in a vacuum oven at 120°C for ~20 hours The procedure is

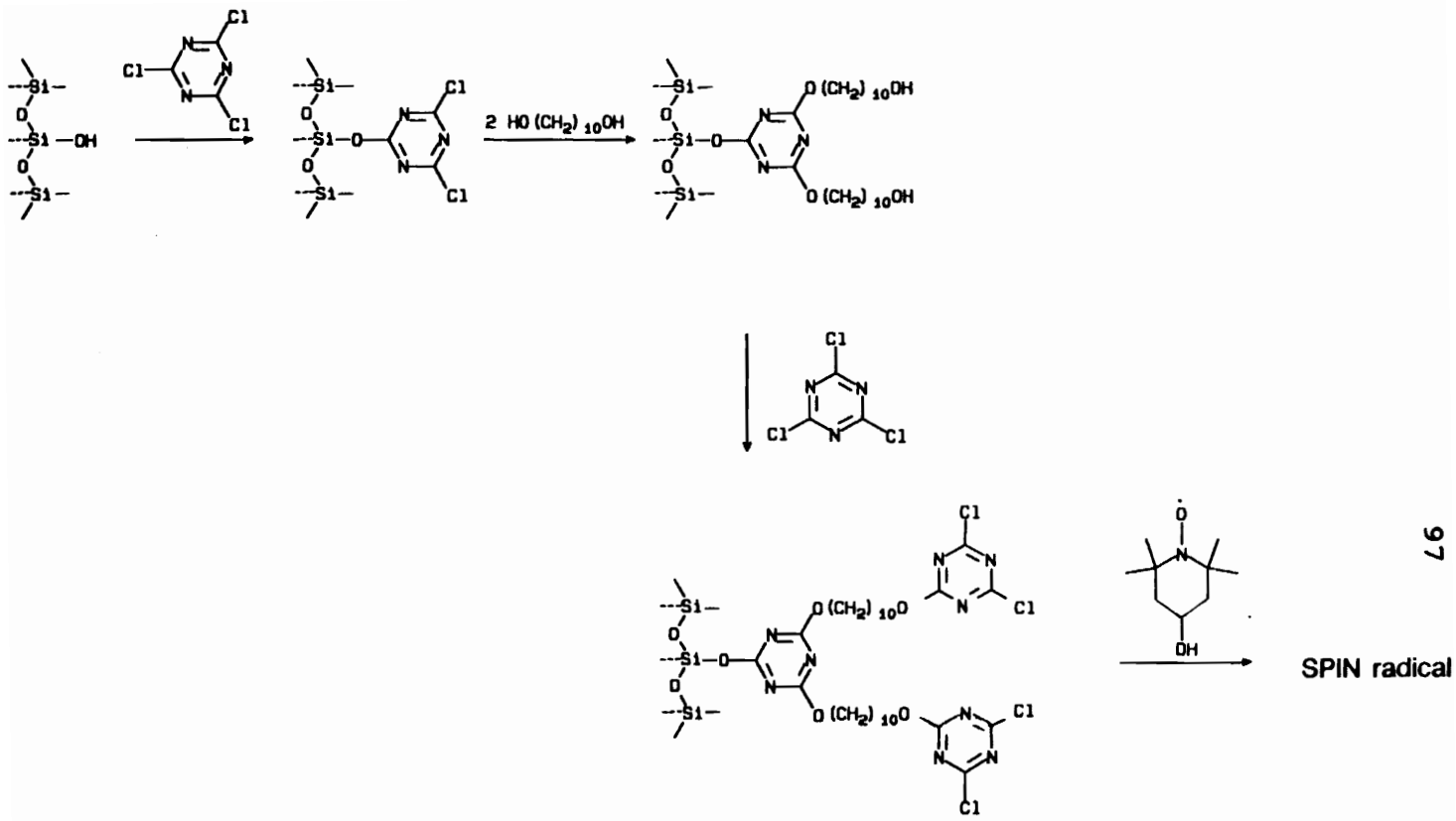

Scheme 5.7 Synthetic route for the preparation of a long-chain SPIN biradical; linking reagent-cyanuric chloride.

outlined below:

In a three-necked flask equipped with a soxhlet extractor containing freshly activated 3 Å molecular sieves was added 5 g of the silica gel and ~25 ml dry benzene. Step one: 0.063 g (0.340 mmol) cyanuric chloride in 25 ml dry benzene was added in the flask dropwise at room temperature and the reaction mixture was refluxed for 4 hours, under nitrogen. The mixture, after standing at room temperature for 12 hours, was filtered and the solid was washed with dry hot benzene. The derivatized silica gel, scheme 5.1, was resuspended in 25 ml of dry benzene and a hot solution of 0.118 g (6.8 mmol) of 1,10-decanediol (Aldrich) was added dropwise to the stirred suspension. The mixture was refluxed under nitrogen for 1 hour, then the silica gel, was filtered, and washed with dry benzene and subsequently ~3 g was refluxed with 0.063 g (0.034 mmol) cyanuric chloride in 25 ml benzene for 3 hours, then filtered and washed. Step two: the derivatized silica gel, was stirred at room temperature with 0.03 g (0.169 mmol) TEMPOL dissolved in 20 ml dry benzene (the TEMPOL solution was added dropwise to the reaction mixture) overnight. The final product was filtered and washed with dry benzene.

Procedure B: Preparation of the Long Chain **SPIN 17** Sample: A separate syntheses utilized 1,8 (chlorodimethyl-

silyl) octane as a linking reagent to prepare another long-chain SPIN sample (Scheme 5.8). 40 μm particle size silica was used. The procedure for the preparation was identical to that reported by Dorn[12]. In addition the same synthesis was carried out in toluene. The SPIN sample prepared in toluene exhibited a larger (by a factor 1.7) surface spin concentration than that for the case of benzene under identical conditions. However, relatively small SLIT DNP enhancements were reported for both cases(benzene and toluene) which was attributed to the relatively low surface spin density for this SPIN system.

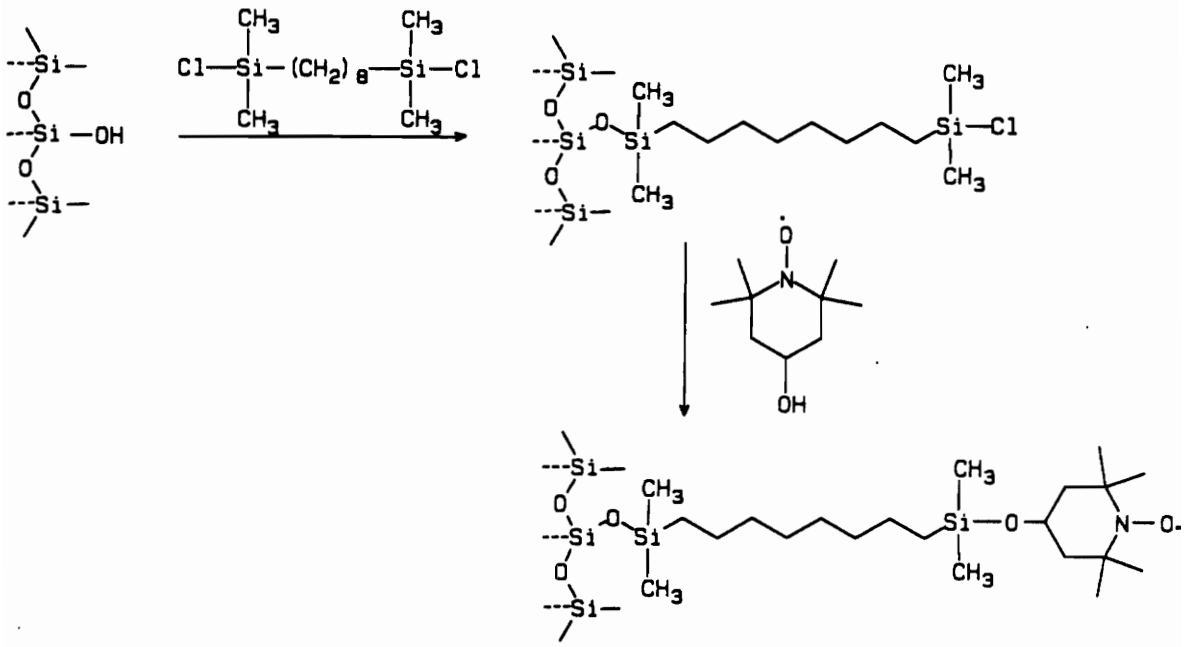

Scheme 5.8 Synthetic route for the preparation of a long-chain SPIN radical; linking reagent- 1,8 bis (chlorodimethyl-silyl) octane.

5.2 EPR Measurements

All EPR spectra were measured at room temperature using an IBM ER 200 D-SRC X-band spectrometer. The number of immobilized radicals in a given sample, N_x was obtained from EPR measurements relative to the number of spins, N_s in a standard sample according to the procedure reported by Swartz et al.[44].

$$N_x = \frac{H_{ms}\sqrt{P_s}\,G_s\Sigma_x}{H_{mx}\sqrt{P_x}\,G_x\Sigma_s}N_s \qquad 5.1$$

where subscript s and x designate the standard and unknown sample, respectively, H_m, the modulation amplitude, P, the microwave power, G, the overall spectrometer gain, and Σ, the integral of the EPR absorption over the entire signal. In our studies, Σ was estimated by the weight of the entire area under the EPR signal. A 2.6 M solution of DPPH (2,2-diphenyl-1-picrylhydrazyl hydrate) free radical in degassed benzene was used as a standard solution. 10 μL in an EPR tube from the solution was used as a standard sample. The absolute number of spins in this DPPH standard sample was $1.5*10^{17}$ spins. Usually about 0.005 g (which corresponds to a comparable magnitude ($\sim10^{17}$ spins) absolute number spins of the sample relative to the number spins of the standard SPIN sample of unknown

concentration in degassed benzene was used for the above measurements. The number spins per gram were calculated from the absolute number of spins (estimated from the weight of the area under the EPR signal) divided by the weight of the SPIN sample used.

It is important to note that this method gives the bulk or average concentration of the spins in the sample. However, the local rather than bulk concentration is the concentration that determines spin-spin interactions and power saturation characteristics. Wyard[47] has reviewed methods for estimating local concentrations, but the latter have not been calculated for the purposes of this study.

5.3 DNP Measurements

5.3.1 Experimental Design

The experimental set-up used for low to high transfer DNP studies was analogues to that used by Tsai[11]. (Fig. 3.3). Specifically, a variable electromagnetic field (B_o^L = 0 ~ 0.6 T) has been placed directly underneath a 4.7 T superconducting magnet. The center of the two magnetic fields are orthogonal and separated by a distance of 1.2 m. The influence of the electromagnet (even at 0.6 T) on the homogeneity of the superconducting magnet was very small[11]. The high magnetic

field (B_o^H) NMR detector is a wideband Jeol FX-200 NMR spectrometer with the ^1H resonance of 199.5 MHz. The NMR probe was homebuilt using a standard capacitor tuning and matching circuit. Helmholtz coils for detection were employed. The liquid sample was recycled by an SSI Model 200 HPLC pump with a flow rate ranging from 0.05 to 9.99 ml/min. The only difference in the experimental set-up in our study was that the microwave source (ω_e = 9.3 GHz) was provided by a Bruker EPR klystron (not shown in Fig. 3.3) and transferred (via low loss cables) to the system. The amount of microwave power was adjusted with an attenuator and subsequently amplified to ~25 Watts with a Varian "K" series TWT amplifier. The variable low field magnet (B_o^L) and the microwave TE_{102} cavity were part of a modified Varian E-3 EPR spectrometer.

Using the above experimental set-up the volume in the microwave region is 160 μl and about 30 μl without and with the immobilized sample respectively. The transfer volume is 15 μl and the NMR detection region volume - 20 μl (for ^1H DNP measurements) and 150 μl (for ^{13}C DNP measurements).
The static ^1H resolution was 3-4 Hz.

5.3.2 Sample Preparation

In all cases 0.1 g of a SPIN sample was packed to a

height of 1 cm and centered in the microwave cavity. The flowing liquids were deoxygenated by bubbling dry nitrogen through the solution prior and during the experiments.

Prior the chiral SLIT DNP measurements, the immobilized chiral SPIN sample in the EPR tube was washed with: ~10 ml 1,4 -dioxane, 12 ml CH_3OD, then flushed with 1,4-dioxane until the NMR signal of CH_3OH disappeared, ~2 ml 1,4-dioxane-d8, and finally with ~2 ml 45% solution of a specific enantiomer of bromo- camphor in 1,4-dioxane-d_8.

5.4 Estimation of the Ultimate Enhancements

The enhancements without either build up or transfer losses, A/K, which correspond to the low field DNP enhancement, A, where estimated from the plot of the observed enhancements, (ln) A_{obs}, versus the inverse floe rate.(see Eq. 3.5). The values of A/K were calculated by a linear regression analysis for the first four points of the linear part of the plot (ln)A_{obs} vs. 1/Flow Rate (That is, flow rate from 1.5 ml/min (or 1/FR =0.67) to 3 ml/min (1/FR = 0.33)). The obtained values were then corrected for saturation, e.i. the enhancements corresponding to complete saturation, A_∞ (or A/K for s=1), were calculated from the plot $1/-A_{obs}$ versus the

inverse power, P^{-1} (see Eq. 2.24). Representative $\ln(A_{obs})$ vs. 1/FR, and 1/-A vs. 1/P plots are presented in Fig. 5.1. For example, for **SPIN 7** the intercept from the saturation plot is ln(0.185) which corresponds to an enhancement at infinite microwave power, A_∞, equal to 5.4. From the ratio of the maximum observed enhancement, A_{obs} (= -4.3), and A_∞ (-5.4) the saturation factor of 0.8 was calculated. From the intercept of the plot $\ln(A_{obs})$ vs. 1/FR, (intercept = ln 1.8) a value of 6.1 was estimated for the A/K factor which corrected for saturation (6.1/0.8) gave a value of 7.6 for A/K (s=1).

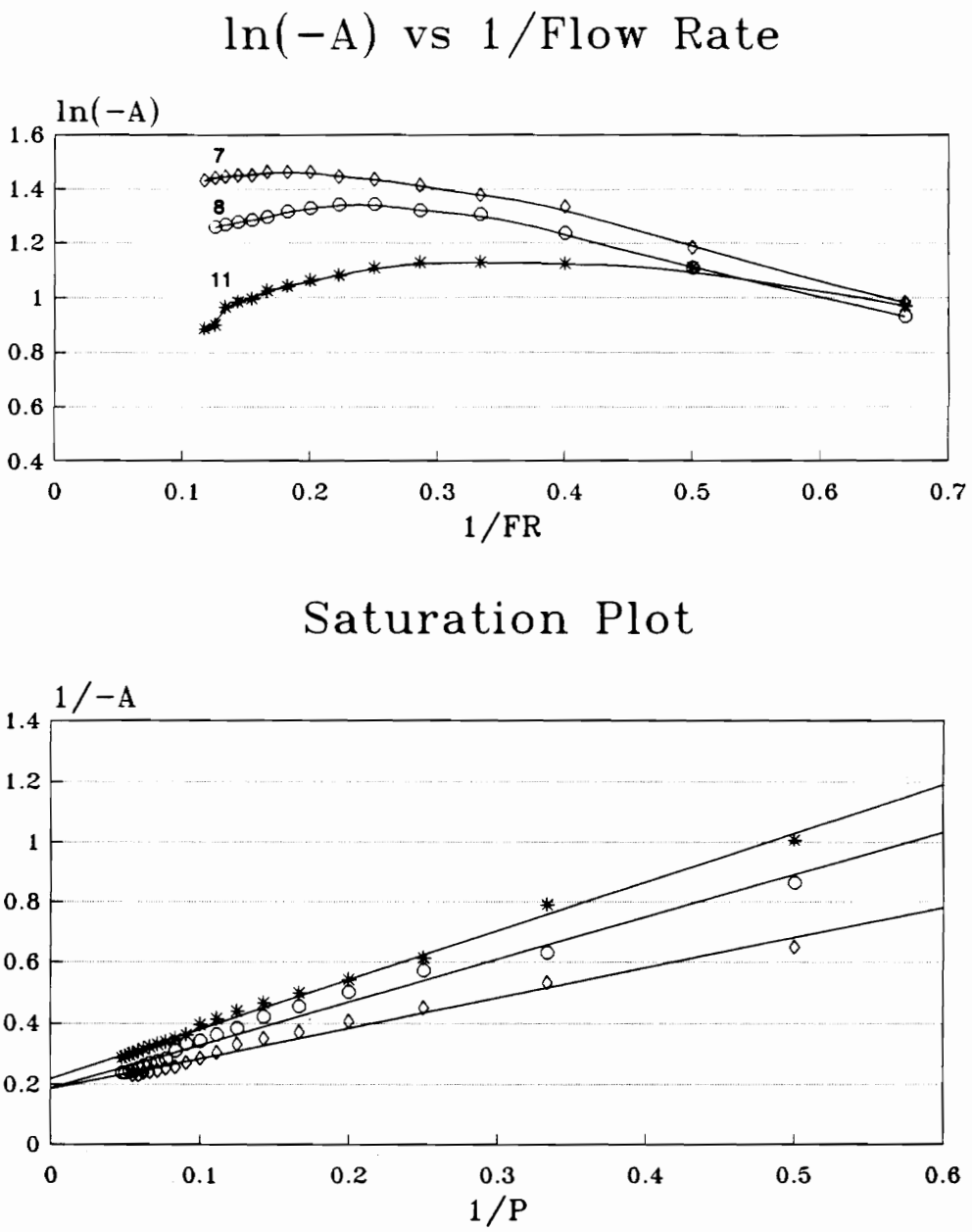

Fig.5.1 Plots for the calculation of: **SPIN 7, 8, 11**/benzene (a) the enhancement without either build up or transfer losses, A/K, and (b) the saturation factor.

CHAPTER 6

RESULTS AND DISCUSSIONS

6.1 EPR Characterization of SPIN Samples.

6.1.1 EPR Characterization of Achiral SPIN Samples.

The EPR spectrum of the long-alkyl chain immobilized nitroxide radical, **SPIN 16** is represented in Fig. 6.1. The preparation of this sample was (see Ch.5.2.1,A) intended to provide a SPIN sample for DNP measurements with a relatively narrow DNP linewidth. As previously mentioned, the long-chain SPIN mono-radical (linking reagent, dimethyldichlorosilane) prepared before exhibited low surface spin concentration and was not utilized for DNP measurement. The preparation of a long-chain biradical (with linking reagent, cyanuric chloride), was expected to provide a SPIN sample with higher mobility (shorter τ_c). Two important features can be concluded in comparing the EPR spectrum of the long-chain SPIN sample Fig. 6.1) to the EPR spectrum of a short-chain SPIN sample, prepared under identical conditions: one is that the observable decrease in the linewidth (for the long-chain SPIN biradical) is very small, and second the area under the entire

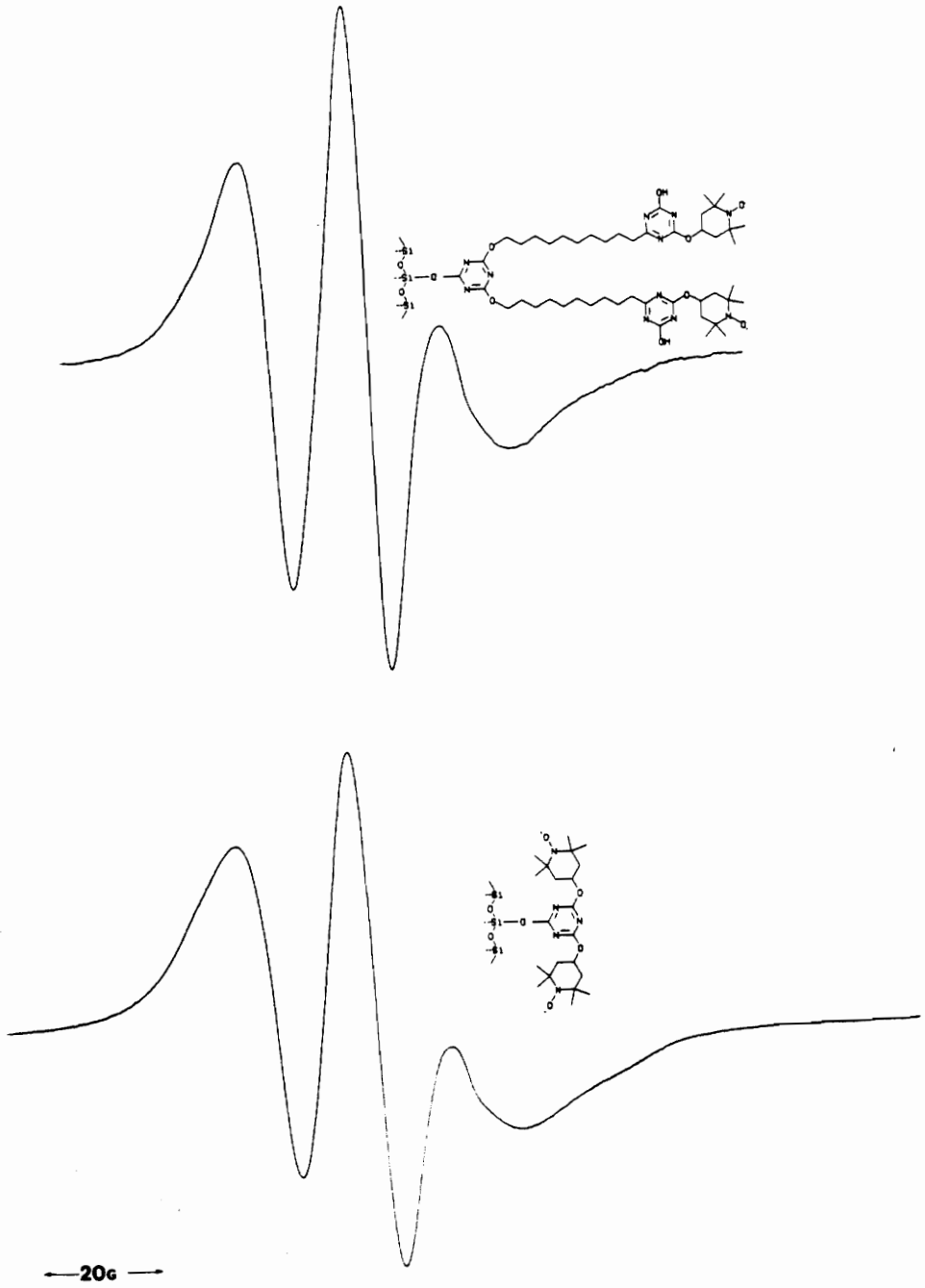

Fig. 6.1 Effect of the length of the alkyl chain on the EPR line width. The EPR spectra of 0.015 g sample in benzene, for both cases, were run under identical conditions.

signal for both samples is comparable (which is what was expected). The decrease in the linewidth can presumably be attributed to higher mobility for the case of the long chain SPIN system. Also, it should be pointed out that the synthetic route outlined in Scheme 5.7 is only a proposed pathway. There was no evidence to support that this was the only (or predominant) reaction pathway. A possible bonding of the chain may cause an attachment of both ends to the surface. Based on both the above result (no drastical change in the EPR line width) and on later study[9], which reported instability ("bleeding" of the spins) for a similar SPIN sample in the presence of polar solvents, the above long-chain SPIN biradical, **SPIN 16**, was not used for DNP measurements.

In Fig. 6.2 are represented the EPR spectra for two SPIN samples, prepared under identical conditions except that the synthesis of **SPIN 3** (Fig 6.2,a) was carried out at room temperature (as reported in previous studies), while for **SPIN 2** (Fig 6.2,b) the reaction mixture was refluxed (see Ch. 5.1.2). It is obvious that the second approach (when the mixture was refluxed) gives a higher spin count (about 16 times higher spin density). In addition, the SPIN sample which was refluxed was found to exhibit better flow characteristics relative to the samples prepared at room temperature.

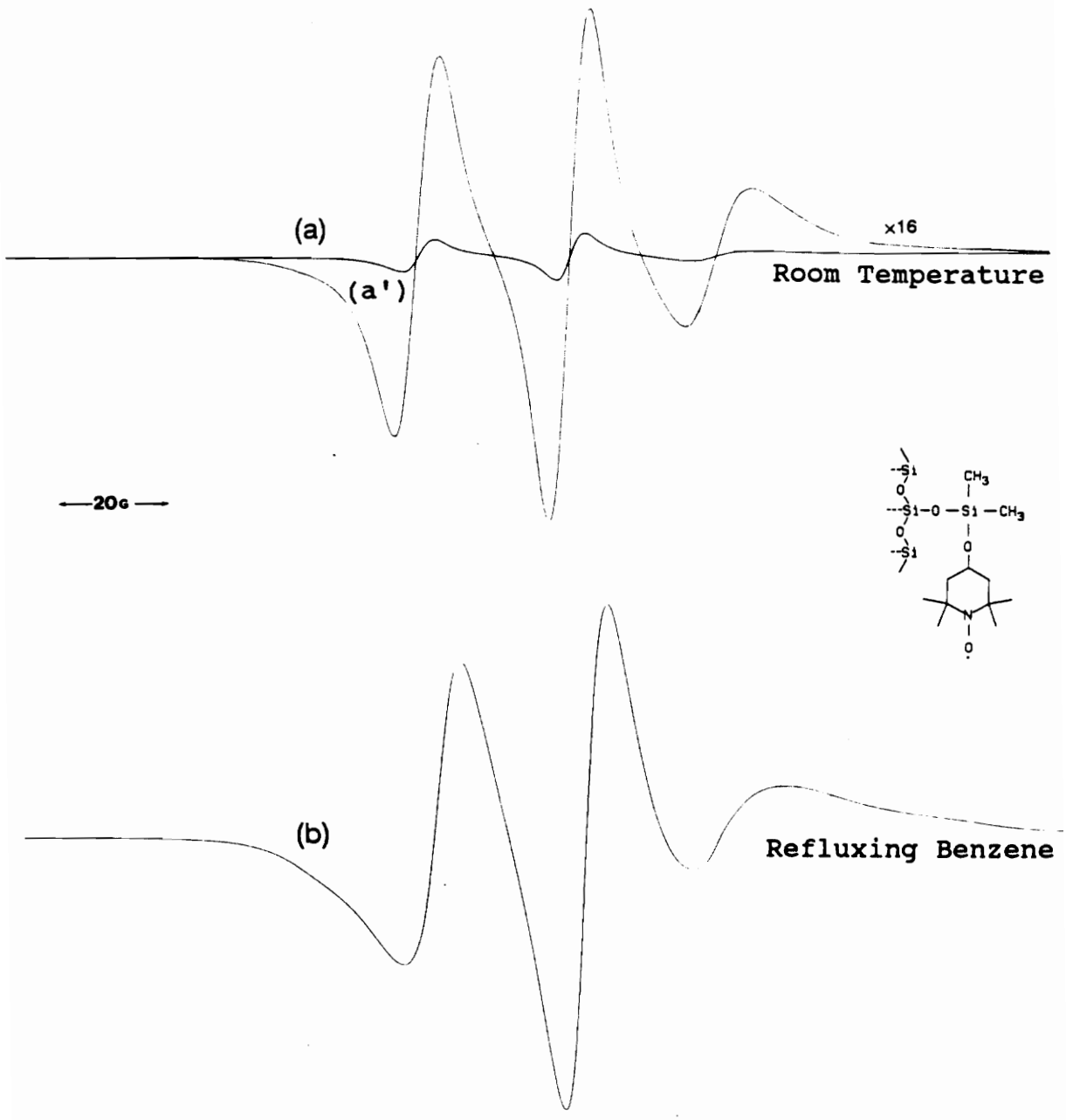

Fig. 6.2 Effect of the reaction conditions on the spin number. 0.015 g sample in benzene was run under identical conditions for (a) and (b). About 16 times larger gain was used for (a')

A separate study, examined the effect of the thermal pretreatment of the silica gel on the achievable surface spin concentration. For the three samples presented in Fig. 6.3, the silica gel was preheated at three different temperatures as follows: 200°C, 400°C, and 600°C for **SPIN 2**, **4**, and **5** respectively. This study was based on the previous results reported by Wagner et al.[36] In their study, large improvements in unpaired spin concentration were reported for 2 samples when the temperature of the silica gel pretreatment was increased from 200 to 600°C, for the ratio of the TEMPOL/LR = 3/1. In contrast, the results from the EPR measurements (Fig. 6.3) in our study show almost no difference in the spin count for the three samples. As discussed by Wagner (see Ch.4), the vicinal silanol groups are removed during the thermal pretreatment of the silica gel. Heating above 200°C causes liberation of water through condensation of hydrogen-bonded silanol pair to give Si-O-Si siloxane linkages thus increasing the fractional population of the isolated silanol groups which are the most reactive groups on the surface. Presumably, the effect of the removal of the vicinal silanol groups is important for higher relative ratio of the linking reagent. Another possible explanation for our results could be the different surface topology (the silica gel used in our

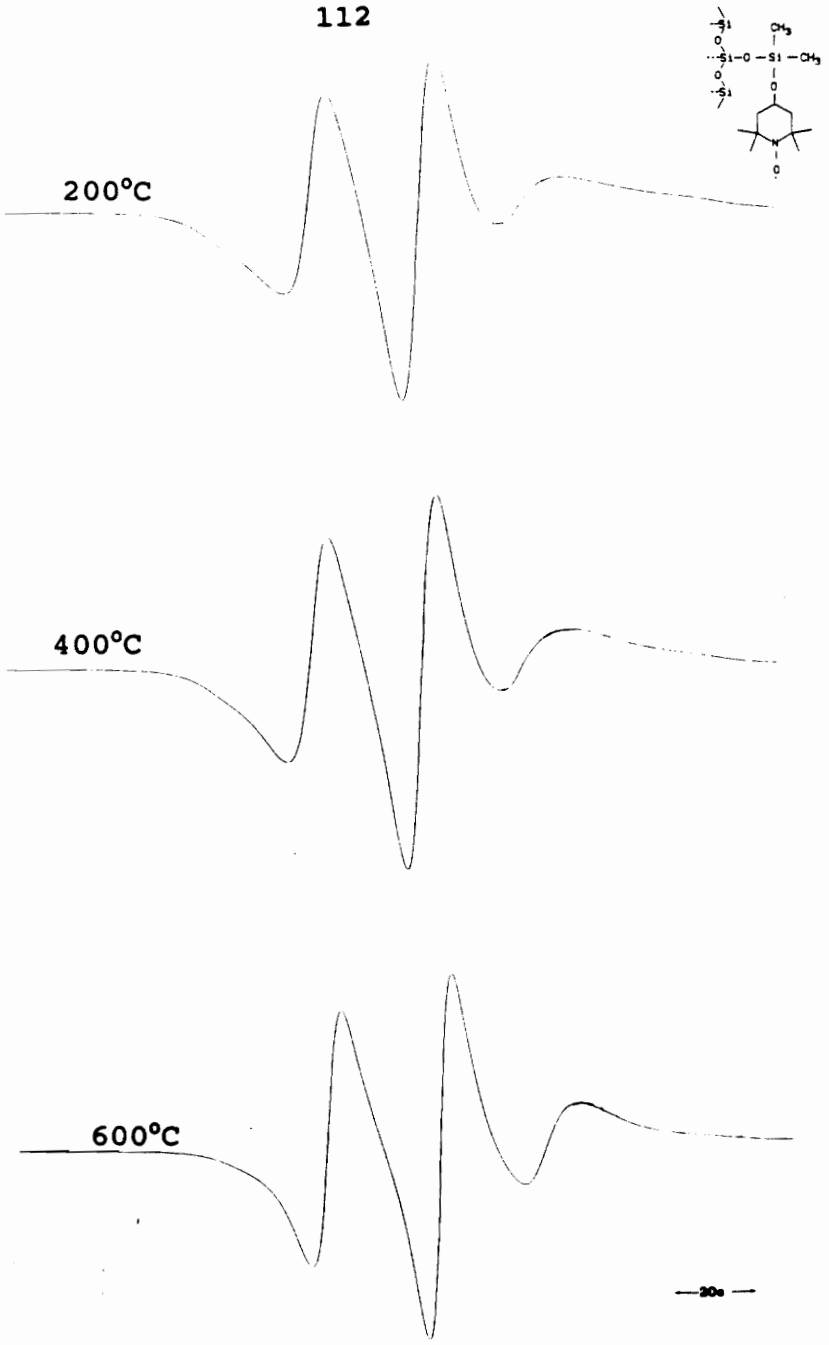

Fig. 6.3 Effect of the silica gel pretreatment on the spin concentration. The EPR spectra (0.015 g sample in benzene) were run under identical conditions for all samples.

study was of smaller particle size and smaller pore diameter) which determines the extent to which the neighboring (vicinal) silanols exist as hydrogen-bonded pairs.

In a different experiment, an attempt to immobilize the amino precursor and consequently oxidize it to the corresponding radical resulted in much smaller surface-spin density relative to that obtained for the direct immobilization of the same radical on the silica gel surface. The EPR spectra for these two samples, **SPIN 5** (the radical was immobilized directly), and **SPIN 6** (the corresponding amine was immobilized and than oxidized) are presented in Fig. 6.4.

In summary, all SPIN samples discussed so far exhibited relatively low surface spin concentration - not much different from the concentration of the SPIN samples used in previous DNP studies[12]. The comparison of the EPR spectra in benzene and methanol of a representative example, **SPIN 5**, (Fig. 6.5) indicates a significant decrease of the EPR line width in the presence of methanol which can be attributed to the increased mobility of the system in the presence of the higher polarity solvent.

Based on the results discussed so far, two SPIN radicals,

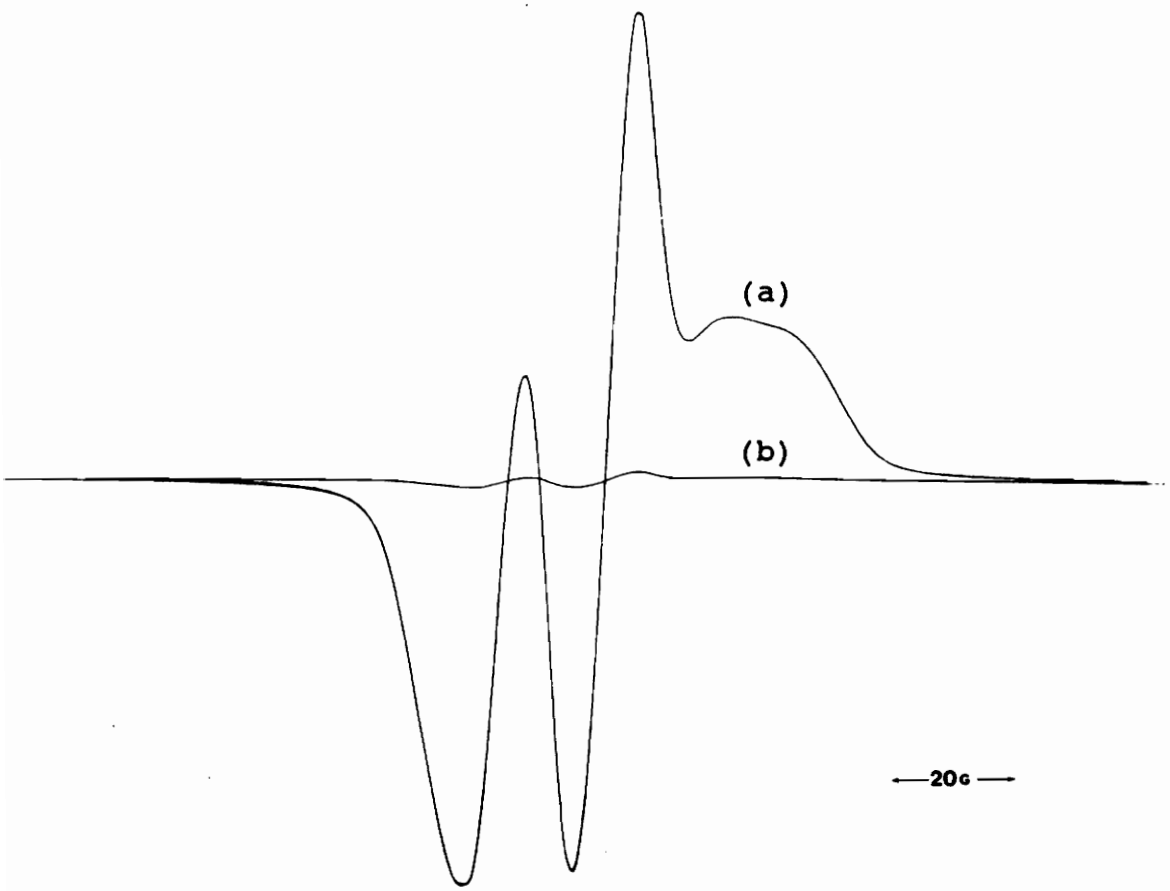

Fig. 6.4 EPR spectra of directly immobilized radical, **SPIN 5** (a), and of the oxidized amino-precursor, **SPIN 6**, (b) 0.015 g sample in benzene.

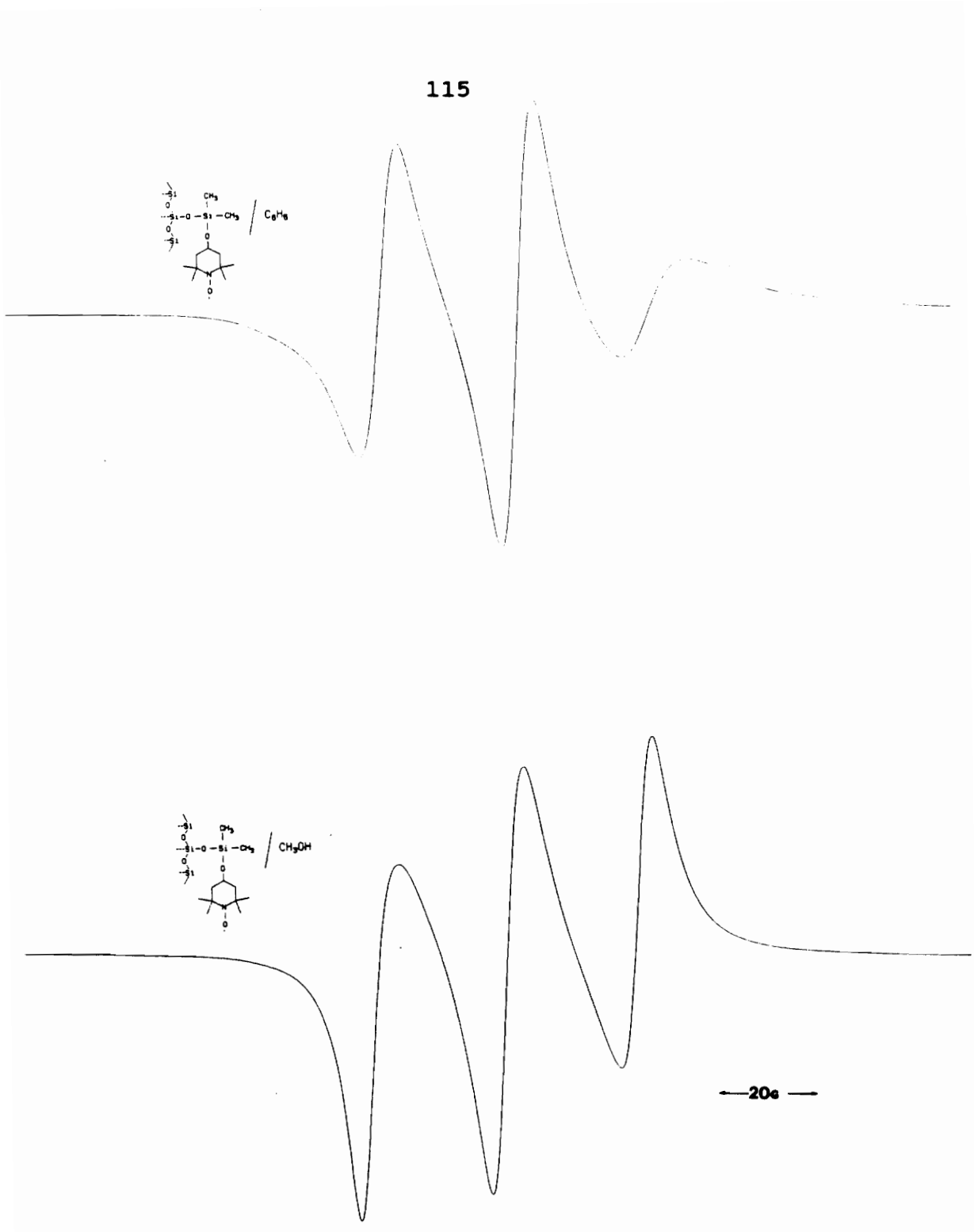

Fig. 6.5 Effect of the solvent on the EPR line width (a) **SPIN 5**/benzene; (b) **SPIN 5**/methanol.

SPIN 8 and **SPIN 11** were prepared using larger particle size and pore diameter silica gel. A 3/1 mole ratio TEMPOL/linking reagent (methyldichloro- and methyltrichloro- silanes) as linking reagents (LR) and refluxing reaction conditions (previously presented in Ch. 5.1.2). Although definitive evidence has not been obtained, it is reasonable to assume that **SPIN 11** is a biradical. The reaction conditions and the number of spins for the two SPIN samples are presented in Table 5.1. A large difference in the number of spins was observed (relative to **SPIN 7**) as a result of different thermal pretreatment for the 150-75 μm silica gel used.(See Table 6.1). Referring to Fig. 6.6 the EPR spectra acquired for the SPIN samples with a higher number of spins are broader which indicates either stronger electron-electron spin interaction and/or reduced mobility for the SPIN samples with higher spin count.

The EPR spectra of the deuterated TEMPOL (TEMPOL-d_{17}), immobilized on 150-75 μm silica gel (**SPIN 9**) and its undeuterated analog (**SPIN 8**) are represented in Fig. 6.7 The EPR line-shape (Fig. 6.7) indicates a dominant ^{14}N hyperfine interaction for both radical systems (immobilized TEMPOL, and immobilized TEMPOL-d_{17}) reflected in broad EPR lines of poorly resolved triplets. Presumably, the dominate electron-nuclear interaction is the ^{14}N hyperfine interaction,

Table 6.1 EPR data and reactant's mole ratios for **SPIN 7, 8,** and **11.**

SPIN System	Sample	Spins/g	Silica gel (g)	LR (mmol)	TEMPOL (mmol)
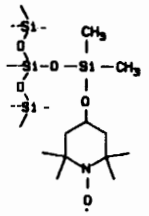	7	$1.7*10^{19}$	2	0.35	1.18
	8	$3.6*10^{19}$	2	0.58	1.74
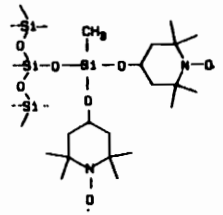	11	$4.9*10^{19}$	2	2.5	7.4

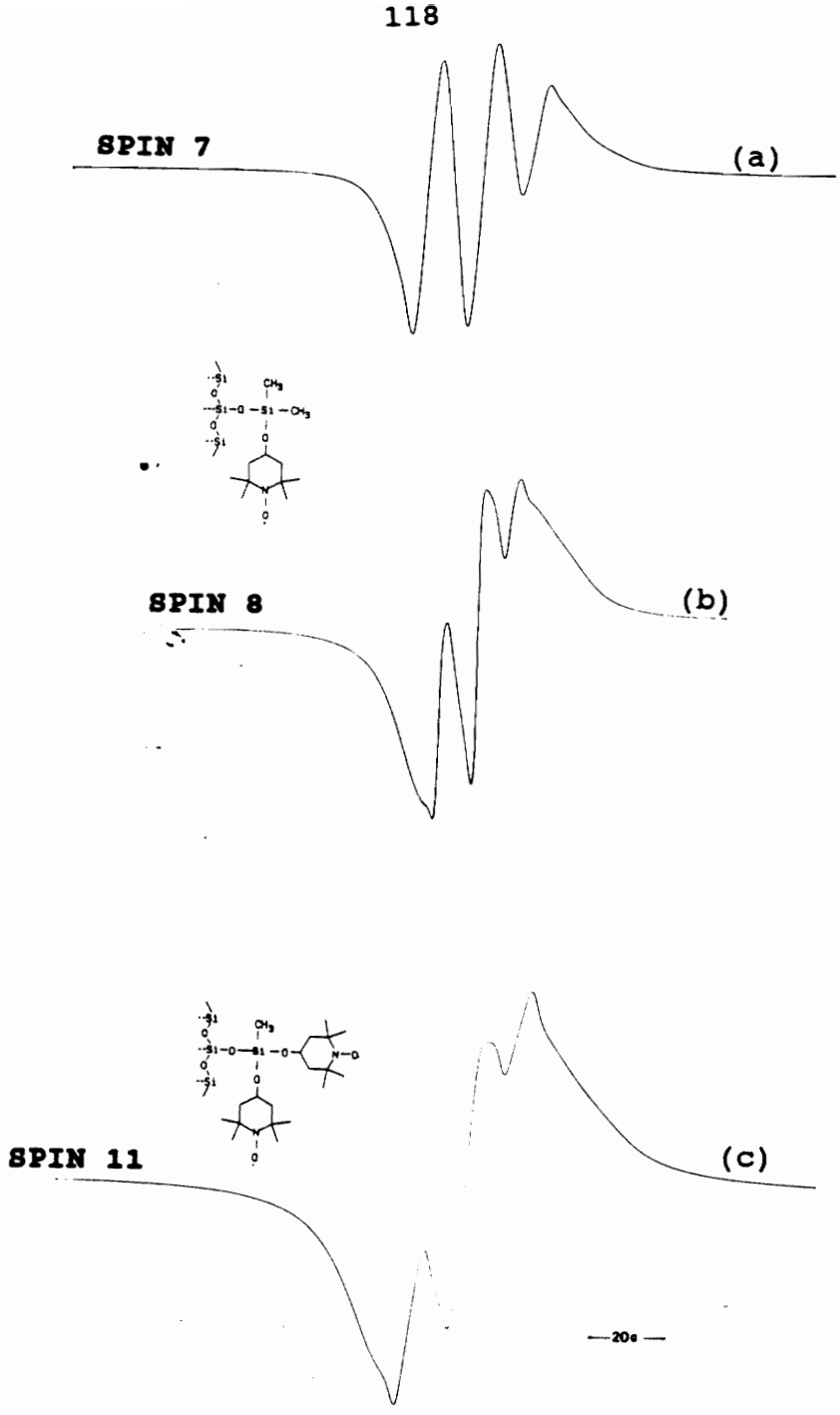

Fig. 6.6 EPR spectra (in benzene) of the SPIN radicals: (a) **SPIN 7**, $1.7*10^{19}$ and (b) **SPIN 8** $3.6*10^{19}$ spins/g, and **SPIN 11**,(c) $4.9*10^{19}$ spins/g

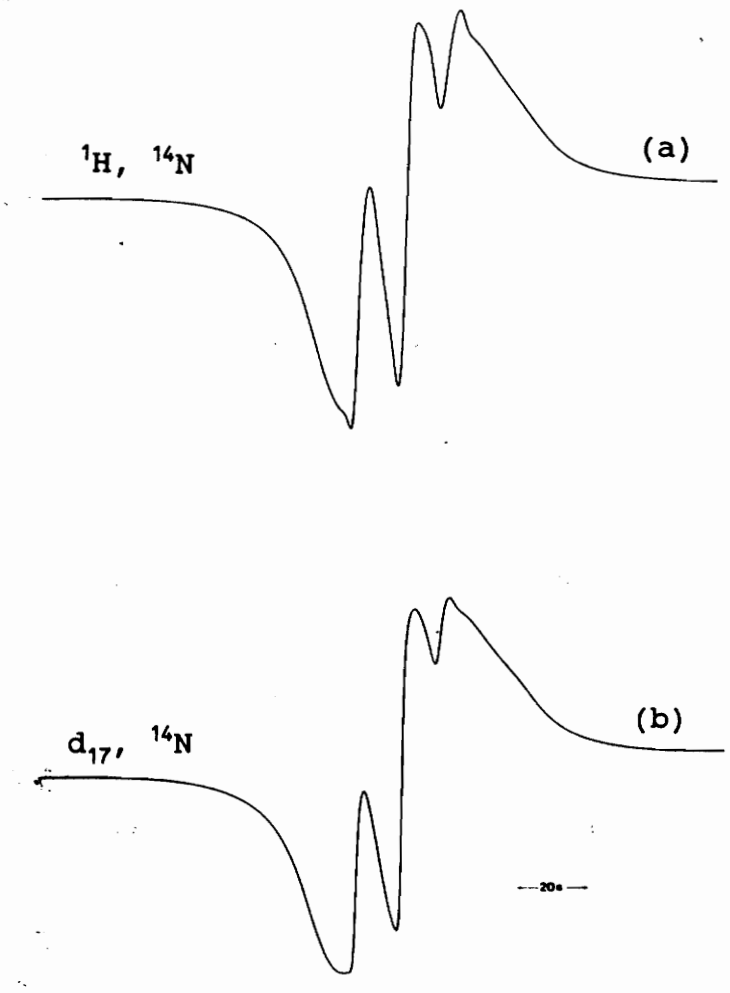

Fig. 6.7 EPR spectra in benzene of: (a) **SPIN 8**, and (b) it deuterated analog, **SPIN 9**.

and is consistent with nearly the same linewidth for both deuterated and undeuterated samples.

The EPR spectrum of ^{15}N substituted TEMPOL-d_{17} (TEMPOL-d_{17},^{15}N), is represented in Fig. 6.8,(b). The poorly resolved asymmetric doublet indicates a dominate ^{15}N hyperfine interaction. The nearly equal enhancements for the ^{14}N and ^{15}N analogs (Table 6.2) suggest significant electron-electron exchange contribution to the EPR line broadening. For comparison, the EPR spectrum of the reference system (immobilized TEMPO), **SPIN 8** is given on the same figure, Fig. 6.8,(a). The ^{1}H and ^{13}C SLIT DNP studies for **SPIN 7, 8, 9, 10,** and **11** are discussed in chapter 6.2.

6.1.2 EPR Characterization of Chiral SPIN Samples

The EPR spectrum of the chiral **SPIN 12** in benzene is represented in Fig. 6.9. The decrease in the linewidth with an increase in the solvent polarity is explained (see Ch.4) by conformational changes on the surface (which result in higher mobility) due to the solvent/(unreacted silanol groups) interactions. For the spin concentration obtained for **SPIN 12**

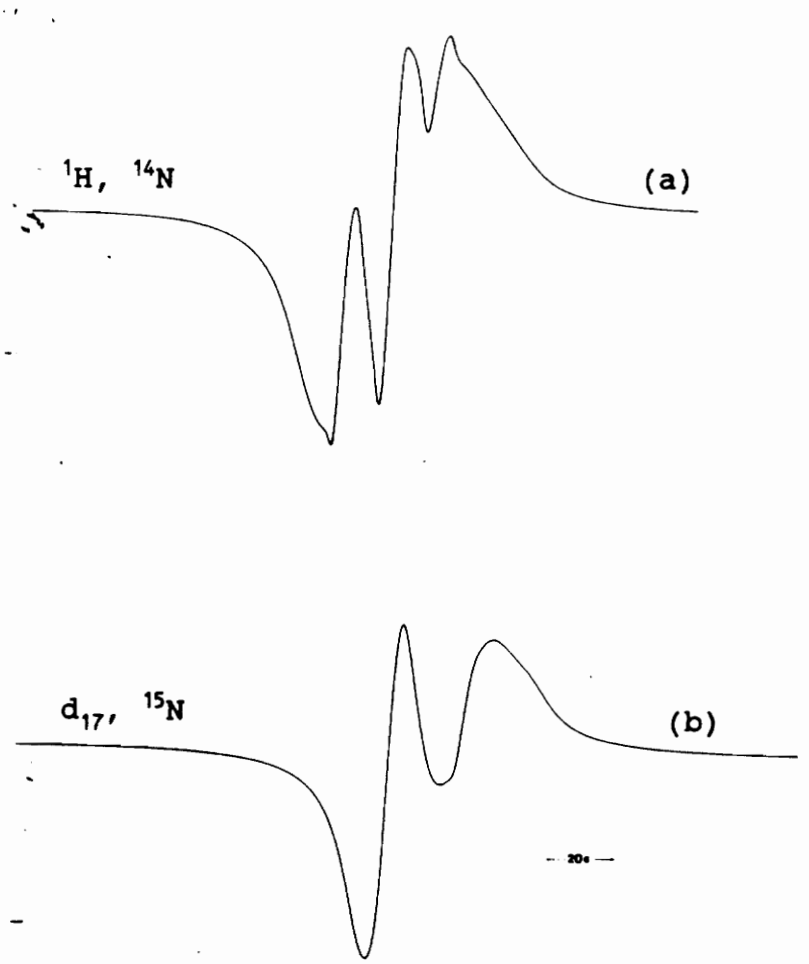

Fig. 6.8 EPR spectra in benzene of (a) **SPIN 8** and (b) it deuterated and ^{15}N substituted analog, **SPIN 10**.

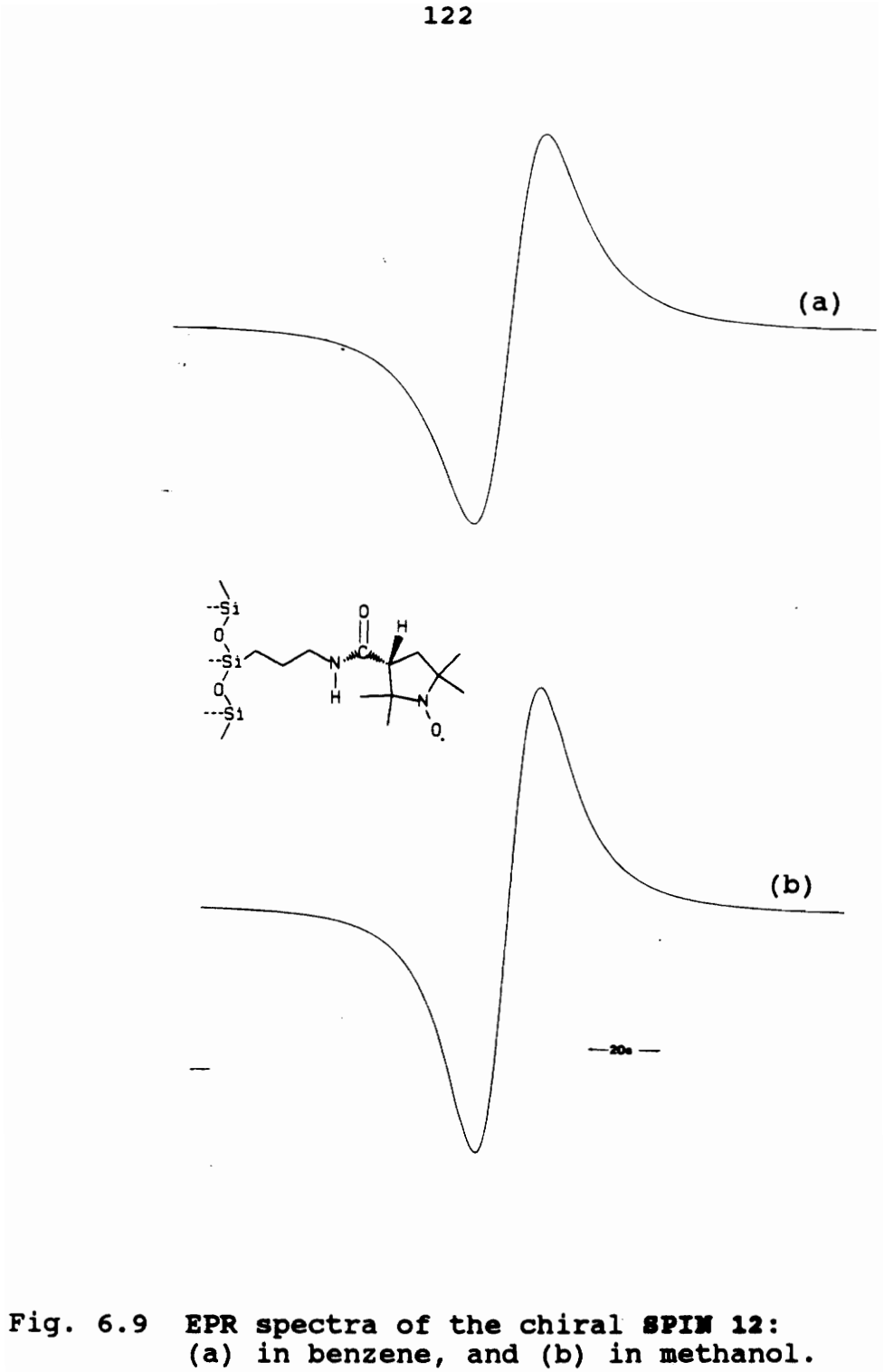

Fig. 6.9 **EPR spectra of the chiral SPIN 12: (a) in benzene, and (b) in methanol.**

($1.3*10^{20}$ spins/gram) the possibility of negligible concentration of the unreacted silanol groups is reasonable. Thus, the relatively smaller change in the mobility of the above system as a function of the solvent polarity could be attributed to a relatively larger contribution of the dipolar electron interaction (relative to the exchange one) and/or to the relatively small concentration of the unreacted silanol groups on the surface for this sample. In any case, the **SPIN 12** exhibited EPR linewidth (regardless of the solvent used) too large for reasonable saturation factors to be obtained. In addition, there were serious problems of maintaining adequate flow during the DNP experiment using this sample. In particular, a maximum flow rate of 1.5 ml/min. (in comparison to ~8-8.5 ml/min for other SPIN samples) was achieved. It should be noted that the 10 μm particle size silica gel used for the preparation of this sample was the largest size aminocapped silica gel, commercially available. The large EPR linewidth and the poor flow characteristics made the use of this sample for SLIT DNP studies virtually impossible.

The EPR spectrum of the chiral **SPIN 13** in benzene is presented in Fig.6.10,(a). As discussed in Ch. 5.1, the system was prepared in order to study the DNP enhancement of different enantiomeric pairs dissolved in the flowing solution. The stability of the chiral **SPIN 13** was examined by

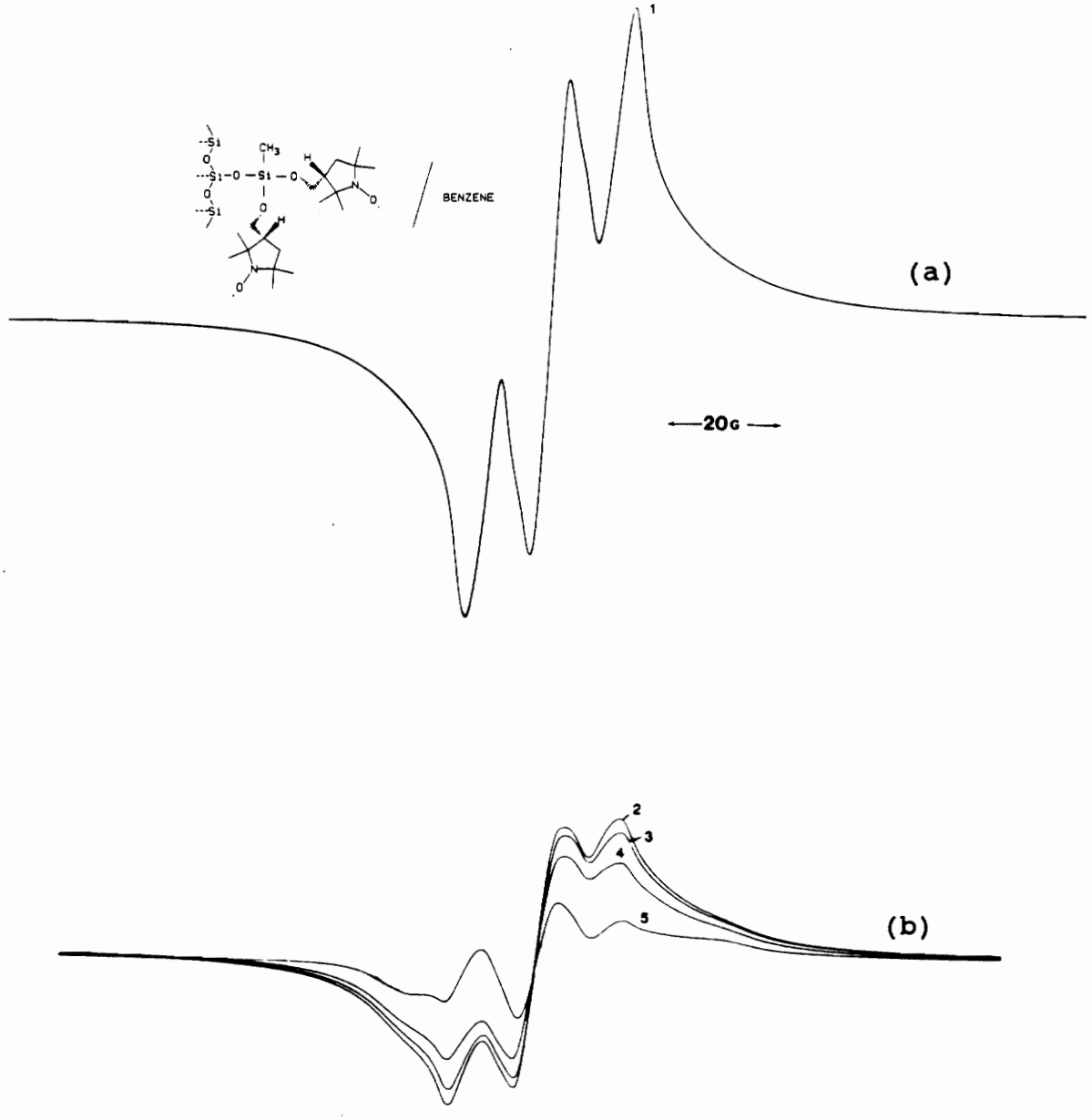

Fig.6.10 EPR spectra of the chiral **SPIN 13:** (A) in benzene, and (b) in benzene in the presence of R-(+)-methyl 2-chloropropionate,as a function of time. Spectra 2, 3, 4, and 5 have times of 5, 10, 15, and 60 min., respectively.

EPR in the presence of the following three enantiomeric pairs:

i). R-(+)-Methyl 2-chloropropionate and
S-(-)-Methyl 2-chloropropionate (Aldrich)

ii). R-(+)-α-Methylbenzylamine and
S-(-)-α-Methylbenzylamine (Aldrich)

iii). [(1R)-endo]-(+)-3-Bromocamphor and
[(1S)-endo]-(-)-3-Bromocamphor (Aldrich).

The chiral **SPIN 13** was not stable in the presence of both enantiomeric pairs (i) and (ii), and the spin concentration decreased rapidly within a time period of about 1 hour. A representative example is given in Fig. 6.10,(b): Spectrum 1 was taken 10 min after the addition of a small amount of R-(+)-Methyl 2-chloropropionate to **SPIN 13** in benzene in a EPR tube. The EPR sample was left in the spectrometer, and spectra 2, 3, 4 and 5 were taken in 5, 10, 15, and 60 min time intervals, respectively.

However, no appreciable change in the number of spins was observed (less than 5% for about 5 hrs. and about 10% for 12 hours) for the **SPIN 13**/bromocamphor system with 1,4 - dioxane as the solvent. This system was used for SLIT DNP studies. The 1,4 -dioxane was used as a solvent because of it relatively low dielectric constant. The EPR spectrum of the **SPIN 13** in 1,4-dioxane is presented in Fig. 6.11.

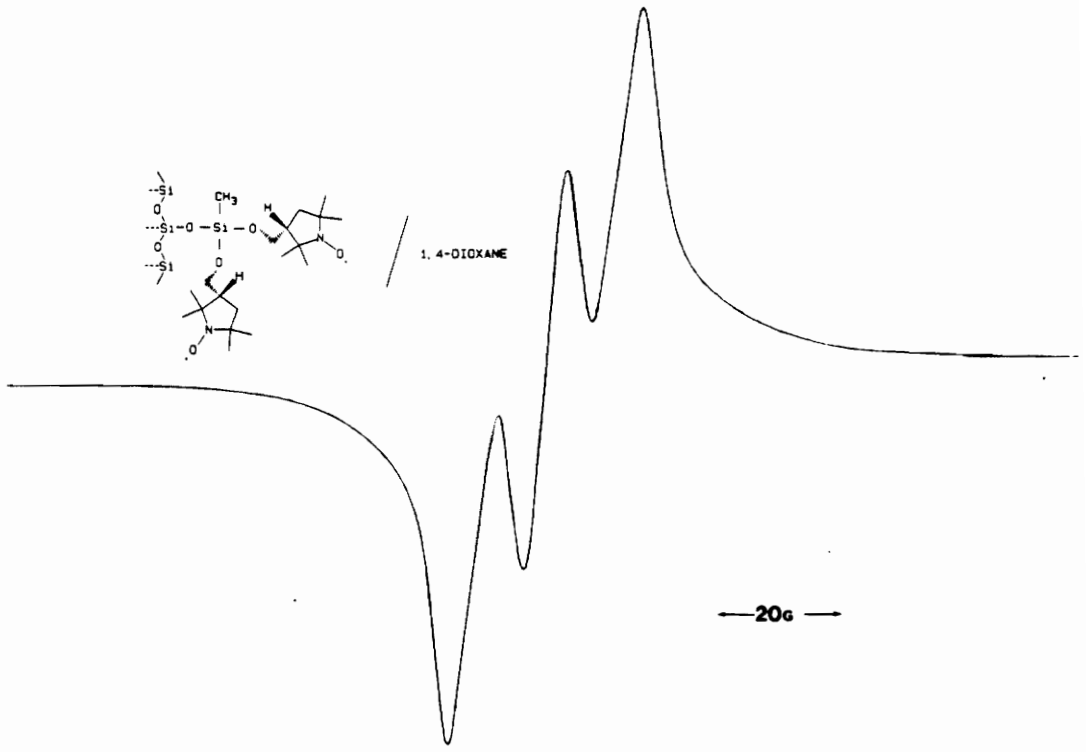

Fig.6.11 EPR spectrum of the chiral SPIN 13 in 1,4-dioxane.

6.2 ^{1}H and ^{13}C SLIT DNP for Achiral SPIN Samples

6.2.1 ^{1}H SLIT DNP Studies of Achiral SPIN Samples.

A). Concentrational Effects on ^{1}H SLIT DNP Studies

The results from the ^{1}H SLIT DNP studies of chloroform for the **SPIN 7**, **8**, and **11** are presented in Table. 6.2. Referring to the results in Table 6.2, we can conclude that the increase in the radical concentration did not appear to offer any advantage for the ^{1}H SLIT DNP studies for the SPIN radicals in question. In fact, the enhancement decreases as a function of the immobilized spins on the surface. As discussed earlier, the increase in the radical concentration, C, results in an improvement of the leakage factor, f, and in an increase the electron-electron exchange interaction rate (e.g. higher enhancements should be observed). On the other hand, no significant difference in the saturation factors, s, as a function of radical concentration is observed (see Table 6.2) Thus the decrease in the enhancements for the samples discussed above (see Table 6.2) can be explained by a decrease in the mobility for the SPIN radicals in question as a function of the unpaired spin surface concentration. Presumably, the necessary requirement, $\omega\tau_c << 1$ for maximum coupling factor to be achieved is not fulfilled which results in a decrease of the enhancement, A_{obs}, with the increase of radical concentration (that is, a decrease of the

Table 6.2 ^{1}H SLIT DNP data for **SPIN 7, 8 and 11.**

SPIN System	Sample	Spins/gr	A_{obs}	A/K	s	A/K (s=1)
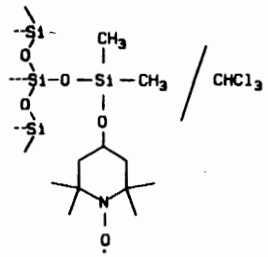	7 8	$1.7*10^{19}$ $3.6*10^{19}$	-4.3 -4.2	-6.1 -5.4	0.80 0.82	-7.6 -6.6
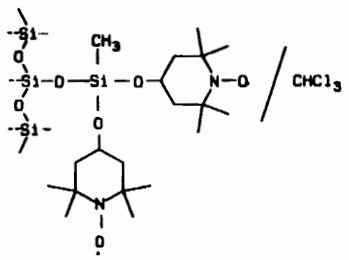	11	$4.9*10^{19}$	-3.5	-3.7	0.77	-4.5

enhancement as a result of restricted mobility at higher concentrations). A comparison to previous results[12] (A_{obs}= -4.6 and A/K = -7.2) shows no improvement in the reported ^1H enhancements within the error of the measurements.

B). Isotope Substitution Effects on ^1H SLIT DNP Studies

The ^1H SLIT DNP enhancements for **SPIN 8** and its deuterated analog, **SPIN 9** were expected to be equal based on the preliminary EPR results which showed equal number of spins as well as comparable linewidths (ΔH_{pp}) for both samples (see Table 6.3. However, the results presented in Table 6.3 indicate that deuteration results in degradation of the ^1H SLIT DNP enhancement. A possible explanation of this observation could be a different DNP mechanism, encountered for the case of the undeuterated **SPIN 8** relative to that for the deuterated **SPIN 9**. In general, a dipolar interaction between the protons and the free radical electrons governs the ^1H Overhauser DNP and the proton polarization is inverted (with the exception of few special cases[45-47] where positive proton enhancements have been observed indicating the presence of scalar interaction). If we speculate that the protons in the radical, in our case, are negatively enhanced then a possible mechanism for polarization transfer could be a transfer of magnetization (via spin diffusion) from the polarized protons in the radical to the protons of the

Table 6.3 ^{1}H SLIT DNP of chloroform for **SPIN 8**, **SPIN 9** and **SPIN 10**.

SPIN System	SPIN radical	TEMPOL	Spins/gr	A_{obs}	A/K	s	A/K (s=1)	ΔH_{pp} (G)
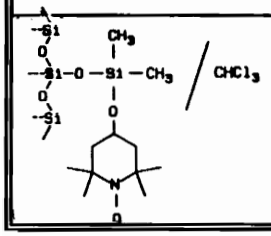	8	$^{1}H, ^{14}N$	$3.6 * 10^{19}$	-4.2	-5.4	0.82	-6.5	8.3
	9	$D, ^{14}N$	$3.6 * 10^{19}$	-4.0	-4.1	0.90	-4.6	8.6
	10	$D, ^{15}N$	$3.4 * 10^{19}$	-2.9	-3.9	0.87	-4.5	8.5

flowing solvent (chloroform in our case) similar to the mechanism which governs the solid-state three-spin effect described in Ch. 2. (It is important to note that spin diffusion can occur from all protons of the radical to all other protons on the surface, such as protons on unreacted silanol groups and protons on the side chain). If this mechanism operates, the net ^{1}H dynamic polarization of the chloroform can be explained in terms of two spin dynamical processes (Fig 6.12 (a)): (1) the usual polarization transfer due to a modulated dipolar interaction between the unpaired electrons and the chloroform protons, and (2) the polarization transfer due to a rapid spin diffusion from the strongly polarized protons in the radical to the chloroform protons. In the case of deuterated immobilized radicals (Fig. 6.12,(b)), the second contribution is expected to be much smaller (because of the smaller electron-deuteron coupling) which explains the smaller DNP enhancements reported for the deuterated case. The assumption that the enhancement depends on the interaction of the sample with the proton spins on the surface is still not clearly understood. For example, previous results, have shown an increase in the ^{1}H and ^{13}C SLIT DNP enhancements of chloroform after washing the surface with D_2O and CH_3OD[29].

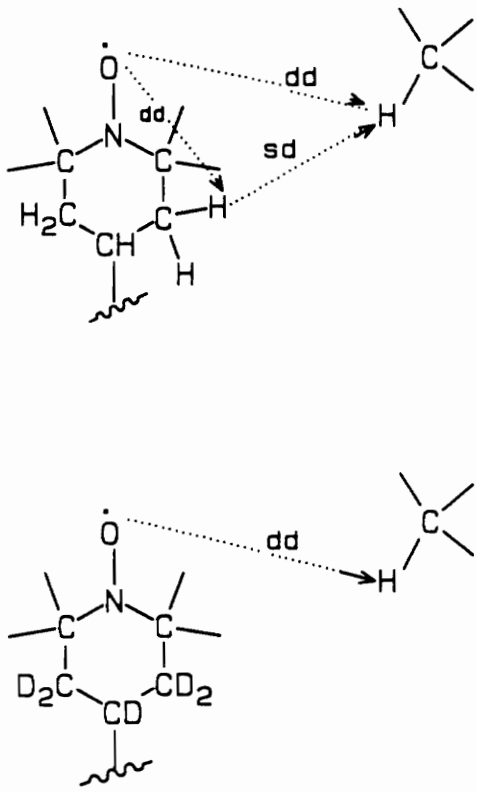

Fig.6.12 **Proposed mechanism for the three-spin effect analog of the solid-state three-spin effect.**
dd - dipolar DNP; sp - spin diffusion.

The mechanism suggested above could be tested experimentally by two separate experiments: (1) deuterium-oxide washing of both deuterated and undeuterated SPIN samples and subsequently monitoring of the ^{1}H and ^{13}C SLIT DNP of $CHCl_3$. No significant difference in the ^{1}H and ^{13}C enhancements before and after the D_2O wash should be observed for the case of deuterated SPIN sample, while the for the case of the undeuterated SPIN samples larger ^{1}H and ^{13}C enhancements should be expected after the D_2O wash. (2) Monitoring ^{13}C SLIT DNP of a model compound which exhibits dipolar dominated ^{13}C DNP enhancements in the presence of deuterated and undeuterated immobilized radicals. The indirect contribution to the ^{13}C enhancement (the three spin-effect) is expected to be stronger in the case of undeuterated immobilized radical, provided that the spin-diffusion mechanism is operative.

A comparison of the DNP data obtained for the ^{15}N substituted immobilized radical (**SPIN 10**) and its ^{14}N analog (**SPIN 9**) indicates no increase of the extrapolated enhancements for the ^{15}N substituted sample. Theoretically, an improvement of a factor of 1.5 in favor of the ^{15}N is expected (see Ch.5.1) for cases of a low electron-electron exchange rate for the separate electron transitions (that is, in the case of a well resolved EPR triplet and doubled for the ^{14}N and ^{15}N respectively). The lack of any difference, in our case is

explained by the presumably large contribution of the electron-electron exchange to the enhancements at this radical concentration.

6.2.2 ^{13}C SLIT DNP Studies of Achiral Samples.

The importance of the ^{13}C SLIT DNP arises from its potential application in LC NMR studies as well as studies of large biological molecules. The ^{13}C SLIT DNP studies offer an advantage of a large NMR chemical shift range and a well separated NMR signal for each carbon in the molecule.

However, the previous ^{13}C SLIT DNP studies were limited to scalar dominated enhancements because of the two major problems encountered in ^{13}C DNP: poor leakage factors and detrimental three-spin effect contribution to the enhancements at relatively low concentrations for the immobilized radicals used.

One of the most important results in this thesis is that for the first time a dipolar dominated ^{13}C SLIT DNP enhancements were observed, utilizing the novel SPIN sample prepared in our laboratory. The SLIT DNP results are discussed

below.

A). Concentrational Effects on the ^{13}C SLIT DNP Studies

The ^{13}C SLIT DNP spectrum of chloroform for the SPIN monoradical, **SPIN 7** is presented in fig. 6.13. The aim of this experiment was to compare the observed ^{13}C enhancements to those reported for previously prepared SPIN systems. The results indicate relatively large scalar dominated enhancements (48 times larger signal relative to the thermal Boltzmann magnetization at 4.7 T), comparable to that reported before[12] (42 times larger signal relative to the thermal Boltzmann magnetization at 4.7 T).

A comparison of the observed ^{13}C SPIT DNP enhancement for the **SPIN 8** (A_{obs} =42), relative to the thermal Boltzmann magnetization) to that reported above for the **SPIN 7** (A_{obs}=48) shows no increase in the observed ^{13}C enhancements as a function of the concentration:

SPIN Sample	Spins/gram	$A_{obs}(^{13}C)$
7	$1.7*10^{19}$	48
8	$3.6*10^{19}$	42

The small difference in the observed enhancements suggests

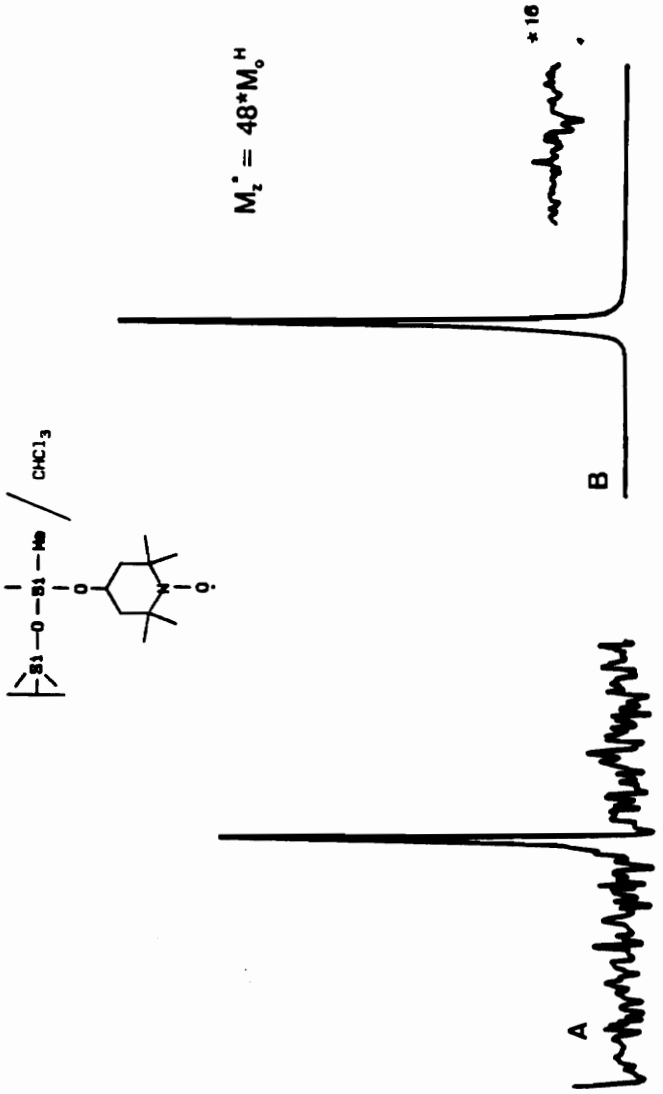

Fig.6.13 ^{13}C SLIT DNP spectrum for **SPIN 7**/$CHCl_3$:
(A) static NMR spectrum, M_o^H,
(B) Flow DNP spectrum, M_z^*.

that reduced motion at higher radical concentration cancels the effect of the improvement of the leakage factor as a function of the radical concentration. Another possible explanation, could be the smaller three-spin effect contribution for the scalar dominated enhancements of the chloroform for the SPIN sample with the higher spin concentration. As stated earlier, the contribution of the three-spin effect (which is larger at smaller radical concentration and causes a positive ^{13}C enhancement) results in a decrease of dipolar dominated enhancements, while an increase of the scalar dominated enhancements is expected. In the above case, a smaller three-spin effect additive contribution is expected for the SPIN sample with the higher spin count, **SPIN 8**, which is in agreement with the smaller enhancements observed in this case.

Since we are interested in observing dipolar dominated enhancements, a model system (a solution of 1-chlorobutane in carbon tetrachloride) which exhibits both dipolar and scalar dominated ^{13}C DNP enhancements has been chosen to test the new, SPIN radicals. The choice of the 1-chlorobutane/CCl_4 flowing system was based on previous ^{13}C LLIT DNP studies[12] which demonstrated selective DNP enhancements (dipolar and scalar) for 1-chlorobutane in the presence of different concentrations of TEMPO free radical (tetramethyl-1-piperidinyloxy free

radical) in the flowing solution. The same previous results, presented in Fig. 6.14, show an increase of the dipolar dominated enhancements (see carbons; C-2, C-3, and C-4) as a function of the radical concentration.

The same features characterize the ^{13}C SLIT DNP spectra for the 1-chlorobutane/CCl_4 50% (v/v), see Fig. 6.15: (1) selective enhancements (scalar dominated for C-1, bonded to the slightly acidic hydrogen atom, and dipolar dominated for the rest carbons - C-2, C-3 and C-4), and (2) an increase of the dipolar dominated enhancements as a function of the radical concentration. The assumption that the dipolar dominated enhancements are subject to three-spin effects is supported by previous ^{13}C SLIT results for benzene and d_6-benzene which exhibited larger dipolar dominated enhancements for the d_6-benzene where the three-spin effect is suppressed by the smaller electron-deuteron interaction. In contrast to the case of chloroform, a small increase in the scalar dominated enhancement (that is the enhancement of carbon C-1 of 1-chlorobutane; see Fig. 6.15 (d) vs (b)) is observed with an increase in the radical concentration. These results suggest that the relative contribution of the different effects on the observed ^{13}C scalar enhancements is hard to predict because of the dependence on the particular system being examined.

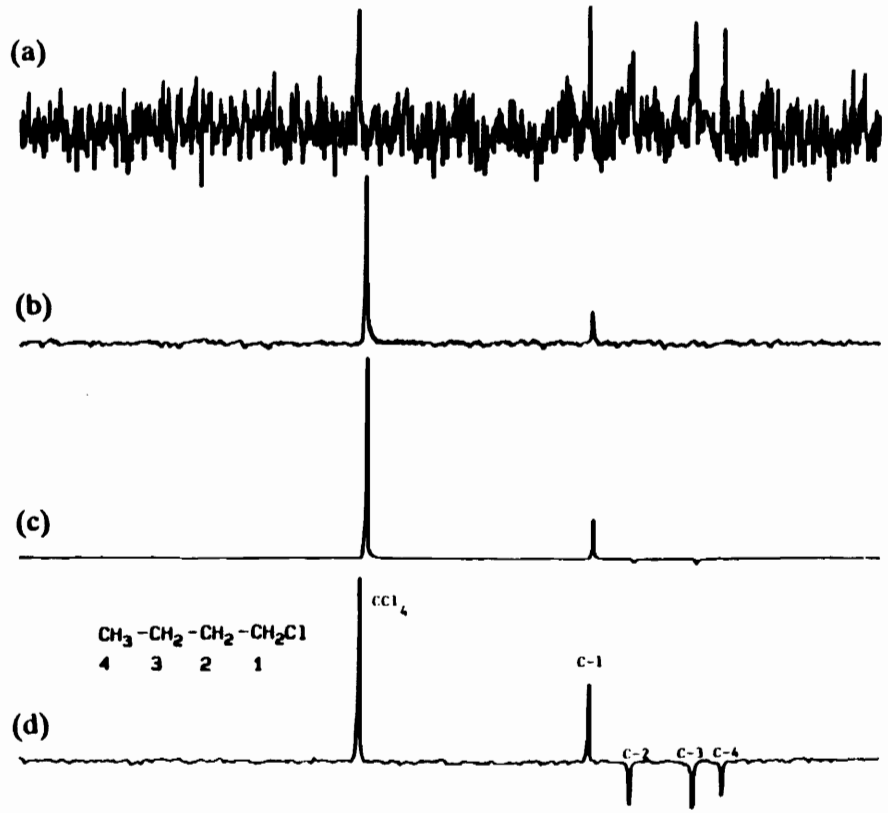

Fig.6.14 : LLIT ^{13}C DNP spectrum (50.1 MHz) for 1-chlorobutane 50% (v/v) in CCl_4: (a) static ^{13}C NMR spectrum M_o^H (40 scans); (b) flow ^{13}C DNP spectrum (240 scans, 7 mL/min, 0.005 M TEMPO); (c) flow ^{13}C DNP spectrum (240 scans, 6 mL/min, 0.010 M TEMPO); (d) flow ^{13}C DNP spectrum (40 scans, 8 mL/min, 0.079 M TEMPO).
From Tsai[11]

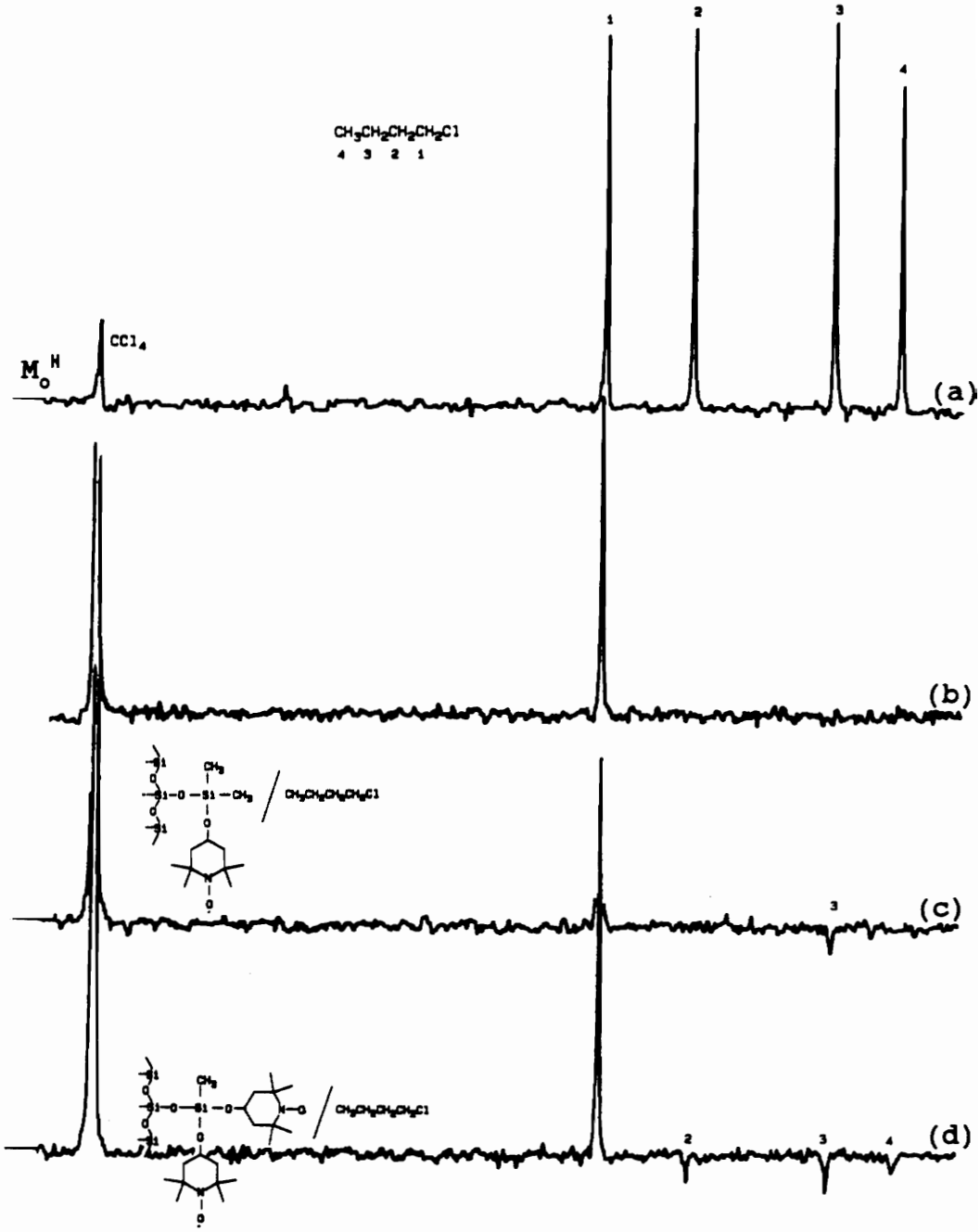

Fig.6.15 SLIT DNP spectra of 1-chlorobutane 50% (v/v) in CCl_4 for SPIN radicals: (b) **SPIN 7**; (c) **SPIN 8**; d) **SPIN 11** at and the static NMR spectrum, M_o^H,(a).

In summary, although the increase in the surface spin concentration did not result in much improvement of the scalar dominated ^{13}C enhancements of the chloroform, it did improve the dipolar dominated ^{13}C enhancements for the case of 1-chlorobutane, presumably by suppressing the detrimental three-spin effect contributions and increasing the leakage factor.

6.3 ^{13}C SLIT DNP for Chiral SPIN Samples

The preparation of a chiral SPIN sample on the silica gel surface was intended to provide a chiral environment for monitoring ^{1}H and ^{13}C SLIT DNP enhancements. As previously indicated (see Ch. 5.1), we hoped to observe different enhancements for flowing solute enantiomers in the presence of an immobilized chiral environment at the solid/liquid surface interface.

The significance of eventual differences in the DNP enhancements depend on diastereomeric interactions, $(R)_{sample}/(R)_{surface}$ and $(S)_{sample}/(R)_{surface}$, which could ultimately provide development of a new method for determination of enantiomeric purity and for determination of the efficacy of chiral chromatographic separations.

Presently, there is an NMR technique which has been extensively employed to determine enantiomeric purity and in favorable cases the absolute configuration of various organic molecules[48-54]. The method is based on the fact that enantiomers in a chiral environment (that is, a chiral solvents or/and chiral NMR shift reagents) yield separate NMR signals. The chemical shift difference critically depends on subtle differences in the electronic environment at a given monitoring nucleus when weak diastereomeric complexes are formed in solution (chiral solvent/(R) enantiomer, chiral solvent/(S) enantiomer.

The major disadvantage of the present NMR technique is the necessity of contaminating valuable samples with the chiral solvent and/or chiral shift reagent. This can be potentially overcome in the present study by employing a SLIT DNP technique for determination of the enantiomeric purity. The "chiral environment" in this case is provided by the immobilized chiral spin labels so that the monitoring enantiomeric pairs are in contact with them only during the time for the polarization transfer in the microwave region. The mechanism which is expected to induce different DNP enhancements in the DNP method is similar to that in the NMR experiment, that is, different "DNP" environment (selective DNP enhancements) for the two enantiomers during the life time

of the weak diastereomeric complexes between the chiral (R) SPIN sample, and the flowing (R)- or (S)- isomers of a given enantiomeric pair.

The chiral **SPIN 13** (see Scheme 5.7) and the [(1R)-endo]-(+) - and [(1S)-endo]-(-)-stereoisomers of bromocamphor were employed as a model system to test the above hypothesis. The choice of the chiral **SPIN 13** was based on its relative ease of preparation and the promising ^{13}C SLIT DNP results for a SPIN samples prepared under similar conditions (see the results for **SPIN 13**/1-chlorobutane). From the discussions in the previous chapter, it is clear that a SPIN radical suitable for the optimization of both ^{1}H and ^{13}C SLIT DNP studies is difficult to achieve. Usually the best sample for ^{13}C DNP (in terms of achievable enhancements) does not yield high ^{1}H DNP enhancements. And indeed, it turned out that the chiral SPIN radical used in our studies was not appropriate for ^{1}H DNP, so that only ^{13}C SLIT DNP will be reported. The latter is not considered as a disadvantage because we were mainly interested in ^{13}C DNP. The choice of the bromocamphor enantiomeric pair was based on the relevant stability of the chiral SPIN radical in the presence of that enantiomeric pair as well as on the previous LLIT DNP results[29] which demonstrated selective (dipolar and scalar) DNP enhancements for this molecule in the presence of 0.1 M TEMPO free radical in carbon tetrachloride.

Based on the above discussions, differences in the ^{13}C DNP enhancements were predicted for the carbon atoms which are close to the assumed site of the weak complex formation, that is C-3 (see Fig. 6.16). The assumption that weak hydrogen-bond complexation occurs between the slightly acidic hydrogen atom at carbon C-3 and the nitoxide group of the immobilized radical was supported by the scalar dominated (positive) enhancements observed for carbon C-3 in contrast to all ather carbons which exhibited dipolar dominated (negative) enhancements in the previous study[11].

A careful inspection of the ^{13}C DNP spectra of both R(+)- and S(-)- stereoisomers of bromocamphor at 2 ml/min flow rate (see Fig. 6.17 shows increases in the intensities in favor of the S(-) isomer for the C-1, C-3, C-7, and C-10.

Although, the difference for all quaternary carbons (C-2, C-1 and C-7) seems most pronounced (see Table 6.4), it is only observable at this particular flow rate (e.g. 2 ml/min). The enhancements for the carbons in question as a function of the flow rate are presented on Fig. 6.18. It should be noted that the observed enhancements, A, were calculated relative to the thermal Boltzmann magnetization at 4.7 T (no correction was made for M^{HL}). Analogous plots, to those in Fig. 6.18, where the enhancements were calculated relative to the intensity of

Table 6.4 ^{13}C SLIT DNP enhancements for R-(+)- and S-(-)-bromocamphor at flow rate 2 ml/min.

	*C-2	*C-1	C-3	**C-4	*C-7	**C-6	**C-5	**C-8	**C-9	**C-10
S(-)	-0.97	-0.67	1.86	0.68	-0.92	0.79	0.69	0.77	0.72	0.59
R(+)	-0.60	-0.24	1.27	0.73	-0.38	0.96	1.02	0.75	0.76	0.81
S/R	1.62	2.79	1.46	1.07	2.42	1.22	1.48	0.97	1.05	1.37

* The enhancements for these carbons are negative and inverted (the smaller absolute value represents a smaller enhancement).

** The enhancements for these carbons are negative but not inverted (the smaller absolute value represents a larger enhancement).

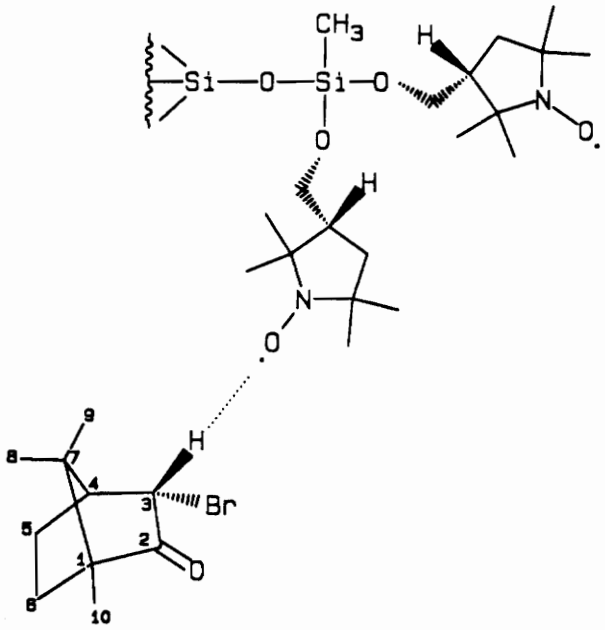

Fig.6.16 Scheme of the R(+)-chiral SPIN/R(+)-bromocamphor model system for SLIT DNP studies.

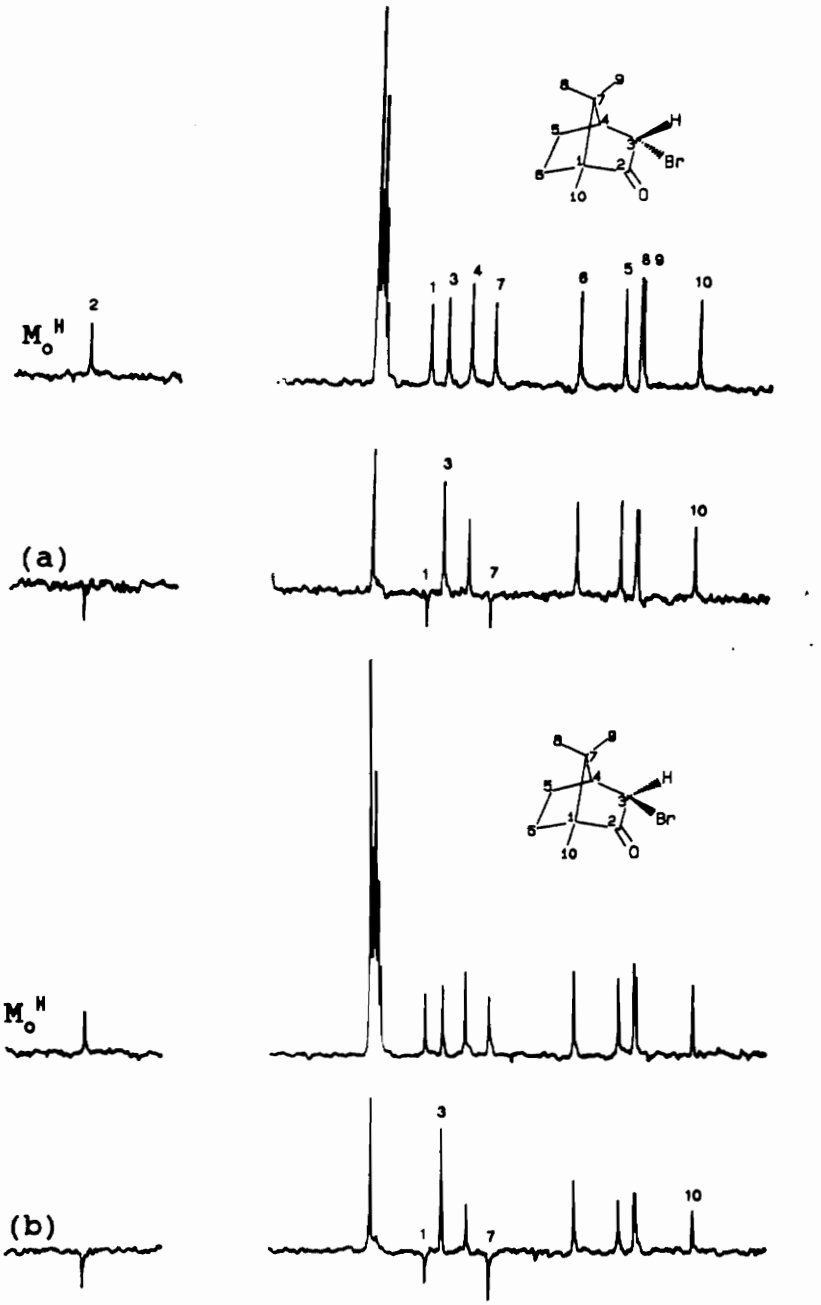

Fig.6.17 ^{13}C SLIT DNP spectra of 45% bromocamphor in 1,4-dioxane: (a) chiral **SPIN 13**/R-isomer; (b) chiral **SPIN 13**/S-isomer; flow rate 2 ml/min.

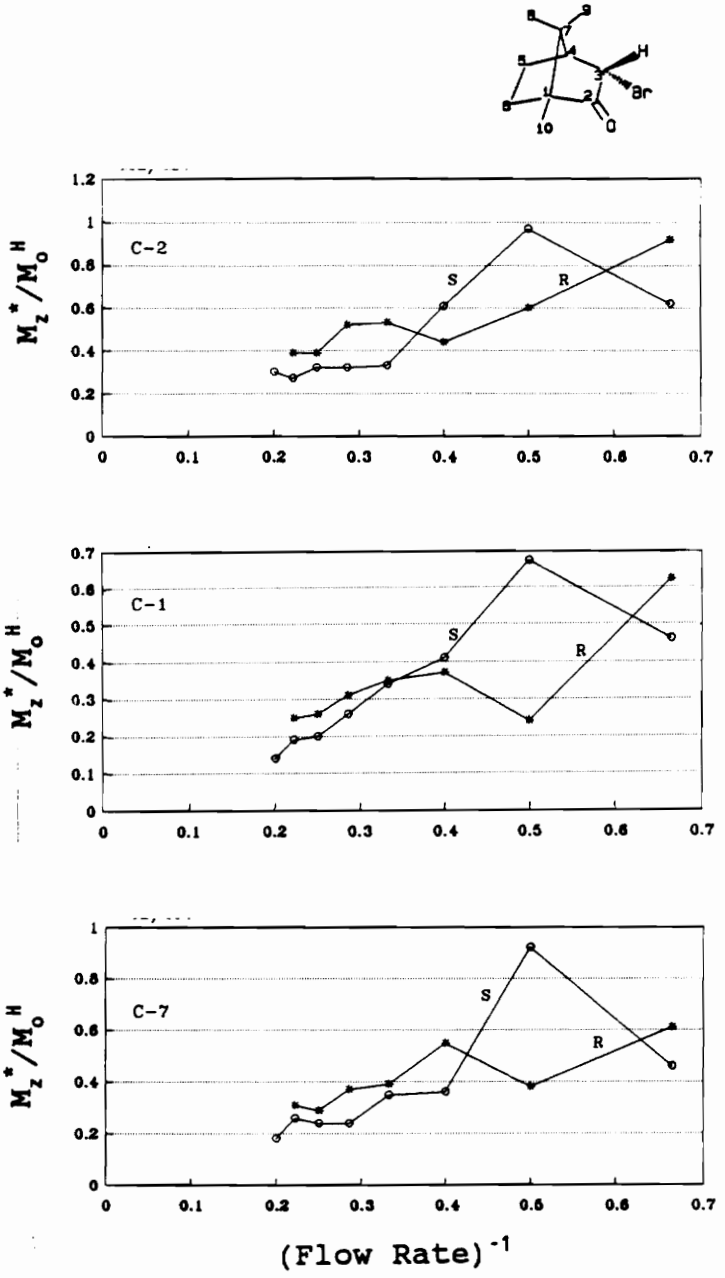

Fig.6.18 Plots of the observed ^{13}C SLIT DNP enhancements, M_z^*/M_o^H, relative to the static Boltzmann magnetization, vs. 1/Flow Rate for carbons C-2; C-1; and C-7.

carbon C-6 (which was used as an internal standard) show the same trend and representative examples are given in Fig. 6.19. (Since the enhancement for carbon C-6 becomes appreciable at higher flow rate, (the denominator becomes smaller - non-inverted negative enhancements), the ratio M_z^*/M_{C-6} becomes a little larger - which explains the difference in the curves between the two plot, M_z^*/M_o^H and M_z^*/M_{C-6} at higher flow rates: see Fig. 6.19). The latter comparison was necessary because of the small magnitude of the observable enhancements.

A common feature characteristic for all quaternary carbons (see Fig. 6.18) is that the enhancements achieve their maximum value at relatively low flow rate (2 ml/min) and subsequently the increase in the flow rate results in a decrease of the enhancements. This is due to the relatively long spin-lattice relaxation time, characteristic for quaternary carbons, which requires long residence time of the flowing bolus in the low field magnet to prevent build up losses in the DNP enhancement due to an incomplete build up of the equilibrium Boltzmann magnetization. (The relaxation times for 1M bromocamphor in CCl_4 are presented in Table 6.5)[29].

An illustration of the change in the enhancements as a function of the flow rate is given in Fig. 6.20. The characteristic decrease in the negatively enhanced (inverted)

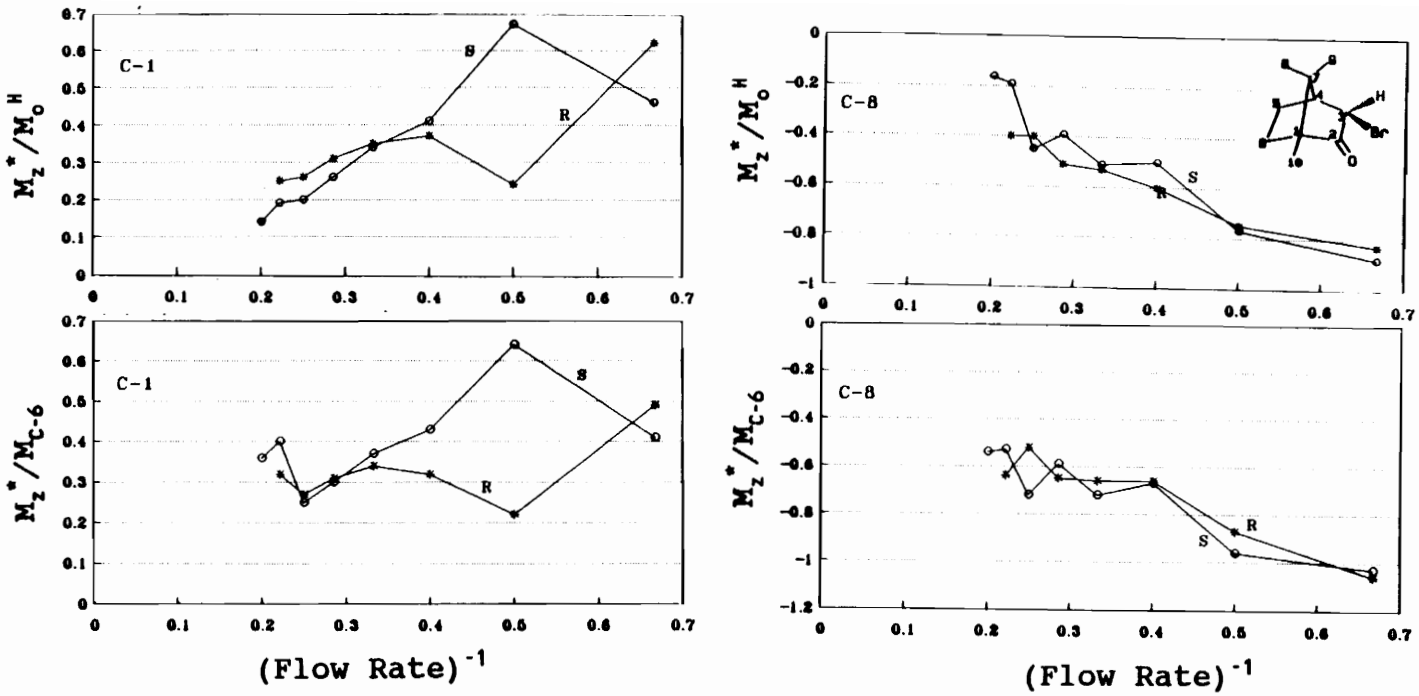

Fig.6.19 Plots of the observed ^{13}C SLIT DNP enhancements, M_z^*, relative to: (a) M_o^H and (b) M_{C-6}, vs. 1/Flow Rate for carbons C-1 and C-8.

Table 6.5 Relaxation times for 1M bromocamphor in CCl_4.[29]

Carbon number	T_{1co} (sec)
1	49.0
2	27.0
3	4.4
4	5.5
5	2.4
6	2.6
7	9.5
8,9	3.4
10	4.0

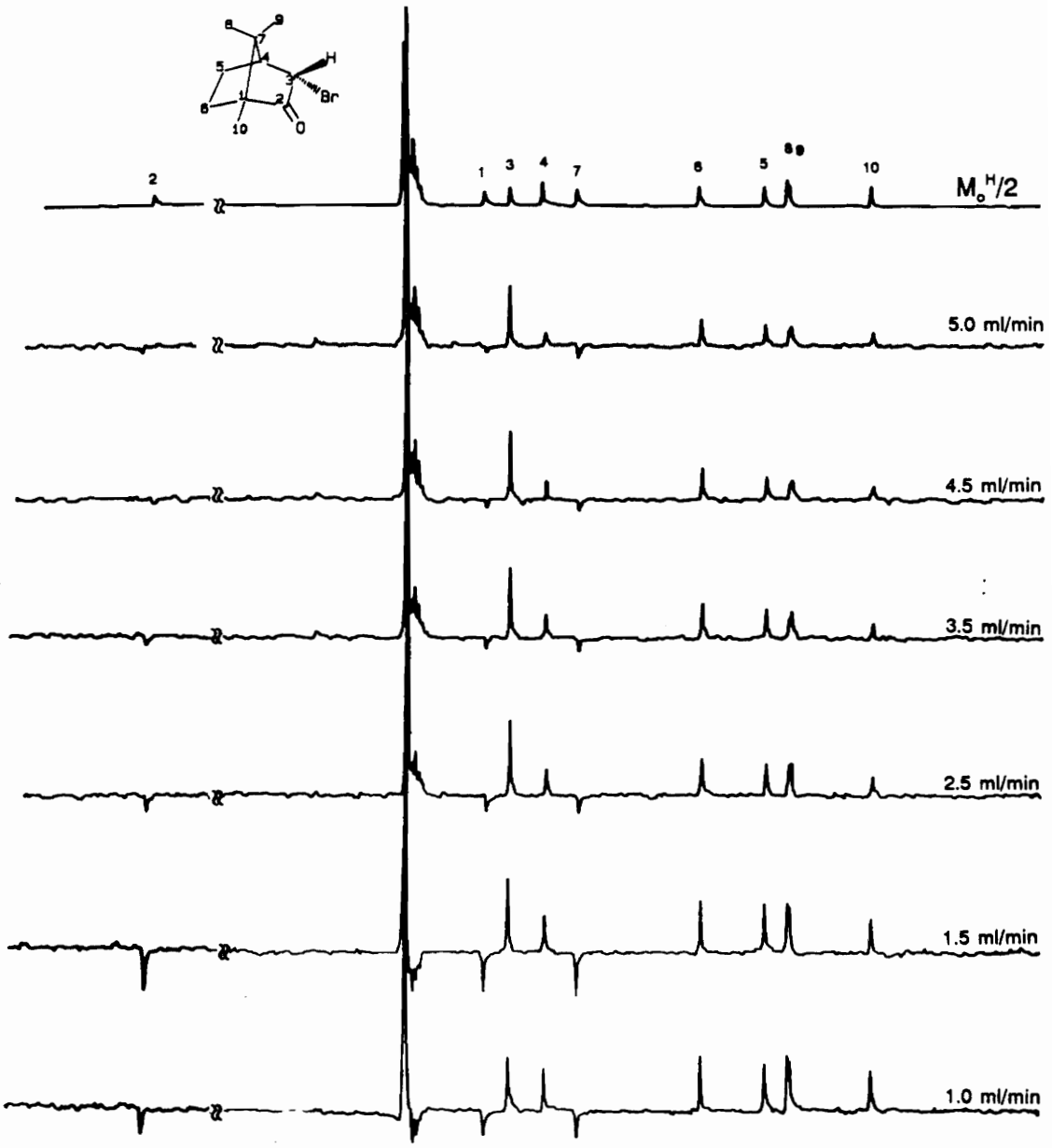

Fig.6.20 (a) Static ^{13}C NMR spectrum of R-(+)-bromocamphor in 1,4-dioxane, M_o^H; (b)-(g) ^{13}C SLIT DNP spectra of (R-(+)-bromocamphor)/**SPIN 13**.

carbons, C-1, C-2 and C-7 with the increase of the flow rate is clearly observed. In contrast, an increase of the negative enhancement for carbon, C-10, is observed which is obviously due to its shorter relaxation time (C-10 bears three hydrogen atoms, $-CH_3$). However, the enhancements for this carbon, C-10, are very small (the peak is not inverted) which can be attributed to the detrimental contribution of the three-spin effect and/or a poor leakage factor, f.

The plots of the observed enhancements for carbon C-10 and carbon C-3 as a function of the inverse flow rate are shown in Fig. 6.21, (a) and (b), respectively and indicate a consistent difference between the enhancements for the R(+)- and S(-)- isomers at low flow rates.

A close inspection of molecular models, suggests the possibility of different orientations for the $-CH_3$ group (that bears carbon C-10) with respect to the surface for one stereoisomer relative to the orientation for the other one. However, it should be strongly emphasized that at the present time we have no concrete evidence for the actual conformation at the chiral site. In analogy to the case of chiral chromatography, where steric interaction contribute to the enantioseparation process (see Ch.1), in our case, there might be an appreciable contribution to the difference in the

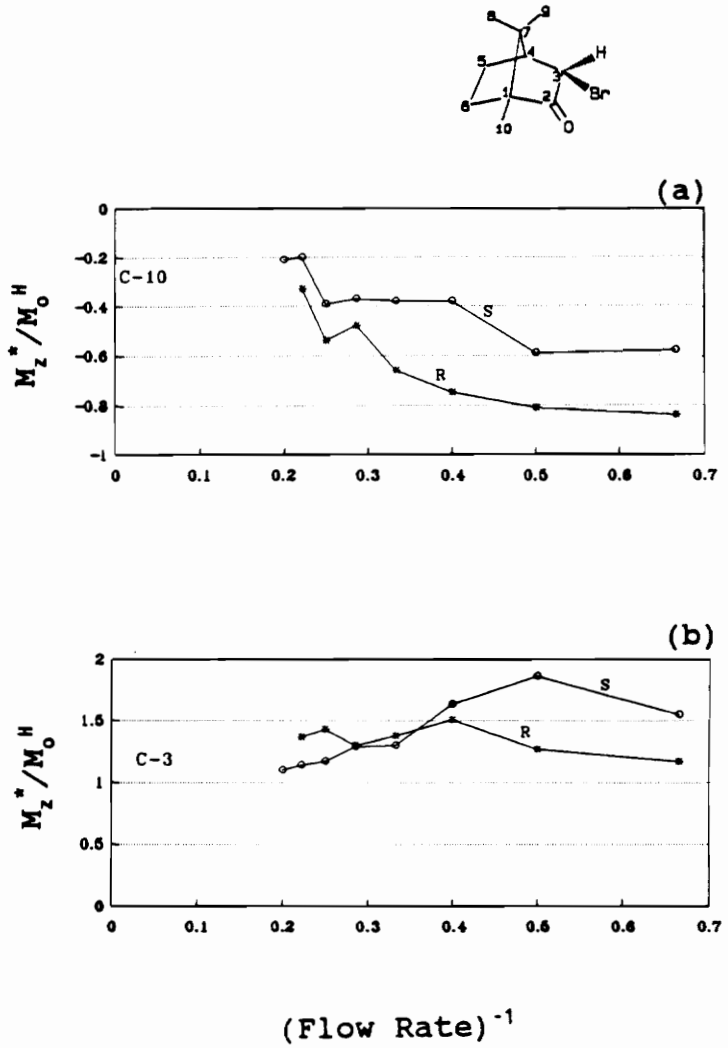

Fig.6.21 Plots of the observed ^{13}C SLIT DNP enhancements, M_z^*, relative to M_o^H vs. 1/Flow Rate for carbons C-10 (a), and C-3 (b).

enhancments due to steric interactions with the strongly polarized spins on the surface for the two stereoisomers. A prediction of such interactions is not trivial, especially for this particular case, where presumably, a biradical was immobilized on the surface.

The difference in the positive (scalar) ^{13}C DNP enhancements for the carbon at the site of assumed complexation that is, C-3 (see Fig. 6.21(b)) could be attributed to a more dominant specific diastereomeric pair -wise $S_{sample}/R_{surface}$ interaction. It should be pointed out that an inspection of the plot on Fig. 6.21(b) indicates a different trend in the change of the enhancements as a function of the flow rate for the two stereoisomers (which can not be concluded considering the plots for other enhanced carbons - see Fig. 6.19). In particular, a slow increase in the enhancement at low flow rates with a consequent achievement of a nearly constant static value is characteristic for the R(+) - stereoisomer. In contrast, the case of the S(-) exhibits a modest increase in the enhancements as the flow rate decreases. The difference in the trend for the two curves at higher flow rates could presumably be attributed to a three-spin effect (which contribution is expected to be large at high flow rate when the proton polarization suffers low transfer losses). Overall, the data

suggest a stronger $(S)_{sample}/(R)_{surface}$ complex interactions and support the higher enhancements for the S(-) - stereoisomer at low flow rates.

Referring to Fig. 6.22, differences in the enhancements for carbon C-9 versus C-8 at higher flow rates can be concluded. The plot for carbon C-8 is included in the same figure for comparison. In both cases a consistent increase in the enhancement as a function of the flow rate is observed. However, the change in the C-8 enhancements for both R- and S-isomers is the same, while some difference is observed between the C-9 enhancements for the two isomers.

It is important to note that a value of only 0.1±0.03 for the saturation factor, s, ($s = 0.1 \pm 0.03$) was obtained in both cases: $(R)_{sample}/(R)_{surface}$ and $(S)_{sample}/(R)_{surface}$.

Regardless of the above discussions, additional experimental evidence in support of the above results is desirable before indisputable conclusion can be made. For example, a SLIT DNP experiment using the same, R, SPIN radical and the racemic mixture, (±)-bromocamphor is expected to average the values of the observed enhancements for the R- and S- enantiomers (at a particular flow rate) which should result in a curve in between the curves for the (R) and (S)

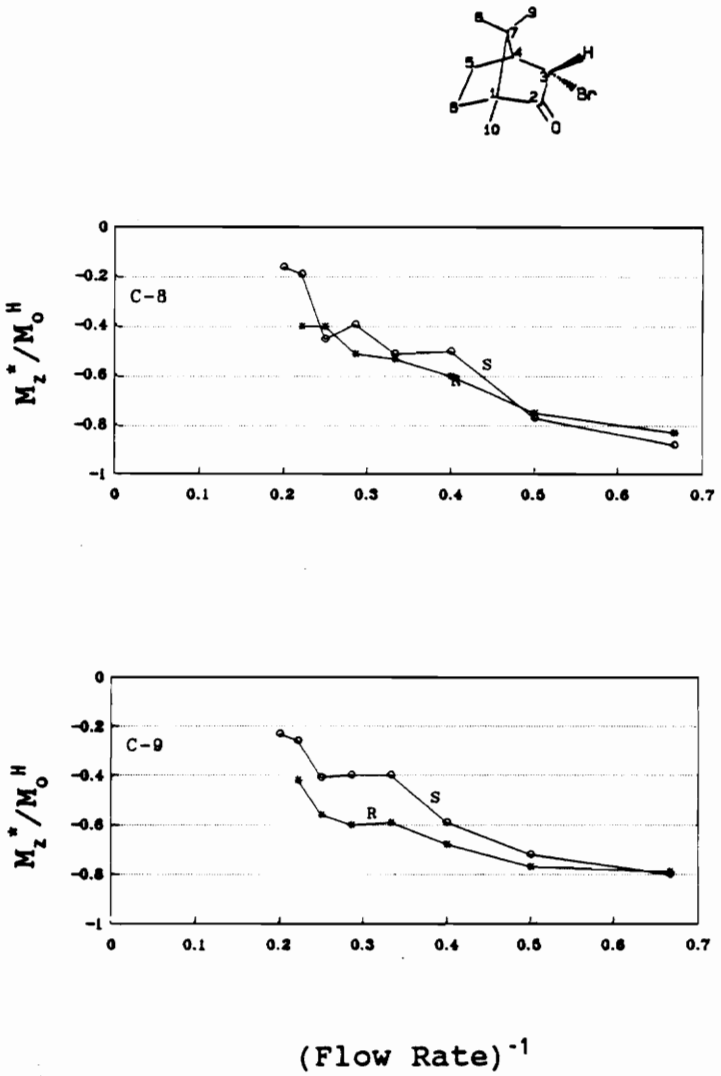

Fig. 6.22 Plots of the observed ^{13}C SLIT DNP enhancements, M_z^*, relative to M_o^H vs. 1/Flow Rate for carbons C-8 and C-9.

enantiomers in a plot similar to that in Fig. 6.21. Also, the assumption for a difference in the enhancement due to non-enantio- selective enhancement could be tested by two separate SLIT DNP experiment utilizing $(R)_{sample}/(\pm)$SPIN sample and $(S)_{sample}/(\pm)$SPIN sample systems where the interactions sample/surface are not enantiospecific.

In conclusion, although the result from this experiment is qualitative, it does suggest that selective enantiomer/chiral SPIN interactions are feasible. Also, the result shows some feature directions for the development of the method. For example, an introduction of π-electron substituents (such as aromatics, nitroaromatics etc.) in the immobilized radicals will insure π-π interaction in addition to the polar interactions (for example, hydrogen bonding) and will hopefully increase the strength of the diastereomeric pairwise interactions between the enantiomers and the surface. Potentially, this will insure larger differences in the enhancements induced by the weak diastereomeric $R_{sample}/R_{surface}$ interactions. This will hopefully allow a prediction of the direction for the difference between the enhancements for a given enantiomeric pair.

CONCLUSIONS

The focal point of this study was to utilize the synthetic approach to provide novel SPIN samples which will hopefully extend the applications of the SLIT DNP approach further.

The introduction of the electron spin system in the DNP experiment via SPIN samples opens the possibility of specific surface/solvent interactions which can influence the observable enhancements. However, it is not trivial to predict which factors are important in the synthetic approach. Accordingly, the syntheses of appropriate SPIN sample for the DNP experiment is difficult and depend on various factors: the topology of the silica gel surface (particle size, surface area and pore diameter); and the relative number of accessible isolated and hydrogen-bonded silanol groups.

A number of achiral SPIN samples were prepared and characterized by EPR spectroscopy in the first part of this study. As a result, the reaction conditions in terms of the type and the thermal pretreatment of the silica gel as well as the reactants mole ratios have been optimized and SPIN samples with about 2.5 to 3.0 times larger surface spin concentration were prepared in this thesis.

The SLIT ^{1}H DNP result showed no improvement of the observed enhancements as a function of the radical concentration. Most likely, the ultimate enhancement is limited by the limited correlation time ($\omega_e \tau_c \sim 1$).

However, the use of SPIN samples with higher surface spin concentration demonstrate for the first time the possibility of detection of dipolar-dominated ^{13}C SLIT DNP enhancements for the case of **SPIN 11**/1-chlorobutane. The significance of this results is important for improved signal/noise ratios in routine LC NMR and other sensitivity limited studies

Deuteration and ^{15}N substituted SPIN samples have been prepared in order to examine the effect of the isotope substitution on the ^{1}H SLIT DNP enhancements. The lack of improvement in the enhancements as a result of the substitution of the deuteron for proton on the surface was assumed to be a result of an appreciable contribution of a solid-state three-spin effect. The substitution of deuterium for proton on the surface presumable suppresses an additional contribution to the enhancement, due to the interaction of the sample with the strongly polarized protons in the radical. The result of substituting ^{15}N for ^{14}N on the surface suggests that this approach has no advantages for studies where high spin concentration is required because of the large electron

-electron exchange interaction .

Two different types of chiral SPIN samples were prepared, in the second part of this study in order to provide a chiral environment to test the hypothesis for obtaining different enhancements for the R- and S- isomers of a given enantiomeric pair. A resolution of a racemic acid and consequently a reduction to the corresponding R-(+)- alcohol was accomplished for this purpose.

The ^{13}C SLIT DNP results show differences in the enhancements for the R-(+)- and S-(-)- isomers of bromocamphor in the presence of the chiral **SPIN 13**. The differences in the enhancements for the carbon atoms were considered to be a result of the different strength of the hydrogen bonding complex formation for the two enantiomers. A contribution to the difference in the enhancements, however, could presumably arise from steric effects which would be different for the R-(+)- and S-(-)-bromocamphor, respectively. The results are considered reliable because the same saturation factors (within the error of the measurement) were obtained in both cases. Nevertheless, an additional experimental support is necessary for indisputable conclusion to be made. However, this experiment does suggest that selective enantiomer/chiral SPIN interactions are feasible.

FUTURE STUDIES

The future development of the SLIT DNP method can be viewed in two areas: synthesis of SPIN samples and instrumentation.

The synthetic approach can be used to study the effect of the different silica supports (in terms of surface area and particle size). Based on the resuls from the DNP experiment, in this study, utilizing a chiral SPIN sample to induce enantioselective ^{13}C enhancements, it is probably advantageous to use the synthetic approach in order to provide a system that will assure maximum enantioselectivity by providing tighter binding between the chiral SPIN radical and the enantiomeric pair.

At this stage of the development of the SLIT DNP method a further improvement from instumentational point of view could be helpful. Some suggestions are given below:

1). The use of a dual EPR cavity will result in an introduction of the SPIN samples in two EPR cells, connected by a short transfer line. Thus, the flowing (through the two EPR cells) bolus will be in contact with about twice larger volume of the SPIN sample which is almost equivalent to an

increase of the radical concentration by a factor of 2. In this case the increase in the leakage factor and/or the suppression of the three-spin effect will not occur at the expense of the saturation factors.

2). The simultaneous irradiation of the proton transitions in the low magnetic field will suppress the three-spin effect thus increase dipolar dominated ^{13}C SLIT DNP enhancements.

3). A possible experiment which utilizes a pulse technique to saturate the three nitroxide transitions simultaneously would also result in an increase of the observable DNP enhancements. However, such an experiment can be applied for dilute SPIN systems only.

APPENDIX

^{13}C NMR Intramolecular Relaxation Studies of Nitroxide Samples.

Because ^{13}C is a dilute spin and usually occurs in molecules in which protons are the only other magnetically active nuclei, its relaxation properties are largely dominated by (C,H) dipolar interactions. Relaxation mechanisms other than the (C,H) dipolar effect are normally negligible for the carbons of large organic molecules, even (in the limit) for quaternary carbons.

Relaxation rates due to different mechanism are additive so that, under the assumption that the contribution of all other than dipole-dipole mechanism are small and can be combine in one term, $(1/T_1)_{others}$, the total relaxation rate can be expressed by:

$$(T_{1total})^{-1} = (T_{1dd})^{-1} + (T_{1o})^{-1} \qquad \text{A-1}$$

Dipolar relaxation can be divided into intra- and inter-molecular contributions:

$$(T_{1dd})^{-1} = (T_{1dd})^{-1}(\text{intra}) + (T_{1dd})^{-1}(\text{inter}) \qquad \text{A-2}$$

It is frequently desired to separate relaxation contributions from different mechanisms. The dipolar term, $(T_{1dd})^{-1}$, (Eq. A-1) can be separated by measurement of the nuclear Overhauser effect which depends on the dipole-dipole interactions only, and for the case of carbon-proton dipolar interactions is given by:[14]

$$NOE = 1 + (\gamma_H/2\gamma_C)(T_{1dd})^{-1}/(T_1)^{-1} \qquad A\text{-}3$$

where $(T_1)^{-1}$ is the total relaxation rate.When the $(T_1)^{-1} = (T_{1dd})^{-1}$ (or when the only relaxation mechanism is (C,H) dipolar interactions) the NOE achieves its maximum value of 2.988. If other relaxation mechanisms contribute to the total relaxation rate, the measurements of both T_{1total} and NOE yields a value for the contribution of T_{1dd} (inter- and intra-). The contributions of all other mechanisms together can then be obtained from eq. A-1.

Intra- and inter-molecular terms can be distinguish by dilution studies, because of the concentration dependence of the intermolecular contribution which is not effective at low concentrations. A plot of the total relaxation rate as a function of the radical concentration should allow the intra-molecular contribution to be estimated from the intercept.

Our study intended to estimate the relative contribution of the intramolecular relaxation rate for the different carbon atoms of a long chain nitroxide radical. In the presence of the radical (at high concentrations), the relaxation of the carbons is dominated entirely by their dipolar interactions with the unpaired electron (S) because of the larger magnetic moment of the electron relative to the of the proton. However, for low radical concentrations the (C,H) intramolecular dipolar interaction becomes comparable with the (C,S) intermolecular dipolar interaction. The relative contribution of the intra-molecular (C,H) and (C,S) dipolar interactions, however depends only on the distance ($\propto 1/r^6$) and carbons which are close to the unpaired electrons will have dipolar intramolecular contribution due to the (C,S) interactions. It should be noted that the (C-S) interaction is not necessarily a dipole - dipole interaction).

In light of the discussion above, the equation for the total relaxation rate when unpaired electrons are present, is given by:

$$(T_{1total})^{-1} = [(T_{1dd})_{intra}^{-1} + (T_{1dd})_{iter}^{-1}]_{C,S} + [(T_{1dd})_{intra}^{-1} + (T_{1dd})_{inter}^{-1}]_{C,H} + (T_1)_o^{-1} \quad \text{A-4}$$

A model system for a long chain nitroxide radical, 4-octanoate-TEMPO, RNO, (Fig. A-1,(a)) and it amino-precursor,

RNH, (Fig. A-1,(b)) was used for the NOE measurements in this study. A concentration range of 0.002 to 0.1 M RNO and 0.2 M RNH in $CDCl_3$ was employed.

We assume that the presence of the relatively high concentration of RNH provides no changes in the molecular correlation time (that is, no change in T_1 due to a different time dependence for the motion) as a function of the radical, RNO, concentration. The above statement holds under the assumption that the intermolecular (C-H) interactions for the RNO/RNH system are identical to that if we used the RNO system only.

The NOE's for the different carbon atoms in the above system at different concentrations of RNO are presented in Table A-1. The ^{13}C NMR spectrum for a 0.2 M RNH in $CDCl_3$ is given in Fig. A-2. The expected decrease of the NOE (that is, decrease in the contribution of the (C-H) dipolar mechanism to the total relaxation rate) with the increase in the radical concentration is observed, but does not appear to be linear with concentration (except for carbons C-12 and C-8).

A separate experiment for the separation of the (C-S) intra- and the (C-S) inter-molecular contribution was attempted by acquiring the total relaxation rate as a function of the radical concentration. The plots for the different

carbon atoms are presented in Fig. A.4. Radical concentrations in the range of 0.05 to 0.2 M were used. The curves do not level off as the radical concentration decreases which suggest an appreciable contribution of the intermolecular (C-S) contribution in that concentration region. Thus an estimation of the (C,S) intramolecular contribution to the total relaxation rate could not be made.

Experimental:

Preparation of 2,2,6,6 - tetramethylpiperidinyloxy-4-octanoate (RNO): An analogous procedure to that described by Waggoner et al[55]. was used as follows: 2.28 ml (11 mmol) of decanoyl chloride dissolved in 10 ml of anhydrous ether was added dropwise (for 1 hr.) to a solution containing 0.81 ml (0.79 g; 10 mmol) of dry pyridine, 1.72 g (10 mmol) of TEMPOL, and 30 ml of diethylether at 0°C in a three-necked flask. After a few minutes the solution was allowed to warm to room temperature. The synthesis was carried out in a N_2 atmosphere. On the next day the solution (red solution + white ppt.) was washed several times with 5% aq. $NaHCO_3$ and filtered through $MgSO_4$. The solvent was removed in vacuo. The resulting red oil was purified by column chromatography: ether/hexane - (5/95), then (10/90), then (20/80).

Preparation of 2,2.6,6-Tetramethylpiperidine-4-octanoate (RNH): The amine was prepared in analogous way: to 1.58 g (10 mmol) $HO(C_9H_{18})NH$ and 2.8 ml (20 mmol) Et_3N in 50 ml CH_2Cl_2 add dropwise 2.28 ml (11 mmol) $CH_3(CH_2)_8COCl$ in 10 ml CH_2Cl_2 for 1/2 hr. Reflux the mixture for 18 hrs., filter, evaporate the solvent in vac.

All samples for the NMR measurements were degassed by means of the freeze-pump-thaw technique directly in the NMR tube. The NMR spectra were measured using 200 MHz BRUKER spectrometer. The inversion recovery method was used for the T_1 measurements and the inverse gated decoupling was employed for the NOE measurements.

Table A.1 NOE data for the RNH/RNO system

	NOE						
Conc. (M) RNH/RNO	C-1 14.0 ppm	C-2 22.6 ppm	C-3 24.9 ppm	C-8 31.8 ppm	C-11 43.6 ppm	C-12 51.9ppm	C-13 68.1 ppm
0.2/0.0	2.57	2.50	3.02	2.72	2.65	2.09	2.63
0.2/0.002	1.42	1.87	2.43	2.09	2.88	2.31	2.74
0.2/0.05	1.86	2.02	2.52	1.97	2.85	1.48	2.51
0.2/0.1	1.74	1.23	1.78	1.72	2.39	1.21	2.10

The NMR spectra were measured using 200 2MHz BRUKER NMR Spectrometer.

The inverse gated decoupling was employed for the NOE measurements.

(a)

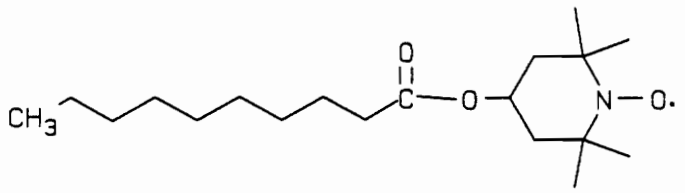

(b)

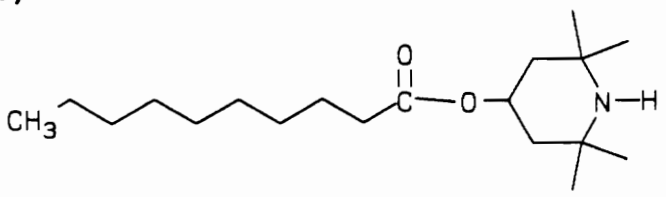

Fig. A.1 (a) long chain nitroxide radical, R-NO, and (b) its amino-precursor, R-NH

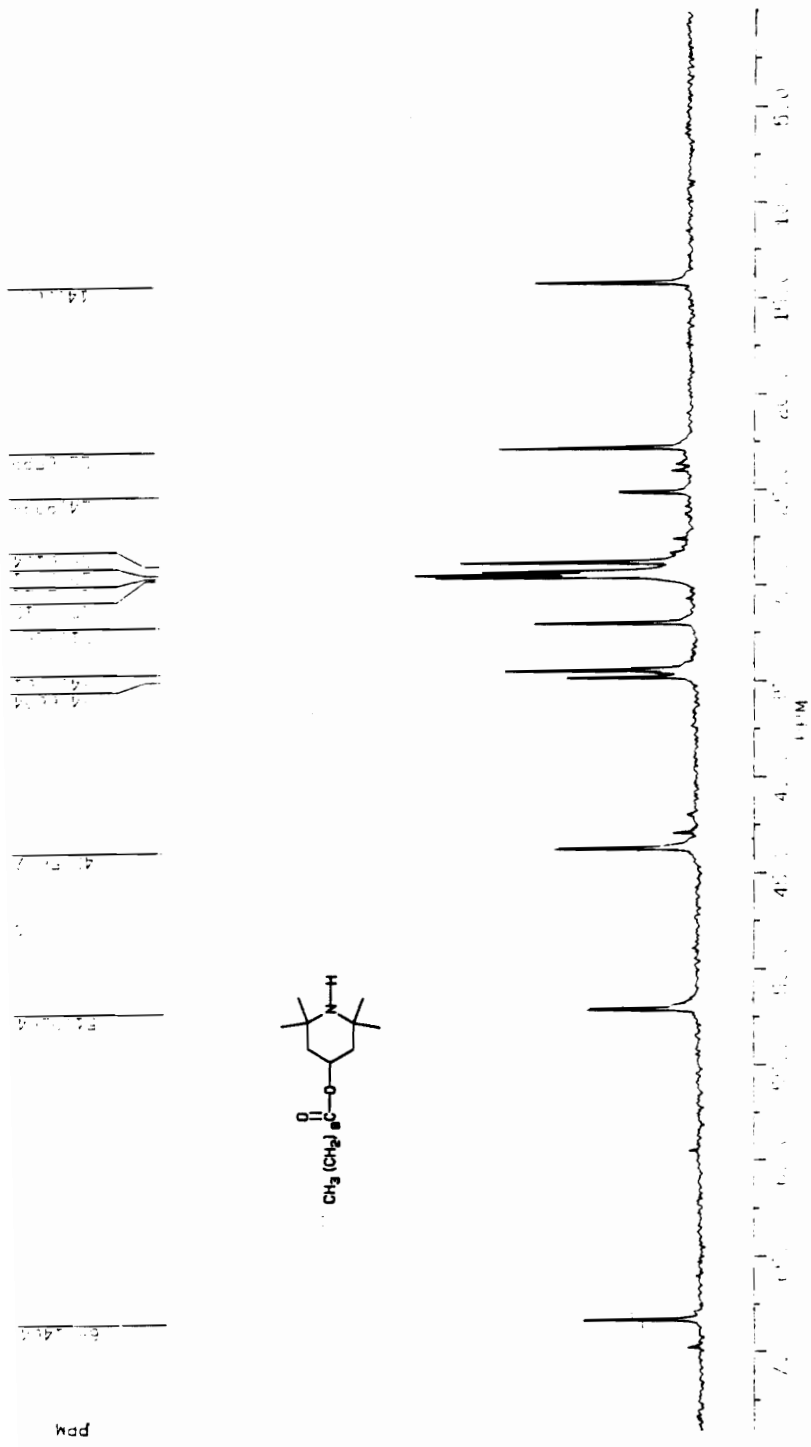

Fig. A.2 ^{13}C NMR spectrum of R-NH in $CDCl_3$

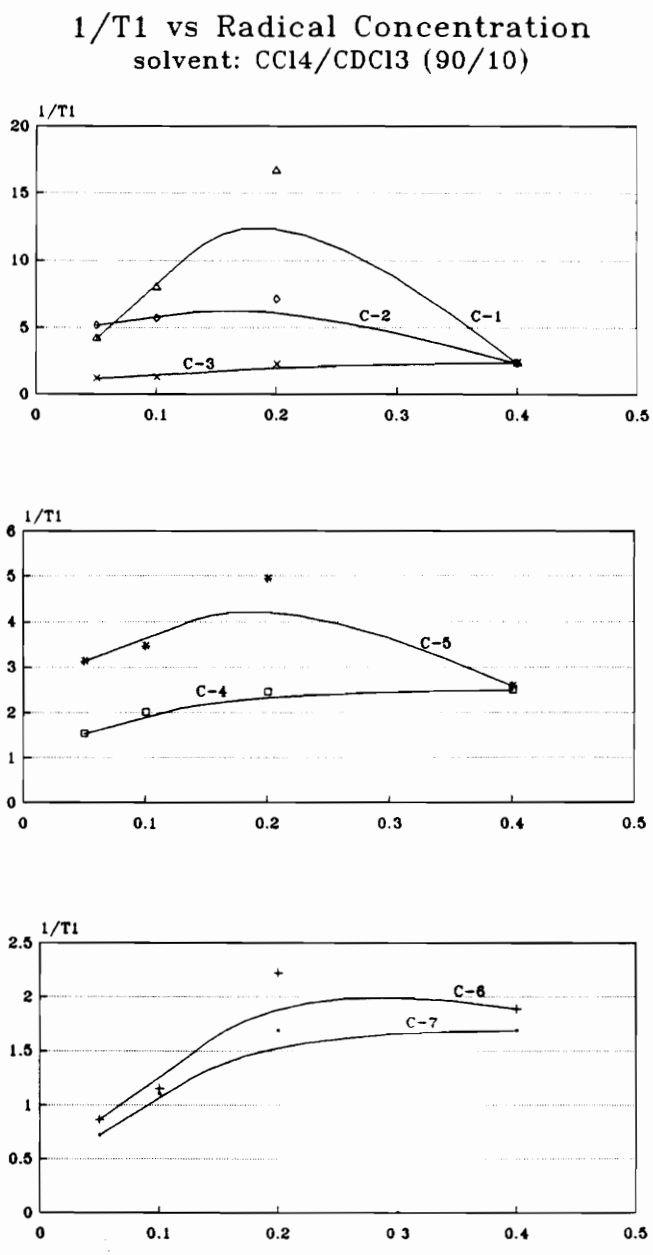

Fig. A.3 Plots of the total relaxation rate, (T_1^{-1}) vs. the radical concentration for carbons C-1 to C-7

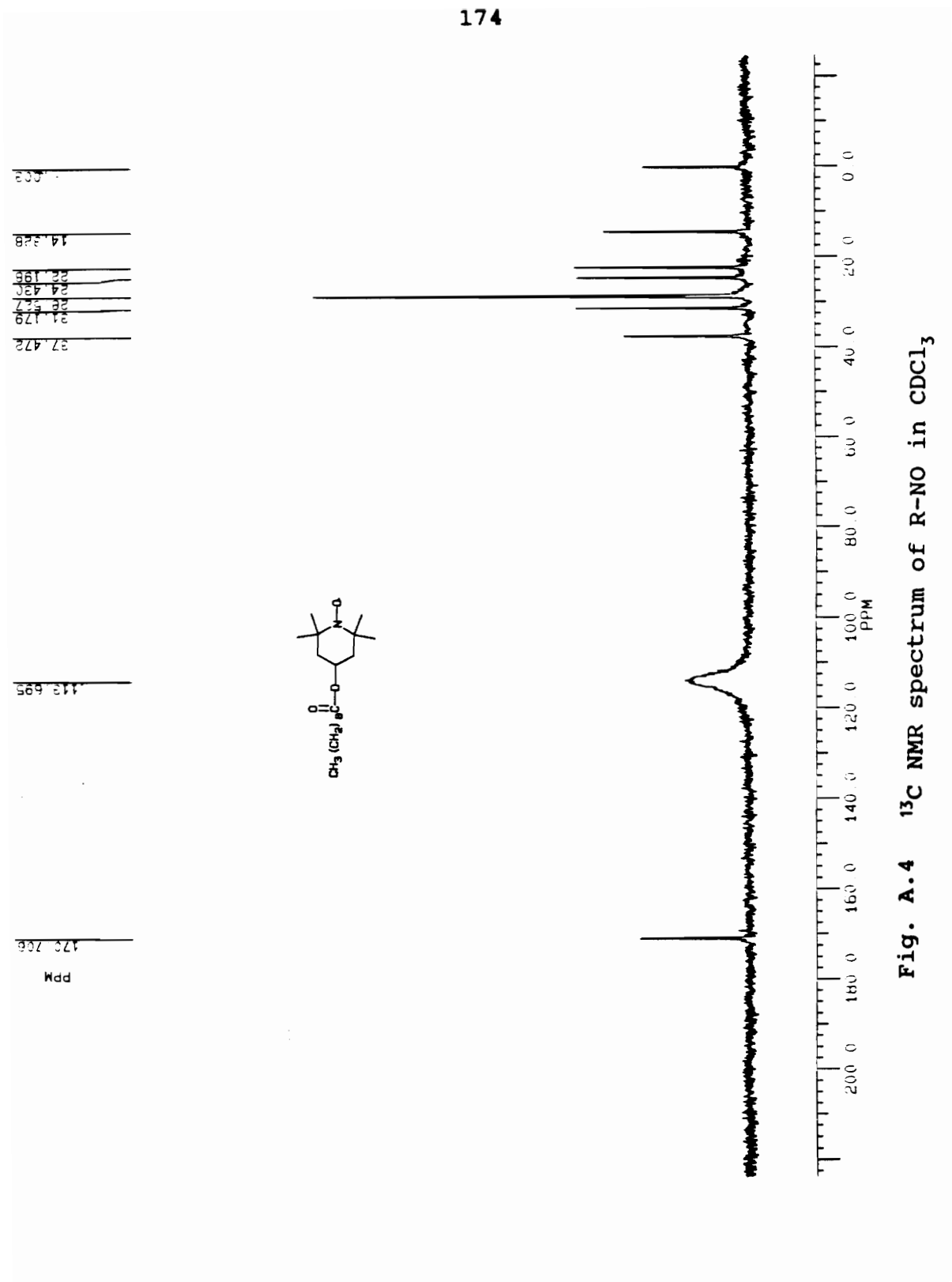

Fig. A.4 ^{13}C NMR spectrum of R-NO in $CDCl_3$

REFERENCES

1. H. J. Jakobsen, S. Linde, S. Sorensen, J.Magn.Reson., **15** (1974) 385.

2. J. H. Noggle, R. E. Schirmer, "The Nuclear Overhauser Effect", Academic Press, New York 1971.

3. A. W. Overhauser, Phys.Rev. **92** (1953) 411.

4. K. H. Hausser, D. Stehlik, Adv.Magn.Reson. **3**(1968) 79.

5. A. R. Dwek, R. E. Richards and D. Taylor, Annu. Rev. NMR Spectrosc. **2** (1969) 293.

6. W. Müller-Warmuth and K. Meise-Gresch. Adv.Magn.Reson. **11** (1983) 1.

7. R. A. Wind, M.J. Duijvestijn, C. Van Der Lugt, A. Manenschijn and J. Vriend, Prog.NMR Spectrosc. **17** (1985) 33.

8. H. C. Dorn. J. Wang, L. Allen, D. Sweeney, and T. E. Glass, J. Magn. Res. **79** (1988), 404.

9. R. Gitti, C. Wild, C. Tsiao, K. Zimmer, T. Glass. and H. C. Dorn, J. Am. Chem. Soc., **110** (1988), 2294.

10. H. C. Dorn, R.K. Gitti, K.H. Tsai, and T.E. Glass, Chem. Phys. Lett. 155 (1989) 227.

11. K. H. Tsai and H. C. Dorn, Applied Magn. Reson., **1** (1990), 231.

12. H. C. Dorn, T. E. Glass, R. K. Gitti, and K. H. Tsai, J. Applied Magn. Reson., **9**, (Vol. 2) (1992),608.

13. H. C. Dorn, C. Tsiao, K. H. Tsai, G. Samaranayake, and G. I. Kingston, J. Org. Magn. Res., **in press.**

14. K. H. Tsai, T. E. Glass, and H. C. Dorn, J. Magn. Reson., **89** (1090), 362.

15. S. G. Allenmark, Chromatographic Enantioseparation: Methods and Applications", John Wiley & Sons, New York, (1988).

16. B. Beilush and E. Gil-Av, Tetrahedron, **26,** (1970), 1361.

17. B. Koppenhofer, H. Allmendinger and G. Nicholson, Angew. Chem., **97**, (1985), 46.

18. B. Koppenhofer and H. Allmendinger, Chromatographia, **21**, (1986), 503.

19. E. Bayer, Z. Naturforsch, **38b**, (1983), 1281.

20. G. Whitesides and D. Lewis, J. Am. Chem. Soc., **92**, (1970), 6979.

21 V. A. Davankov, A. A. Kurganov and A. S. Bochov, Adv. Chromatog. **22**, (1983), 71.

22. A. Dobaski, K. Oha and S. Hara, J. Am. Chem. Soc., **102**, (1980), 7122.

23. R. K. Harris, Nuclear Magnetic Resonance Spectroscopy, Pitman, 1983.

24. A. Abragam, The Principles of Nuclear magnetism, at the Clarendon Press, Oxford, **44** (1961), 308.

25. G. N. LaMar, ed., NMR of Paramagnetic Molecules, 1973.

26. P. S. Hubbard, Proc. Roy. Soc. **A291** (1966), 537.

27. I. Noack, G. J. Kruger, W. Müller-Warmuth and R. Van Steenwinkel, Z. Naturforsch, **22a** (1967), 2102.

28. I. Solomon. Phys. Rev., **99** (1955), 559.

29. K. H. Tsai, Ph.D. Thesis, Virginia polytechnic institute and State University, (1991).

30. K. H. Hauser and D. Stehlik, in Adv. in Magn. Res., vol. 3, ed. J.S. Waugh, Academic Press, New York (1968).

31. G. G. Maresch, R. D. Kendrick, and C. S. Yannoni, J. Magn. Res. **82** (1989), 41.

32. R. Gitti, M.S., Virginia Polytechnic Institute and State University, 1988.

33. E. G. Bagrganskaya, N. I. Andrievich, Yu. A Grishin, and R. Z. Sagdeev, Chem. Phys., **135** (1989), 123.

34. D. Bruck, B. Dudly, C. S. Fyfe, and J.V. Delden, J. Magn. Reson. **42** (1981), 51.

35. R. K. Giplin, A. Kasrur, and E. Gelerinter, Anal. Chem., **59** (1987) 1177.

36. B. E. Wagner J. N. Helbert, E. H. Poindexter, and R. D. Bates Surf. Sci. **67** (1977), 251.

37. D. Griller and K.U. Ingold, Acc. Chem. Res. **9** (1976), 13.

38. D. W. Sindorf and G. E. Maciel, J. Am. Chem Soc., **105** (1983), 1848.

39. R. D. Bates, and W.S. Drozdoski, J. Chem. Phys., **67** (1977), 4038.

40. R. D. Bates, J. Magn. reson., **48** (1982), 111.

41. B. A. Bates, M. E. Johnson, and B. L. Currie, Journal of Labelled Compounds and Radiopharmaceuticals **XX**, No.1 (1082), 33.

42. K.Flohr, R.M. Paton, and E.T. Kaiser, J. Amm. Chem. Soc. **97** (1975), 1209.

43. S. Hara and A. Dobashi, J. High Resol. Chromatog; Chromatog. Commun., **2** (1979), 531.

44. H. M. Swartz, J. R. Bolton, and D. C. Borg, Biological Applications of Electron Spin Resonsnce, John Wiley & Sons Inc. 1972, p. 121.

45. K.H. Hausser, H. Brunner, and J. C. Jochims, Mol. Phys., **10** (1966), 529.

46. R. A. Dwek, J.G. Kenworthy, and R. E. Richards, Mol. Phys., **11** (1966), 421.

47. D. Stehlik and K. H. Hausser, Z. Naturforsh, **22a** (1967), 914.

48. T. G. Burlingame and W. H. Pirkle, J. Am. Chem. Soc., **88** (1966), 4294.

49. W. H. Pirkle and S. D. Beare, J. Am. Chem. Soc., **89** (1967), 5485.

50. W. H. Pirkle and S. D. Beare, J. Am. Chem. Soc., **90** (1968), 6250.

51. W. H. Pirkle and S. D. Beare, J. Am. Chem. Soc., **91** (1969), 5150.

52. R. E. Sievers, Ed., "Nuclear Magnetic Resonance Shift Reagents", Academic Press, Inc.: New York, (1973).

53. T. J. Wenzel, "NMR Shift Reagents", CRC Press, Inc., Boca Raton, Florida (1987).

54. T. C. Moril, Ed., "Lanthanide Shift Reagents in Stereochemical Analysis", Vol. 5, VCH Publisher, Inc., New York (1986).

55. A. S. Waggoner and A. D. Eith, J. Phys. Chem., **72** (1968), 4129.

VITA

Rossitza Gitti was born May 13, 1949 in Bulgaria. She graduated with a Diploma in Chemical Engineering from Chemical Technological Institute, Sofia, Bulgaria in 1976. After that she has worked in the Institute of Organic Chemistry, Bulgarian Academy of Science. She came to the United States October, 1984 and started her graduate studies in VPI & SU in January, 1985. She received the Master of Science Degree in Chemistry in 1988. The same year, she began her Ph. D. graduate studies at VPI & SU under the guidance of Dr. Harry C. Dorn.